Tectonics

FEATURE ARTICLE
10.1029/2018TC005312

GRAND CHALLENGES CENTENNIAL COLLECTION

Innovations in (U–Th)/He, Fission Track, and Trapped Charge Thermochronometry with Applications to Earthquakes, Weathering, Surface-Mantle Connections, and the Growth and Decay of Mountains

Alexis K. Ault[1], **Cécile Gautheron**[2], **and Georgina E. King**[3]

[1]Department of Geosciences, Utah State University, Logan, UT, USA, [2]GEOPS, Université Paris-Sud, CNRS, Université Paris-Saclay, Orsay, France, [3]Institute of Earth Surface Dynamics, University of Lausanne, Lausanne, Switzerland

Key Points:
- Challenges in low-temperature thermochronometry involve resolving complex thermal histories in recent or deep time
- We summarize method advances and new applications in (U–Th)/He, fission track, and trapped charge thermochronometry
- Innovations in methods, materials science, multimethod approaches, and modeling will enable new Earth science discoveries in coming years

Correspondence to:
A. K. Ault,
alexis.ault@usu.edu

Citation:
Ault, A. K., Gautheron, C., & King, G. E. (2019). Innovations in (U–Th)/He, fission track, and trapped charge thermochronometry with applications to earthquakes, weathering, surface-mantle connections, and the growth and decay of mountains. *Tectonics*, *38*. https://doi.org/10.1029/2018TC005312

Received 7 MAY 2019
Accepted 7 AUG 2019
Accepted article online 24 AUG 2019

Abstract A transformative advance in Earth science is the development of low-temperature thermochronometry to date Earth surface processes or quantify the thermal evolution of rocks through time. *Grand challenges* and new directions in low-temperature thermochronometry involve pushing the boundaries of these techniques to decipher thermal histories operative over seconds to hundreds of millions of years, in recent or deep geologic time and from the perspective of atoms to mountain belts. Here we highlight innovation in bedrock and detrital fission track, (U–Th)/He, and trapped charge thermochronometry, as well as thermal history modeling that enable fresh perspectives on Earth science problems. These developments connect low-temperature thermochronometry tools with new users across Earth science disciplines to enable transdisciplinary research. Method advances include radiation damage and crystal chemistry influences on fission track and (U–Th)/He systematics, atomistic calculations of He diffusion, measurement protocols and numerical modeling routines in trapped charge systematics, development of $^{4}He/^{3}He$ and new (U–Th)/He thermochronometers, and multimethod approaches. New applications leverage method developments and include quantifying landscape evolution at variable temporal scales, changes to Earth's surface in deep geologic time and connections to mantle processes, the spectrum of fault processes from paleoearthquakes to slow slip and fluid flow, and paleoclimate and past critical zone evolution. These research avenues have societal implications for modern climate change, groundwater flow paths, mineral resource and petroleum systems science, and earthquake hazards.

Plain Language Summary Documenting the timing and rates of transformations to Earth's surface and crust helps scientists understand how and why geologic processes occur and improves predictions of future changes to our planet. The field of low-temperature thermochronometry, which quantifies the temperature ($T < 250$ °C) evolution of minerals and rocks through time, is uniquely suited to address these challenges. We highlight development of three techniques: fission track (damage tracks from spontaneous fission), (U–Th)/He (abundances of uranium and thorium compared to helium), and trapped charge (electrons trapped in crystal defects) thermochronometry. Innovations in these methods enable breakthroughs on long-standing and emerging Earth science problems. For example, low-temperature thermochronometry can document dramatic changes to Earth's surface through erosion and plate tectonics, such as past earthquakes or detect subtle surface changes that are connected to deep (mantle) Earth processes. Thermochronometry research has implications for climate change, geologic exploration of other planets, subsurface water, resource development, and earthquake hazards.

1. Thermochronometry and Earth Processes

Many Earth processes result in a change in Earth's thermal structure. Temperature changes impart distinct geochemical and isotopic fingerprints on minerals and rocks. A transformative advance in Earth science is the development of thermochronometry, which utilizes these fingerprints to quantify the thermal evolution of rocks through time as they move through Earth's subsurface. Radioisotopic systems sensitive to a range of temperatures place specific ages on Earth materials from the oldest preserved rocks and minerals to the most recently formed, as well as dates on processes that cool, weather, transport, and deposit them. Low-

temperature thermochronometry has become a cornerstone of tectonics, geomorphology, and sedimentary systems research. G*rand challenges* in low-temperature thermochronometry involve pushing the boundaries of these techniques to constrain the evolution of Earth's landscape and upper crust over seconds to hundreds of millions of years, in recent to deep geologic time, by leveraging perspectives from the scale of atoms to mountain belts. Addressing these challenges advances our understanding of how Earth materials deform, fault zones evolve, sedimentary basins fill, continental margins develop, Earth's surface responds to mantle flow, and orogens are built and decay through the interplay of tectonic and erosional processes.

Thermochronometric methods involve the measurement of ratios of fission tracks (FTs), isotopes creating parent-daughter decay systems, and trapped electrons in crystal defects. Annealing of FTs, loss of daughter isotopes, and ratios of parent-daughter isotopes and trapped charges reflect the thermal history of the sample in which they are measured. The temperature sensitivity of a particular thermochronometer is described using the concept of "closure temperature" (T_c; e.g., Dodson, 1973; Guralnik et al., 2013). The T_c reflects the transition from open- to closed-system behavior (i.e., retention of noble gases and trapped charge and preservation of FTs). The concept of T_c applies to monotonic cooling histories, is cooling rate and grain size dependent, and serves as a useful metric for comparing different thermochronometric systems.

Low-temperature thermochronometry systems (250 °C > T_c > 25 °C) are uniquely suited to decipher upper crustal and Earth surface thermal histories owing to their low-temperature sensitivity (Figure 1). Here we highlight recent advances in FT, (U–Th)/He, and trapped charge thermochronometry. We focus on these systems due to their complementary T_c (Figure 1) and because addressing grand challenges in low-temperature thermochronometry requires integration of observations from multiple systems. Recent method and application advances enable fresh perspectives on fundamental Earth science problems and connect these tools with new users across disparate Earth science disciplines to facilitate transdisciplinary research. These developments mirror innovation in moderate (i.e., ^{40}Ar–^{39}Ar; e.g., Lovera et al., 1991) and high temperature (i.e., U–Pb; e.g., Blackburn et al., 2011; Cochrane et al., 2014; Schoene & Bowring, 2007) thermochronometry systems, as well as the development of noble gas paleothermometry (e.g., Tremblay et al., 2014; Tremblay et al., 2017), which are not the focus of this contribution. Ongoing work in ^{40}Ar–^{39}Ar and U–Pb thermochronometry and noble gas paleothermometry enable researchers to tackle a range of Earth science problems from crustal deformation to surface processes and mountain building (e.g., Gottardi et al., 2018; Hodges et al., 2005; Resor et al., 1996; Schneider et al., 2013; Tremblay et al., 2019; van der Pluijm et al., 2001; and many others).

In this contribution, we first review the fundamentals of the FT, (U–Th)/He, and trapped charge thermochronometry systems. We then highlight some of the discoveries and method improvements that are advancing the field to address grand challenges. Innovative applications leverage these advances and multisystem data sets and include but are not limited to landscape evolution, connecting Earth surface changes with the deep Earth processes, documenting the spectrum of fault processes from paleoearthquakes to slow slip and fluid flow, and paleoclimate changes and critical zone (CZ) evolution in deep geologic time.

2. Foundation

2.1. FT Thermochronometry

FT thermochronometry exploits the natural production of tracks formed during the spontaneous fission of ^{238}U and time-temperature-dependent annealing of FTs. The first observations of charged-particle tracks were reported in the late 1950s (Silk & Barner, 1959; Young, 1958), and Price and Walker (1962a, 1962b, 1962c) discovered that tracks created by fission fragments are revealed by chemical etching. The foundation of the FT dating method, developed by Fleischer et al. (1975) and Naeser (1967), involves measuring U concentration, a ^{238}U fission decay constant, and the FT density in a crystal, the accumulation of which is a function of time. Although many phases contain U, FT thermochronometry is predominantly applied to apatite and zircon, owing to suitable U concentrations (10-1000s ppm) that generate FT densities associated with relatively precise dates. Apatite and zircon FT (AFT and ZFT) are now routinely used to constrain geological processes occurring over 10^6–10^9 years, as well as high-temperature (i.e., >800 °C), short-duration (seconds to minutes) phenomena.

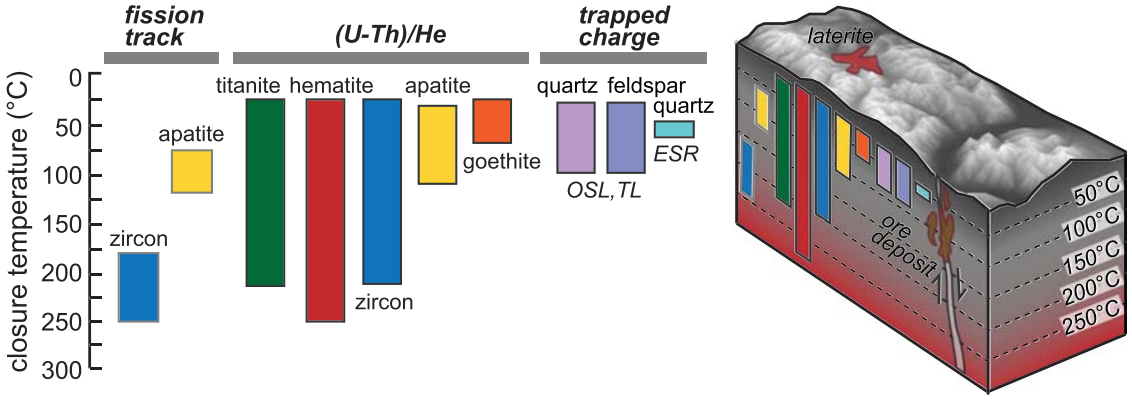

Figure 1. Closure temperature (T_c) ranges for fission track (FT), selected (U–Th)/He, and trapped charge thermochronometry systems. T_c ranges for FT and (U-Th)/He assume a 10 °C/Myr cooling rate (Baughman et al., 2017; Bernet, 2009; Flowers et al., 2009; Gautheron et al., 2009; Guenthner et al., 2013; Ketcham et al., 2007; Shuster et al., 2005). T_c ranges for trapped charge thermochronometry are determined relative to the minimum resolvable cooling rate (cf Grün et al., 1999; Guralnik et al., 2013; Guralnik, Jain, et al., 2015; King, Guralnik, Valla, & Herman, 2016; Biswas et al., 2018). Conceptual sketch at right shows topography, isotherms that increase with depth, and projected T_c values for each system on left. ESR = electron spin resonance; OSL = optically stimulated luminescence; TL = thermoluminescence.

An AFT or ZFT date is obtained by counting the density of spontaneous FTs in a suite of epoxy-mounted crystals, revealed in an acid-etched polished surface. The spontaneous track density is compared with a U concentration, determined either by counting induced tracks from ^{235}U neutron activation in an irradiated mica (i.e., external detector method; Gleadow, 1981) or by laser ablation inductively coupled plasma mass spectrometry (ICPMS; Chew & Donelick, 2012; Hasebe et al., 2004). Refinement and standardization of etching protocols, combined with consideration of compositional proxies (i.e., D_{par}), have improved FT thermochronometry applicability (Donelick et al., 1999; Ketcham et al., 1999; Murrell et al., 2009; Sobel & Seward, 2010) and refined data interpretations (e.g., Stevens et al., 2016).

FTs are not permanently preserved in minerals, and they can shorten, fade, and segment (e.g., Ketcham, 2005). Annealing of FTs in apatite and zircon is primarily a function of the thermal history and grain chemistry (Barbarand et al., 2003; Carlson et al., 1999; Green et al., 1986; Ketcham et al., 1999; Ketcham et al., 2007; Tagami et al., 1998; Yamada et al., 1995). More specifically, FTs anneal by temperature-controlled atomic diffusion, observed from the microscopic to atomic scales (Barbarand et al., 2003; Laslett et al., 1987; Li et al., 2011; Li et al., 2014). The T_c for the AFT and ZFT systems are ~80–120 °C and ~180–250 °C (e.g., Bernet, 2009; Ketcham et al., 2007; Figure 1). The measurement of the track length distribution in a given sample provides additional constraints on the sample's thermal history (Gleadow et al., 1986; Green et al., 1985).

2.2. (U–Th)/He Thermochronometry

(U–Th)/He thermochronometry exploits decay of ^{238}U, ^{235}U, ^{232}Th, and ^{147}Sm isotopes, associated alpha particle (^{4}He) production, and temperature-dependent ^{4}He diffusion through a crystal lattice (e.g., Farley, 2000; Strutt, 1909; Wolf et al., 1996; Zeitler et al., 1987). Because the Sm contribution to the He budget is limited, this method is historically referred to as (U–Th)/He, with (U–Th–Sm)/He used more recently for phases with measurable Sm content. (U–Th)/He dating has a historical perspective, with Ernest Rutherford reporting the first radioisotopic date using a U–He system in 1904. In the last three decades, a resurgence of interest in dating minerals with ^{4}He ingrowth has been facilitated by an improved understanding of the behavior of He in minerals (Farley, 2000; Flowers et al., 2009; Gautheron et al., 2009; Guenthner et al., 2013; Lippolt et al., 1994; Reiners et al., 2004a; Shuster et al., 2006; Shuster & Farley, 2009; Stockli & Farley, 2004; Wolf et al., 1996; Zeitler et al., 1987) and development of robust analytical techniques (Farley, 2002; Farley et al., 1999; Guenthner et al., 2016). This method can be applied to address geological problems operative over 10^5 to 10^9 years, as well as high-temperature, short-duration thermal pulses.

(U–Th)/He dates are calculated using the ^{4}He, U, Th, and Sm content. An alpha ejection correction factor is applied to account for the fraction of ^{4}He lost from the crystal during alpha decay (Farley et al., 1996; Ketcham et al., 2011), most recently via mapping the 3-D grain-shape and parent nuclide distribution

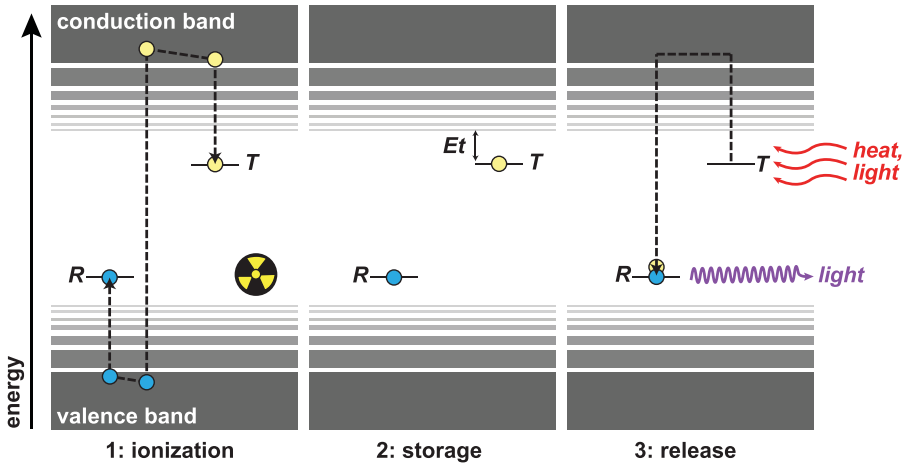

Figure 2. Fundamentals of trapped charge thermochronometry. (1) Exposure of quartz or feldspar minerals to ionizing radiation (i.e., from decay of naturally occurring U, Th, and K) causes electrons (yellow circles) to become excited and to migrate from their ground state in the valence band to the conduction band. Some electrons become trapped in lattice defects (*T*), creating holes (blue circles) that form recombination centers (R). (2) The trapped charge population is metastable over geological time, requiring energy E_t (eV) to escape the electron trap. (3) Stimulation of the mineral with heat or light results in the electrons obtaining sufficient energy to overcome E_t and escape the trap. Electrons diffuse to R, dissipating excess energy as light which can be measured (luminescence). Electron spin resonance dating measures the trapped charge population directly, circumventing Stage 3.

(Fox, McKeon, & Shuster, 2014; Glotzbach et al., 2019; Herman et al., 2007). Whole, pristine crystals (e.g., apatite) are selected, measured, or mapped, and, typically, individual grains are loaded into pure metal (e.g., Nb) tubes or foils. Zircon crystals can be purposefully selected to leverage the range of intrasample visual metamictization, a qualitative proxy for accumulated radiation damage and intrasample geochemical variability (Ault et al., 2018). Hematite aliquots can be targeted by grain size or texture, proxies for the range in T_c, and formation process, respectively (Jensen et al., 2018; McDermott et al., 2017). ^{4}He content is determined by He release from the samples by laser heating or ablation under vacuum, gas purification, and analysis using a noble gas quadrupole or magnetic sector mass spectrometer (Boyce et al., 2006; Farley et al., 1999; Horne et al., 2016, 2019). U, Th, and Sm content are measured using an ICPMS by laser ablation or after aliquot dissolution using appropriate acids (e.g., Evans, Byrne, et al., 2005; Reiners, 2005). Elemental concentrations are traditionally determined by aliquot dimensional mass. Elemental concentrations can also be determined via ICPMS measurement of the Ca and Zr content of apatite and zircon crystals, respectively, and stoichiometry to calculate aliquot mass (Guenthner et al., 2016).

Many common accessory phases including apatite, zircon, titanite, rutile, magnetite, and monazite, and secondary minerals such as calcite, fluorite, hematite, and goethite incorporate trace but measurable amounts of U, Th, and Sm into their crystal structure and negligible initial He. Together with ^{4}He retentivity over geologic timescales, these factors make minerals amenable to (U–Th)/He thermochronometry. The apatite (U–Th)/He (apatite He), zircon (U–Th)/He (zircon He), and titanite (U–Th)/He (titanite He) systems, for example, have T_c of ~30–120 °C (Farley, 2000; Flowers et al., 2009; Gautheron et al., 2009; Shuster et al., 2006; Shuster & Farley, 2009), ~20–200 °C (Guenthner et al., 2013; Reiners et al., 2004a), and ~20–210 °C (Baughman et al., 2017; Reiners & Farley, 1999; Figure 1). Additional T_c ranges for various (U–Th)/He systems are described in section 4.4.

2.3. Trapped Charge Thermochronometry

Trapped charge thermochronometry is based on the dynamic equilibrium between rates of charge trapping and thermally stimulated rates of charge detrapping. Free electronic charge (electrons or holes) is trapped at defects in a mineral lattice (i.e., atomic interstitials, atomic vacancies, and elemental substitutions) due to environmental or ionizing radiation (Figure 2). Electrons are excited by ionizing radiation and both the electron and hole left behind migrate to lower-energy positions or crystal defects. The trapped charge concentration is measured indirectly by a luminescence signal produced when the charge is evicted from a trap by

either light (Aitken, 1998; Huntley, 1985) or heat (Aitken, 1985; Figure 2). The trapped charge concentration of a mineral can also be measured directly using electron spin resonance (ESR; Grün et al., 1999; Rink, 1997), which permits nondestructive charge quantification. The potential of trapped charge systems for determining the thermal history of rocks was recognized >65 years ago (Houtermans et al., 1957). However, since 2010, this technique has been the subject of intense research in an effort to develop a new low-temperature luminescence thermochronometer. To date, the focus has been on the development of optically stimulated luminescence (OSL; Guralnik, Jain, et al., 2015; Herman et al., 2010; King, Herman, Lambert, et al., 2016; Li & Li, 2012) and thermoluminescence (TL; Biswas et al., 2018; Brown et al., 2017) thermochronometry. These approaches benefit from a foundation in the established trapped charge method of luminescence dating (Roberts & Lian, 2015).

Although many minerals produce luminescence (e.g., Marfunin, 2012), defects, trapping capacities, and kinetic parameters are best characterized and thus understood in quartz and feldspar (see Table 2 in King, Guralnik, Valla, & Herman, 2016). Luminescence signals in other phases may not be stable or have such a high and variable environmental radiation dose that they are saturated at short timescales or the dose rate is challenging to calculate. Quartz and feldspar are extracted from bedrock samples with care because the trapped charge is light and heat sensitive. The exterior >1 cm of sample material is removed, and samples are gently hand crushed to extract minerals under subdued red light to avoid potential signal resetting. Samples are sieved to extract the desired grain size range (typically 180–220 μm), followed by treatment with HCl and H_2O_2 to remove carbonates and any organic material, respectively. Density separation isolates quartz and feldspar-enriched fractions. Quartz fractions are then etched in HF acid to remove any contaminating feldspar as well as the outer ~10 μm of the grain that has been affected by alpha irradiation. Feldspar grains may be etched in dilute hydrofluoric acid (e.g., Guralnik, Jain et al., 2015).

Trapped charge dates (ka), in their simplest form, are given by the following equation:

$$Date = \frac{D_e}{\dot{D}} \tag{1}$$

where D_e is the number of trapped charge, or the equivalent dose (Gy), and $\dot{D}$ is the environmental dose rate (Gy/ka). The accumulated dose from environmental radiation, rate of signal saturation, and saturation level are measured via the natural signal using heat (TL), light (OSL), or microwaves (ESR). Kinetic parameters of trapped charge signals, such as signal loss in response to heat for quartz and feldspar, as well as athermal signal loss from feldspar, are documented using isothermal decay and anomalous fading measurements, respectively. TL and OSL measurements use automated systems such as a Risø TL/OSL reader (Bøtter-Jensen et al., 2000) and ESR measurements are typically made with an X-band ESR spectrometer. The rate of signal trapping is calculated from the sample-specific environmental radiation dose rate, which is a function of the U, Th, and K concentrations within the surrounding rock matrix, as well as grain size and mineral type (cf. Durcan et al., 2015). Radioisotope concentrations are measured via ICPMS or by sample activity, constrained with high-resolution gamma spectrometry, alpha, and/or beta counting.

Trapped charge systems have T_c ranging from ~30 °C to ~90 °C, depending on the mineral and signal investigated (Figure 1; Biswas et al., 2018; Guralnik, Jain, et al., 2015; King, Herman, & Guralnik, 2016). In contrast to other thermochronometric systems, these systems are used to infer changes in rock cooling over finite time periods of 10^5 years for OSL and TL dating and 10^6 years for ESR dating because these systems saturate. The saturation limit and low T_c means that trapped charge thermochronometry is applicable for documenting recent rapid exhumation or for late Quaternary paleothermometry (Guralnik, Jain, et al., 2015; Herman & King, 2018; King, Herman, & Guralnik, 2016). Below the T_c, the rate of charge trapping is governed by the environmental radiation dose rate and the grain size distribution of the analyzed aliquots (cf. Durcan et al., 2015).

3. Analytical Uncertainties, Models, and Interpretations

3.1. FT and (U–Th)/He Systems

Resolving complex thermal histories using FT and (U–Th)/He data is a function of analytical precision, our evolving understanding of variables that control FT annealing and He diffusion as well as our ability to accurately model these phenomena, and the questions posed. Reported FT dates utilize pooled, central, or

arithmetic means from large ($n = 20–100$) single-grain data sets (Galbraith & Laslett, 1993; Vermeesh, 2009). These dates may comprise single or multiple populations with different annealing kinetics. Track density and track length analysis (Gleadow et al., 1986) collectively provide a powerful constraint on a sample's thermal history. Primary sources of analytical uncertainty in FT thermochronometry are undersaturation or oversaturation of FTs due to low or high U concentrations, respectively, and analyst bias in track counting and track length measurements (e.g., Donelick et al., 2005; Ketcham et al., 2015). Ketcham, van der Beek, et al. (2018) provide a review of laboratory intercomparison of FT and (U–Th)/He dates and the sources of variability within each system and between the two systems.

Analytical uncertainties for individual (U–Th)/He dates are typically ~3–4% (not accounting for uncertainty in the alpha ejection correction). However, mean (U–Th)/He dates are commonly overdispersed, with standard deviations of the means exceeding analytical precision. Overdispersion is due to various factors that control He diffusivity and thus influence T_c and dates, including diffusion-domain length scale and cooling rate (Dodson, 1973; Farley, 2000; Jensen et al., 2018; Reiners & Farley, 2001), radiation damage accumulation (Baughman et al., 2017; Flowers et al., 2009; Gautheron et al., 2009; Guenthner et al., 2013, 2017; Shuster & Farley, 2009), grain chemistry (Gautheron, Barbarand, et al., 2013), and grain breakage (Brown et al., 2013). Additional variables that cause He data dispersion include implantation of parentless He by adjacent U–Th-rich phases (Gautheron et al., 2012; Murray et al., 2014; Spiegel et al., 2009), parent isotope zonation (Ault & Flowers, 2012; Farley et al., 2011; Gautheron, Barbarand, et al., 2013; Guenthner et al., 2013; Hourigan et al., 2005; Meesters & Dunai, 2002; Orme et al., 2015), microvoids or crystal defects (McDannell, Zeitler, Janes, et al., 2018; Zeitler et al., 2017), and inaccuracies in the alpha ejection correction factor owing to grain geometry or zoning (Farley et al., 1996, 2011; Glotzbach et al., 2019). Relationships between individual apatite, zircon, titanite, and hematite He dates and radiation damage, grain chemistry, and grain size can be leveraged to extract a more precise time-temperature history from rocks, as described in section 4.1.

3.2. Trapped Charge Thermochronometric Systems

OSL signals can be measured with <5% precision in the laboratory (Murray & Olley, 2002). Precision of TL and ESR analyses may be lower, owing to sensitivity changes throughout laboratory analyses and lack of automated instrumentation, respectively. However, the largest source of uncertainty for trapped charge dates is derived from the environmental dose rate, with uncertainty increasing with sample date (cf. equation (1)). Calculation of the environmental dose rate ($\dot{D}$) is especially challenging for trapped charge thermochronometry because the sample grain size distribution is lost during sample preparation (Durcan et al., 2015; Guralnik, Jain, et al., 2015), and approaches to overcome this issue are discussed in section 4.6.

Constraining the signal saturation level is essential for accurate modeling of trapped charge data (Wintle & Murray, 2006), with the possible exception of the Al center in ESR analysis. A laboratory-irradiated calibration curve is generated for every aliquot under investigation (Murray & Wintle, 2000, 2003). However, some studies suggest that laboratory measurements do not mimic natural observations (e.g., Chapot et al., 2012; Tsukamoto et al., 2018). The cause of this discrepancy is not known but may relate to the creation of new defects or changing charge trapping probabilities throughout laboratory measurement. Furthermore, the trapped charge in feldspar is affected by athermal detrapping thought to be caused by the tunneling of charge to recombination centers (i.e., anomalous fading; Visocekas et al., 1994; Wintle, 1973), resulting in an underestimation of trapped charge concentrations and an overestimation of cooling rates. Laboratory measurements of anomalous fading rates and trapped charge concentrations for samples in field saturation (i.e., where rates of charge trapping are in equilibrium with rates of athermal charge detrapping) match modeled signal saturation values to within ~10% (Huntley, 2006; Kars et al., 2008; King et al., 2018). Thus, it is unlikely that cooling rates will be reported for samples that are saturated, providing appropriate screening of signal saturation (e.g., Guralnik, Jain, et al., 2015; King, Herman, & Guralnik, 2016; King, Herman, Lambert, et al., 2016; Valla, Lowick, et al., 2016).

In common with all thermochronometric systems, thermal kinetic parameters estimated in the laboratory must be extrapolated over geological time, potentially introducing significant uncertainties. Various numerical models have been proposed to extract kinetic parameters from luminescence decay measured in response to isothermal holding (e.g., Guralnik, Jain, et al., 2015; Li & Li, 2012). However, to date, none of these models yield physically plausible values (Riedesel et al., 2018).

Despite this challenge, all currently employed models are validated against the known thermal history German Continental Deep Drilling Program (KTB) borehole using the experimental data of Guralnik, Jain, et al. (2015).

3.3. Thermal History Modeling of Thermochronometry Data

Thermochronometry results, reported as dates and saturation ratios, reflect a mineral's *integrated* thermal history. FT and (U–Th)/He data are modeled using computer-based numerical simulation programs, such as QTQt and HeFTy (Gallagher, 2012; Ketcham, 2005) or numerical codes that simultaneously invert thermochronometry data and additional thermal constraints, such as vitrinite reflectance data (Issler et al., 2005). Trapped charge data are modeled using Monte Carlo inversion approaches (Guralnik, Jain, et al., 2015; King, Herman, Lambert, et al., 2016). Simulations use kinetic models that describe how the FT, (U–Th)/He, and trapped charge systems respond as a function of temperature and time. These programs predict dates for a given time-temperature path or yield time-temperature paths that are consistent with thermochronometric data and independent geologic (e.g., unconformities and overburden estimates) and thermochronologic constraints. Owing to the subjectivity of imposed time-temperature constraints and choices in kinetic models and data visualization, thermal history models should be viewed as interpretations and transparency in model inputs and outputs is necessary (Flowers et al., 2015; Ketcham, van der Beek, et al., 2018). Simultaneous simulation of multiple low-temperature thermochronometers (i.e., AFT and apatite He or zircon He) has the potential to improve the reliability of thermal history information and/or provide intermethod calibration (e.g., Fox et al., 2019; Mackintosh et al., 2017; Winn et al., 2017).

Thermal histories derived from thermochronometry data are converted into burial and unroofing histories assuming appropriate geothermal gradients and surface temperatures. Surface temperature can be a critical parameter in some of these models, owing to the low T_c of select (U–Th)/He and trapped charge thermochronometric methods (Figure 1). In some trapped charge systems, for example, a sample that does not appear to be in athermal saturation may in fact be in thermal steady state, reflecting equilibrium with the surface temperature (Guralnik & Sohbati, 2019). Codes have been devised to convert thermochronometric dates to surface erosion or exhumation rates (e.g., Fox, Herman, et al., 2014; Willett & Brandon, 2013) and variable erosion rates (Biswas et al., 2018). Models such as Pecube (Braun, 2003; Braun et al., 2012) use a finite element method to solve the 3-D heat transport equation and predict thermal histories of rocks. Outputs from Pecube and other complementary models are compared with low-temperature and trapped charge thermochronometric data to constrain tectonic and erosion rates (Batt & Braun, 1997; Braun, 2003; Stüwe & Hintermüller, 2000; Whipp et al., 2009). Pecube is also coupled with landscape evolution models to infer surface processes (Braun et al., 2012; Herman et al., 2010; van der Beek et al., 2002). Midland Valley's Move kinematic modeling software has been linked with finite element advection-diffusion thermal models to predict thermochronometric dates from deformation-specific thermal histories (Lock & Willett, 2008; McQuarrie & Ehlers, 2015).

4. Advances in Thermochronometry Systematics

4.1. Radiation Damage and Chemistry Controls on (U–Th)/He and FT Thermochronometry

The recognition that radiation damage accumulation and crystal chemistry impact He mobility and FT annealing and, consequently, T_c and (U–Th)/He and FT dates has transformed our ability to apply these techniques to a range of Earth science problems. Damage to the crystal lattice develops from self-irradiation from the natural decay of isotopes of U, Th, and Sm by ionization and electronic excitation and heavy nuclide recoil during alpha decay, as well as spontaneous fission (e.g., Weber & Matzke, 1986). This discovery is rooted in materials science approaches to characterize apatite, zircon, and titanite using X-ray diffraction, infrared and Raman spectroscopy, in situ transmission electron microscopy analysis, and hardness analysis via nanoindentation (Beirau et al., 2018; Ginster et al., 2019; Hawthorne et al., 1991; Holland & Gottfried, 1955; Li et al., 2017; Lumpkin et al., 1991; Nasdala et al., 1995, 2004; Woodhead et al., 1991). Damage anneals at high temperatures and thus cumulative damage is a function of a sample's initial U, Th, and Sm content and its thermal history.

Radiation damage impacts He diffusivity in apatite (Flowers et al., 2009; Gautheron et al., 2009; Gerin et al., 2017; Recanati et al., 2017; Shuster et al., 2006; Shuster & Farley, 2009; Willett et al., 2017), titanite (Baughman et al., 2017; Guenthner et al., 2017), and zircon (Ginster et al., 2019; Guenthner et al., 2013;

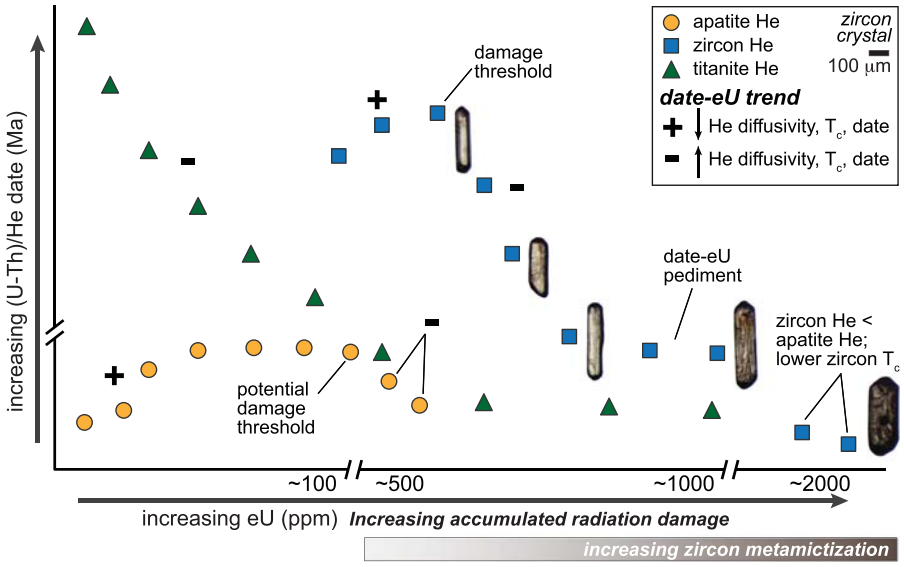

Figure 3. Patterns of relative individual apatite, zircon, and titanite (U–Th)/He (apatite He, zircon He, and titanite He, respectively) dates as a function of relative effective U concentration (eU), a proxy for radiation damage provided aliquots experience the same thermal history, for slowly cooled bedrock. Empirical data and damage-diffusivity models yield positive apatite He date-eU trends (Flowers et al., 2009; Gautheron et al., 2009), and recent work shows apatite He dates can decrease at high eU values (Recanati et al., 2017). Zircon He dates can yield positive and/or negative relationships with eU (Guenthner et al., 2013) and increasing visual metamictization (see zircon images) tracks with increased eU (Ault et al., 2018). Young, uniform zircon He dates at high eU (and thus high radiation damage) define a date-eU "pediment," reflecting residence at temperatures low enough to accumulate sufficient damage to yield low closure temperatures combined with subsequent heating followed by relatively rapid cooling across a range of closure temperature (T_c)—equivalent to apatite fission track and apatite He T_c (e.g., Ault et al., 2018; DeLucia et al., 2018; Johnson et al., 2017; Mackintosh et al., 2017). High eU zircon He dates can be younger than apatite He dates reflecting low T_c. Titanite He dates similarly yield an inverse date-eU relationship and older dates owing to lower eU values and higher T_c (Baughman et al., 2017; Guenthner et al., 2017).

Hurley, 1952; Reiners, 2005). Provided grains experience the same thermal history, the measured effective U concentration (eU, where eU is calculated as [U] + 0.234 * [Th] + 0.0046 * [Sm]; Gastil et al., 1967) corresponds to relative radiation damage. Figure 3 illustrates relationships between eU, radiation damage, and (U–Th)/He dates for apatite, zircon, and titanite in slowly cooled rocks. Radiation damage effects are manifest in samples with a span of eU values that experience slow cooling, which involves sufficient time for the He retentivities of variably damaged grains to diverge. In the apatite He system, increasing amounts of radiation damage from alpha recoil impede He diffusion, resulting in a higher T_c (Flowers et al., 2009; Gautheron et al., 2009; Shuster et al., 2006). The influence of radiation damage can yield a positive relationship between apatite He date and eU, depending on the thermal history (Figure 3; e.g., Ault et al., 2009; Flowers, 2009; Flowers & Kelley, 2011; Flowers et al., 2007; Gautheron, Barbarand, et al., 2013; Murray et al., 2016; Weisberg et al., 2018). Recent work by Recanati et al. (2017) reveals damage accumulation in high eU apatite reaches a threshold reflecting damage interconnection. This results in a decrease in He retentivity, T_c, and apatite He date, analogous to radiation-damaged zircon (Figure 3). Radiation damage may also influence FT annealing and thus FT dates (Hendriks & Redfield, 2005; McDannell et al., 2019). However, additional work is required to evaluate this and deconvolve complex relationships between alpha damage accumulation, FT annealing, and other parameters such as grain chemistry (McDannell et al., 2019).

The radiation damage effect is magnified in the zircon and titanite He systems owing to higher eU content (~100–10,000 ppm) and crystal self-healing properties requiring higher annealing temperatures than the apatite He system. In zircon, accumulating damage initially disrupts *c* axis-parallel diffusion pathways but reaches a threshold causing damaged portions of the crystal lattice to become interconnected and diffusivity to increase (Figure 3; Guenthner et al., 2013; Ketcham et al., 2013). Thus, low eU zircon grains yield low damage, decreased diffusivity, higher T_c, and older dates, provided that grains share a common thermal

history. High eU grains result in comparatively higher damage, increased diffusivity, lower T_c, and younger dates (Figure 3). Given a spread in eU values, individual grains from a single sample can develop positive and/or negative date-eU relationships depending on the thermal history (Figure 3; Guenthner et al., 2013). Titanite reaches a damage threshold causing increased He diffusivity at lower damage levels than zircon, potentially due to larger damage zones (Baughman et al., 2017; Ewing et al., 2000). However, titanite He dates record higher temperatures and older dates than zircon for the same thermal history, owing to lower eU (Figure 3; Baughman et al., 2017; Guenthner et al., 2017).

Apatite, zircon, and titanite date-eU relationships (e.g., Figure 3) are a powerful tool for reconstructing protracted thermal histories characteristic of ancient bedrock (Ault et al., 2009, 2013; Ault et al., 2018; Baughman & Flowers, 2018; DeLucia et al., 2018; Flowers, 2009; Flowers et al., 2007; Guenthner et al., 2013, 2014, 2017; Johnson et al., 2017; Mackintosh et al., 2017; Orme et al., 2016; Powell et al., 2016; Weisberg et al., 2018). Damage-diffusivity patterns can be predicted given a thermal history or inverted to derive a thermal history using HeFTy or QTQt. Current radiation damage-diffusivity models for apatite and zircon available to the larger community (Flowers et al., 2009; Gautheron et al., 2009; Gerin et al., 2017; Guenthner et al., 2013) are now used to resolve thermal histories from bedrock data sets that were previously considered uninterpretable. This is because crystals with variable eU and thus damage yield different temperature sensitivities, in essence providing multiple thermochronometers within one sample to improve model resolution. However, applying a damage-diffusivity model in HeFTy or QTQt implies that observed intrasample dispersion in bedrock samples can be explained by radiation damage or diffusion-domain length scale effects. Thermal history information should only be derived from bedrock samples that exhibit date-eU and/or date-grain size patterns, including uniform dates regardless of eU or grain size values (Flowers & Kelley, 2011). Samples yielding overdispersed (U–Th)/He dates uncorrelated with eU or grain size should either not be modeled or more information is required to understand the date scatter (Flowers & Kelley, 2011; Fox et al., 2019).

Crystal chemistry and lattice defects also influence FT annealing and He diffusion in apatite and ultimately the T_c in both FT and apatite He thermochronometry. For example, Cl substitution, as well as some cations (Fe, Mn, Na, Sr, and Mg) and rare Earth elements (La and Ce) that substitute for Ca, impact FT annealing resulting in an increase in the T_c (Barbarand et al., 2003; Carlson et al., 1999; Ketcham et al., 2007; Ravenhurst et al., 2003). Cl substitution also alters He mobility and increases the apatite He T_c (Djimbi et al., 2015; Gautheron, Barbarand, et al., 2013). Because current damage-diffusivity models assume alpha recoil damage anneals at temperatures analogous to FTs in fluorapatite, chemical variability also influences the annealing model in (U–Th)/He systems (Gautheron, Barbarand, et al., 2013). In addition, microvoids and strain dislocations in the apatite crystal lattice can either trap He or alter the He diffusion pathway, resulting in a higher T_c (McDannell, Zeitler, & Schneider, 2018; Zeitler et al., 2017). New work suggests alpha recoil damage anneals at higher temperatures compared to FTs in both apatite and zircon and damage-diffusivity models are being refined (Ault et al., 2018; Fox & Shuster, 2014; Garver & Kamp, 2002; Gerin et al., 2017; Ginster et al., 2019; Willett et al., 2017).

4.2. Atomistic Perspectives on He Diffusion

A realistic, atomic level description of He diffusion behavior in minerals is required to understand the role of chemical composition on diffusion, mechanisms modifying diffusivity by radiation damage, and noble gas diffusion in a range of mineral structures. He diffusion behavior in perfect crystal lattices has been investigated for different minerals at atomic to crystal scales using computing advances. In this approach, a crystal cell is constructed using density functional theory (DFT), or a computational quantum mechanical model that predicts material behavior. This method determines the ground energy state of the crystal by solving the Schrödinger equation for all bonds in the atomic structure. Different model codes can be applied to calculate He insertion sites, or interstitial positions, and energetic pathways in a crystal lattice (e.g., Reich et al., 2007). Most studies use the Vienna Ab Initio Simulation Package (Kresse & Furthmüller, 1996a, 1996b; Kresse & Hafner, 1993) for DFT calculations to optimize crystal lattice models for a perfect (i.e., damage free) crystal. Ab initio algorithms were first developed for the theoretical chemistry community but are now applied to geological problems.

To characterize the 3-D diffusion of He in minerals, the size of the cell used (i.e., number of atoms in the structure) is optimized to minimize the crystal relaxation effect due to the incorporation of a He

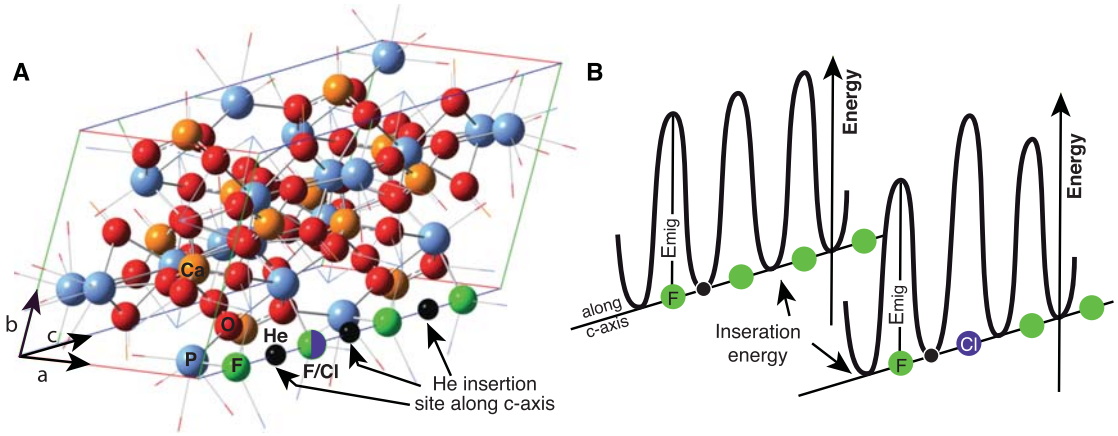

Figure 4. Example of apatite crystal framework for density functional theory calculations to explore He diffusion. (a) Apatite crystal cell with He insertion sites along the *c* axis. (b) Required migration energy (E_{mig}) for He diffusion through the crystal lattice two scenarios: F atoms only (back left) and when one Cl atom is substituted (front right). Modified from Djimbi et al. (2015).

atom. For example, an optimized apatite crystal model comprises 84 atoms representing a double apatite cell ($Ca_{10}((PO_4)_6F_2)_2$; Djimbi et al., 2015). The minimum migration energy between He insertion sites is obtained using the nudged elastic band method (Jónsson et al., 1998; Mills et al., 1995). Figure 4 shows He diffusion pathways in apatite with associated insertion types along the *c* axis (Djimbi et al., 2015). A 3-characterization of the apatite He diffusion coefficient including the activation energy (E_a) and the frequency factor (D_0) is calculated using a Monte Carlo random walk, using all insertion and migration energies along the *a*, *b*, and *c* crystal axes (Figure 4; Djimbi et al., 2015; Gautheron & Tassan-Got, 2010). Calculation details for a damage-free apatite crystal structure and associated 3-D He diffusion coefficients at 0 K are found in Saadoune and De Leeuw (2009) and Djimbi et al. (2015). Computed 3-D He diffusion in apatite and hematite mirrors experimental data on real specimens, supporting the veracity and applicability of this theoretical approach (Balout et al., 2017; Djimbi et al., 2015).

DFT calculations with large numbers of atoms (>200–2,000) cannot be performed at present owing to computational limitations, thus limiting the application to alpha recoil damage and quantifying the damage-induced trapping energy of He diffusion. However, atomic investigation of He diffusion in zircon yields non-retentive results (Bengtson et al., 2012; Reich et al., 2007; Saadoune et al., 2009; Saadoune & De Leeuw, 2009), which differs from retentive behavior in natural zircon (e.g., Reiners et al., 2002; Reiners et al., 2004b). This comparison reveals that processes such as the creation of radiation damage-induced traps significantly alter He diffusion in zircon. In addition, the impact of chemical substitution or single vacancies can be investigated using DFT (Djimbi et al., 2015; Gerin et al., 2017; Saadoune & De Leeuw, 2009). Thus, atomistic calculations of He diffusion in perfect crystal lattices identify parameters that alter diffusion, providing new perspectives when diffusion coefficient measurements are not available or difficult to perform.

4.3. Double and Triple Dating With U–Pb, FT, and (U–Th)/He Systems

FT and (U–Th)/He thermochronometry are now routinely applied to detrital minerals (e.g., Carter, 2019, and references therein). Detrital apatite and/or zircon crystals can trace sediment sources in orogenic systems (Bernet & Garver, 2005; Glotzbach et al., 2011; Horton et al., 2010; Stock et al., 2006), quantify the basin burial and exhumation phases (Guenthner et al., 2015; Ketcham, Mora, & Parra, 2018; Schwartz et al., 2017), and track the source to sink evolution of sedimentary basins (Calzolari et al., 2016; Carter, 2019; Tranel et al., 2011; Zattin et al., 2014). Detrital thermochronometry from catchments also informs the timing and tempo of source area exhumation related to tectonism (e.g., Bernet et al., 2006; Bernet et al., 2009; Espurt et al., 2010; Filleaudeau et al., 2012; Gautheron, Espurt, et al., 2013), glacial processes (e.g., Ehlers et al., 2015; Enkelmann & Ehlers, 2015), or the interplay between the two.

FT and (U–Th)/He data can be acquired on crystals previously analyzed for U–Pb geochronology, aided by analytical advances of laser ablation and noble gas mass spectrometry analyses. This approach includes "double" U–Pb and FT or He analysis of apatite or zircon (Campbell et al., 2005; Carter & Moss, 1999;

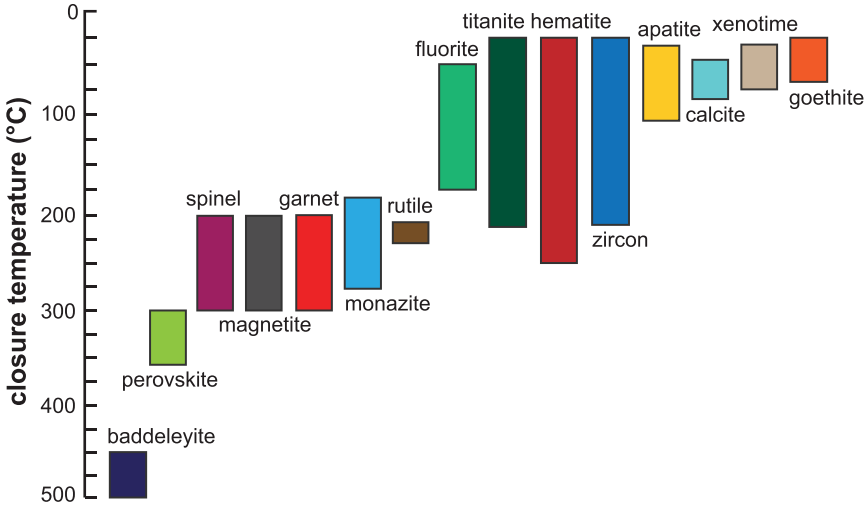

Figure 5. T_c ranges, assuming a 10 °C/Myr cooling rate, for a variety of conventional and new (U–Th)/He thermochronometry systems. See text in section 4.4 for associated references.

Fosdick et al., 2015; Lease, Haeussler, & O'Sullivan, 2016; Odlum & Stockli, 2019; Rahl et al., 2003; Reiners et al., 2005; Ternois et al., 2019; Thomson et al., 2017) or U–Pb, FT, and (U–Th)/He "triple" dating (e.g., Carrapa et al., 2009; Danišík, 2019; Danišík et al., 2010). Integration of data from two or more thermochronometric systems with different temperature sensitivities in the same mineral permits a more detailed reconstruction of the thermal history in these settings. These detailed time-temperature histories allow researchers to discriminate between different source regions, constrain protracted postdeposition burial histories, or capture the source to sink dynamics including sediment recycling. The ability to more fully characterize a basin's thermal evolution also has implications for georesource exploration, as temperature constraints through time are critical for understanding the maturation, expulsion, and trapping of hydrocarbons.

4.4. New (U–Th)/He Thermochronometers

Apatite, zircon, and titanite He continue to be the most widely applied (U–Th)/He thermochronometers, but new mineral systems have been developed in the past three decades that extend the application of these techniques to tackle new research questions (Figure 5). For example, primary and secondary Fe oxides are amenable to (U–Th)/He dating. Hematite He thermochronometry has been successfully applied to constrain deformation, hydrothermal, and diagenesis histories (Ault, Reiners, et al., 2015; Ault et al., 2016; Calzolari et al., 2018; Evenson et al., 2014; Farley & Flowers, 2012; Farley & McKeon, 2015; McDermott et al., 2017; Moser et al., 2017; Wernicke & Lippolt, 1993, 1994). Hematite occurs as polycrystalline aggregates and exhibits polydomain He diffusion behavior (Evenson et al., 2014; Farley, 2018; Farley & Flowers, 2012). Individual crystallites are the He diffusion domains and the hematite He T_c, which is ~25–250 °C (10 °C/Myr cooling rate), increases with increasing domain (grain) size (Balout et al., 2017; Evenson et al., 2014; Farley, 2018; Farley & Flowers, 2012; Jensen et al., 2018). Goethite He has a T_c ~25–60 °C with possible He loss at surface conditions and is used to date supergene alteration and deep weathering profiles (Deng et al., 2017; Heim et al., 2006; Miller et al., 2017; Monteiro et al., 2014; Riffel et al., 2016; Shuster, Vasconcelos, et al., 2005; Shuster et al., 2012; Vasconcelos et al., 2013). Magnetite He thermochronometry is used to date intermediate to mafic volcanic rocks (Blackburn et al., 2007) and serpentinization (Cooperdock & Stockli, 2016). This system has a T_c of ~250 ± 50 °C (Blackburn et al., 2007), although components of ^{4}He diffusion data suggest potential multidomain diffusion behavior.

A variety of accessory phases in igneous and metamorphic rocks can serve as (U–Th)/He thermochronometers. Baddeleyite, for example, has a T_c ~450–500 °C (Metcalf & Flowers, 2013). Perovskite has a T_c >300 °C and has been used to date kimberlite emplacement (Stanley & Flowers, 2016). Rutile has a T_c of ~220–235 °C and has the potential to quantify midcrustal exhumation when paired with well-characterized petrologic and geochemical context (Stockli et al., 2007; Wolfe, 2009). Garnet, common in metamorphic

rocks, has a T_c of ~200–300 °C (Seman et al., 2014), although ^{3}He diffusion experiments using nuclear reaction analysis yield T_c >450 °C (Roselieb et al., 2006). Spinel, a primary phase in mantle peridotites, has a T_c of ~200–300 °C based on empirical constraints comparing spinel He and ZFT results (Cooperdock & Stockli, 2018). This technique may constrain the timing of oceanic crust formation and mantle exhumation. Monazite, common in peraluminous granites and pelitic rocks, has a T_c of ~180–280 °C that is dependent on chemical composition (Boyce et al., 2005; Farley, 2007). Fluorite He thermochronometry has a T_c of ~50–170 °C, and this tool has potential for investigating ore deposits and hydrothermal systems (Evans, Wilson, et al., 2005; Wolff et al., 2015; Wolff et al., 2016). Xenotime yields a T_c of ~35–75 °C (Anderson et al., 2019; Farley, 2007; Farley & Stockli, 2002).

In addition to detrital zircon and apatite He thermochronometry, calcite and bioapatite are useful (U–Th)/He tools for reconstructing the thermal history of sedimentary rocks. Calcite, a constituent of limestone, mudstone, and fossils, has a T_c of ~40–80 °C and common (initial) ^{4}He issues are mitigated by analyzing samples that have experienced significant postdepositional reheating (Copeland et al., 2007; Copeland et al., 2015; Cros et al., 2014). Conodont microfossils (bioapatite) are a target for (U–Th)/He analysis applied to carbonates and shales and the T_c mirrors that of the traditional apatite system (~60 °C; Landman et al., 2016; Peppe & Reiners, 2007). Ongoing research aimed at quantifying the diffusion kinetics of each of the aforementioned systems, coupled with textural and geochemical information and data comparisons with established low-temperature thermochronometry systems, will continue to expand the utility of new (U–Th)/He thermochronometers.

4.5. ^{4}He/^{3}He Thermochronometry: Grain-Specific Diffusion Kinetics and Thermal Histories

Recent and ongoing development of ^{4}He/^{3}He thermochronometry permits recovery of aliquot-specific diffusion kinetics and a sample's detailed thermal history (Farley, 2018; Farley & Flowers, 2012; Fox, McKeon, & Shuster, 2014; Shuster et al., 2004; Shuster & Farley, 2004, 2005; Shuster, Vasconcelos, et al., 2005). This approach quantifies the distribution of ^{4}He in a single crystal or polycrystalline aggregate. Stepwise degassing of an aliquot containing synthetic, uniformly distributed, proton-induced ^{3}He constrains the ^{4}He distribution, which is a function of the initial U and Th distribution (Farley et al., 2010) and the thermal history. Combined with additional geochronological and thermochronological (i.e., the (U–Th)/He date) or geologic information, the ^{4}He concentration profile can be used to more narrowly constrain a sample's thermal history. The ^{3}He Arrhenius relationship yields information about the aliquot's diffusion domain(s) and diffusion kinetics (e.g., Farley, 2018).

The apatite ^{4}He/^{3}He method can resolve cooling histories down to ~20–30 °C (Shuster & Farley, 2004). Owing to its low temperature sensitivity, this technique has been used to quantify the timing and tempo of glacial erosion and related relief generation (Christeleit et al., 2017; Shuster, Ehlers, et al., 2005; Shuster et al., 2011; Valla et al., 2011), exhumation of mountain ranges (Tremblay et al., 2015; Valla et al., 2012), and canyon incision including carving of Grand Canyon (Flowers & Farley, 2012; Fox et al., 2017; Schildgen et al., 2010; Winn et al., 2017). Zircon ^{4}He/^{3}He thermochronometry has been applied to the fast-cooled Fish Canyon Tuff zircon standard and zircon crystals from the Sierra Nevada batholith in the vicinity of the Little Devil's Postpile intrusion (Tripathy-Lang et al., 2015). This tool has also been used to constrain the diffusion kinetics and thermal history of hematite (Evenson et al., 2014; Farley, 2018; Farley & Flowers, 2012; Farley & McKeon, 2015), goethite (Allard et al., 2018; Deng et al., 2017; Shuster, Vasconcelos, et al., 2005; Vasconcelos et al., 2013), and Mn oxides (Garcia et al., 2017).

4.6. Measurement and Modeling Advances in Trapped Charge Thermochronometry

The recent development of trapped charge thermochronometry means that methods and kinetic and thermal models are rapidly improving. Advances center on numerical models that describe the equilibrium between charge trapping and thermal and athermal charge detrapping (e.g., Biswas et al., 2018; Brown et al., 2017; Guralnik, Jain, et al., 2015), measurement protocols (Guralnik, Jain, et al., 2015; King, Herman, Lambert, et al., 2016), and method validation against samples of known thermal history (Guralnik, Jain, et al., 2015). Ongoing development of ESR thermochronometry (Fang et al., 2018; Grün et al., 1999) may overcome the limitation of signal saturation. ESR signals saturate over timescales of up to ~2 Myr (Rink, 1997), potentially extending the applicability of trapped charge thermochronometry methods to more environmental settings (e.g., Bartz et al., 2018) and longer timescales.

A sample's environmental radiation dose rate determines the rate of signal accumulation (i.e., charge trapping) for trapped charge thermochronometric systems. For samples in thermal steady state within the partial retention zone, dose rate exerts only a logarithmic control on the trapped charge concentration, and thus has a low impact on the palaeotemperature determined (Guralnik et al., 2013; Guralnik, Jain, et al., 2015). However, for samples that record cooling, the effect of dose rate will vary from linear to logarithmic as sample saturation (steady state) is approached (Guralnik et al., 2013). This means that, in rapidly cooled settings, a change in dose rate of 30% results in an equivalent shift in the calculated cooling rate (King, Herman, Lambert, et al., 2016).

Grain size exerts a significant control on environmental dose rate, but grain size information is commonly lost during the sample preparation by hand crushing. Grain size distributions can be quantified via thin-section petrography (Guralnik, Jain, et al., 2015). Consideration of end member and/ average observed grain size distributions can provide bounds on dose rate calculations (Guralnik, Jain, et al., 2015) and Monte Carlo modeling can evaluate the impact of heterogeneous grain size distributions on the dose rate of minerals extracted from bedrock (Fang et al., 2018). Accurate estimation of the grain size distribution and chemical composition of K-feldspar are important owing to an internal dose rate component, which can cause a significant change in the total dose rate (Fang et al., 2018). K positioning within the K-feldspar lattice contributes a beta dose, which may increase with increasing mineral size (Buylaert et al., 2018).

Trapped charge systems yield multiple luminescence signals with different optical and thermal stabilities, which can be conveniently measured within the same analytical run. This means that multiple constraints on the cooling history of a single sample are obtained, overcoming potential uncertainties associated with combining data from different thermochronometric systems. For example, King, Herman, Lambert, et al. (2016) demonstrated the utility of multiple OSL signals to derive high-precision cooling and thus exhumation histories in geological settings. Combining four infrared stimulated luminescence signals measured from K-feldspar, with T_c of ~30–90 °C, permits inversion of a more precise cooling history than from single-system inversion (King, Herman, Lambert, et al., 2016). Biswas et al. (2018) developed this approach for TL thermochronometry, measuring a continuum of charge with different thermal stabilities and 10 different signals to constrain cooling rate variations. In addition, a new algorithm now allows for inversion of multiple trapped charge data sets to constrain cooling and thus erosion rate variations (Biswas et al., 2018). Model outputs are more robust, because physically impossible cooling histories are rejected from the inversion and a time series of cooling rate changes are generated. Following the success of these studies, similar approaches have been applied to samples from other rapidly exhuming terranes (Herman & King, 2018).

5. Low-Temperature Thermochronometry Applications

New applications of low-temperature thermochronometry utilize the aforementioned method advances in the FT, (U–Th)/He, and trapped charge systems, as well as numerical modeling approaches. In this section, we highlight efforts to push the boundaries of these techniques to address Earth science problems including landscape evolution, surface-mantle connections in deep time, fault zone processes, and weathering. We emphasize that these examples represent only a fraction of the innovative applications of low-temperature thermochronometry. Figure 6 depicts the diverse science questions that are currently being investigated across continents worldwide using FT, (U–Th)/He, and trapped charge thermochronometry.

5.1. Landscape Evolution

Understanding the tempo of erosive processes that sculpt Earth's surface is at the core of geomorphology and Earth science more broadly. This information has fueled debates into how passive margins evolve via scarp retreat, sediment dispersal and routing from source to sink, and relationships between tectonics and climate. Bedrock and detrital low-temperature thermochronometry, coupled with other chronologic, geologic, and geophysical insights, inform these debates (Figure 6). For example, thermal histories derived from AFT and apatite He dating characterize the topographic evolution of passive continental margins and rates of escarpment retreat associated with supercontinent breakup (Figure 6). Low-temperature thermochronometry provides new perspectives on the relative importance of lithospheric flexure, isostasy, and structural inheritance controlling escarpment development and degradation. Examples of FT and (U–Th)/He thermochronometry applications to passive margins include southern Africa (Brown et al., 1990, 2000; Brown et al.,

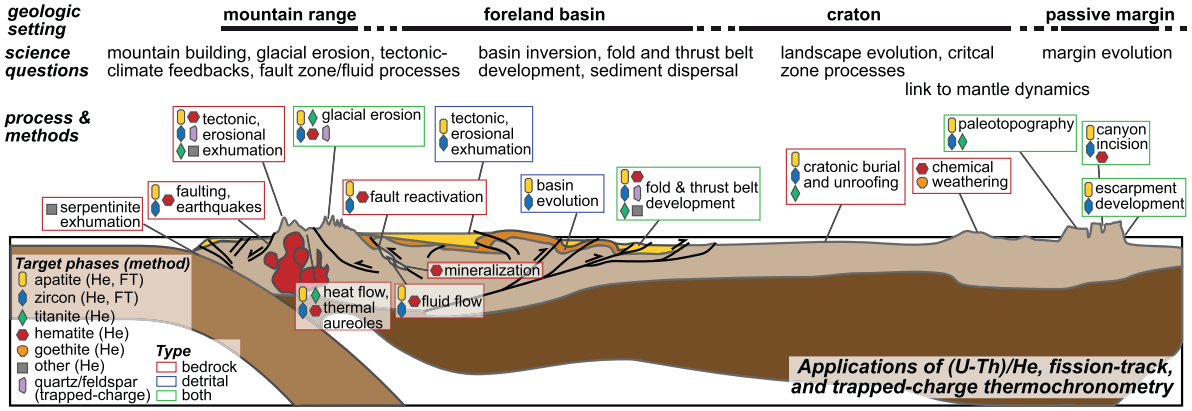

Figure 6. Schematic cross section of a continent illustrating the application of fission track, (U–Th)/He and trapped charge thermochronometry to address diverse Earth science questions. These methods, applied to target phases from both bedrock and detrital systems, are used to understand process and address science questions in a range of geologic settings.

2002; Cockburn et al., 2000; Flowers & Schoene, 2010; Gallagher & Brown, 1999; Kounov et al., 2009; Tinker et al., 2008; Wildman et al., 2016), Fennoscandia (Hendriks & Redfield, 2005), Brazil (Gallagher et al., 1994; Hackspacher et al., 2004), and Baffin Island and West Greenland (Japsen et al., 2009; Jess et al., 2018; Jess et al., 2019).

In active orogenic settings, landscape evolution is driven by the interplay between surface uplift via tectonics and climate-modulated surface processes. FT, (U–Th)/He, and $^{4}He/^{3}He$ thermochronometry of basement rocks, sedimentary rocks, and sediments quantify the timing and tempo of erosional and tectonic exhumation in orogens (Figure 6). In mountain ranges that develop in convergent orogens, these tools lay the foundation to investigate relationships between rapid erosion and surface uplift (e.g., Avdeev & Niemi, 2011; McDermott et al., 2019; Spencer et al., 2019; and many others), propagation of deformation into the foreland (e.g., Gautheron, Espurt, et al., 2013; Lease, Ehlers, & Enkelmann, 2016; Thomson et al., 2017), rapid Quaternary exhumation (Blythe et al., 2007; Shuster et al., 2011; Valla, Rahn, et al., 2016; Yang et al., 2018), and Quaternary climate influences on sediment storage and erosion (e.g., Lang et al., 2018).

Conventional low-temperature thermochronometers traditionally cannot precisely resolve *variations* in Quaternary erosion rates. Trapped charge thermochronometry is able to span this temporal gap and has been successfully applied to understand the Quaternary evolution of the Southern Alps of New Zealand (Herman et al., 2010), the Western Arunachal Himalaya (De Sarkar et al., 2013), the Eastern Himalayan syntaxis (King, Herman, & Guralnik, 2016), and the Japanese Alps (Herman & King, 2018). For example, Figure 7 illustrates that the combination of OSL thermochronometry, together with higher temperature thermochronometric systems, reveals an acceleration in exhumation rates from <1 to >6 mm/year over the past ~1 Myr at Namche Barwa in the eastern Himalayan syntaxis (King, Herman, & Guralnik, 2016). More recent work using TL thermochronometry, which has a lower T_c and thus records more recent changes in rock cooling and exhumation, suggests exhumation rates may have exceeded ~10 mm/yr at ~40 ka, followed by rates of ~2–8 mm/yr over the past 20 ka (Biswas et al., 2018). Regardless of method, trapped charge-derived erosion rates are greater than those inferred from higher-temperature thermochronometry systems. Based on their results, King, Herman, and Guralnik (2016) suggest that tectonics is the key control on the location of rapid exhumation in this region. Future research directions coupling trapped charge with FT and (U–Th)/He thermochronometry, as well as comparing $^{4}He/^{3}He$ and trapped charge data that have similar T_c, will help decipher variations in exhumation rate and thus evaluate the relative roles of tectonics and surface processes in orogenic systems.

5.2. Deep Time Thermochronometry

The ability to reconstruct low-temperature thermal histories spanning billions of years, known as deep time thermochronometry (e.g., DeLucia et al., 2018; Flowers, 2009; Flowers et al., 2006), has implications for the recognition of dynamic topography in the rock record, identifying if and how surface processes are coupled

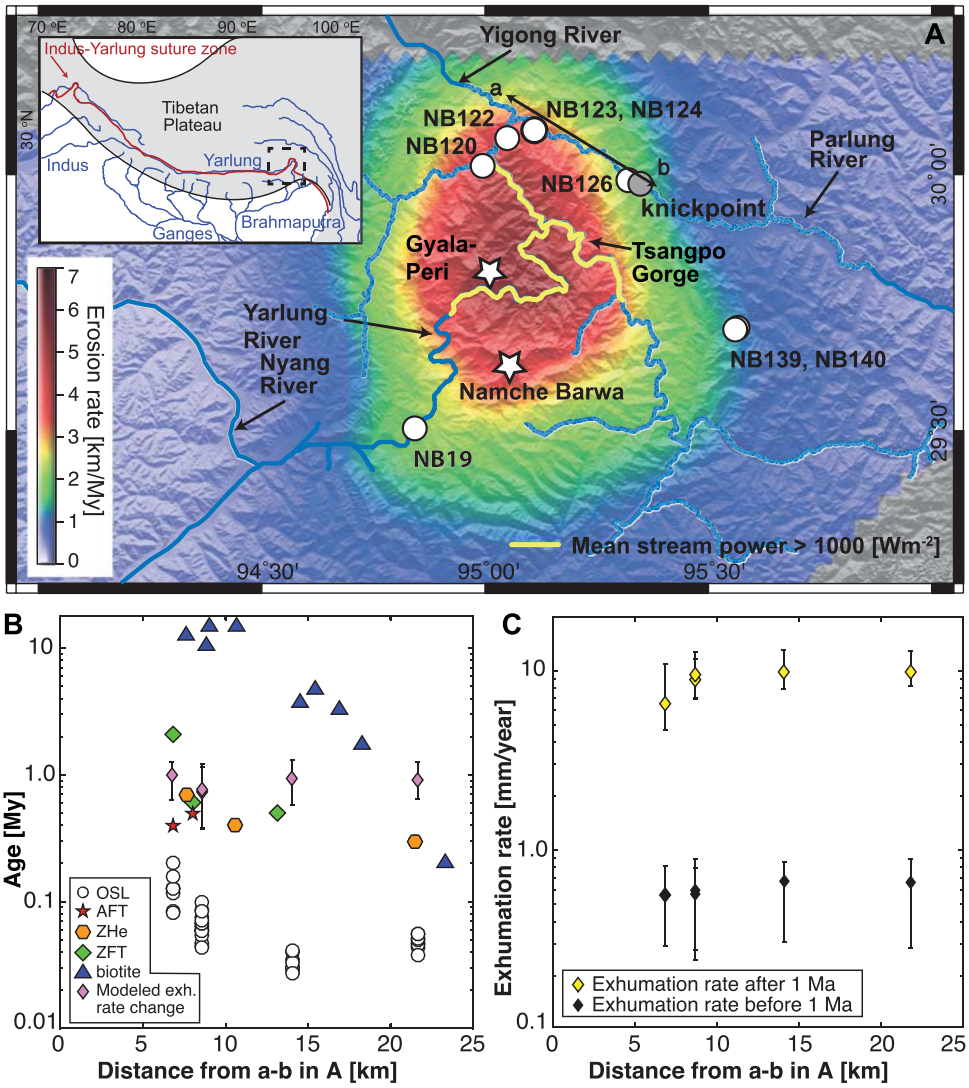

Figure 7. Example of combined trapped charge and low-temperature thermochronometry data from eastern Himalayan syntaxis, Namche Barwa, modified from King, Herman, Lambert, et al. (2016). (a) Erosion rates over 2 million years derived from apatite fission track (AFT) and zircon fission track (ZFT), zircon (U–Th)/He (ZHe), and biotite $^{40}Ar/^{39}Ar$ thermochronometry from prior work. Regions of high stream power (yellow) previously identified as coincident with high exhumation rates; circles denote optically stimulated luminescence (OSL) sample locations of King, Herman, Guralnik (2016). (b) Multi-OSL and low-temperature thermochronometry results, as well as modeled exhumation (exh.) rate changes (pink diamonds) from these data, as a function of distance along A-B line in (a). (c) Data comparison and inversion reveals exhumation rates increased an order of magnitude in the last 1 Ma.

or decoupled from deep-seated (mantle) processes through geologic time, understanding how supercontinent cycles shape Earth's landscape, and documentation of feedbacks between weathering, erosion, and global paleoenvironmental change. AFT thermochronometry can decipher long-term thermal histories of ancient rocks exposed in cratons (e.g., Feinstein et al., 2009; Gleadow et al., 2002; Kohn et al., 2002; Kohn et al., 2005; McDannell et al., 2019). In addition, the low-temperature sensitivity and radiation damage influences on the apatite He system make it ideal for quantifying the timing, magnitude, and extent of low (<2 km) amplitude deposition and denudation episodes in cratonic regions, even when the deposited rocks have been completely eroded from the rock record. Apatite He date-eU relationships inform long-term thermal histories linked to these surface processes (e.g., Ault et al., 2009, 2013; Ault, Flowers, & Bowring, 2015; Flowers, 2009; Flowers et al., 2012; Guenthner et al., 2017; Mackintosh et al., 2017). Figure 8 presents apatite He, AFT, and zircon He data patterns from across the

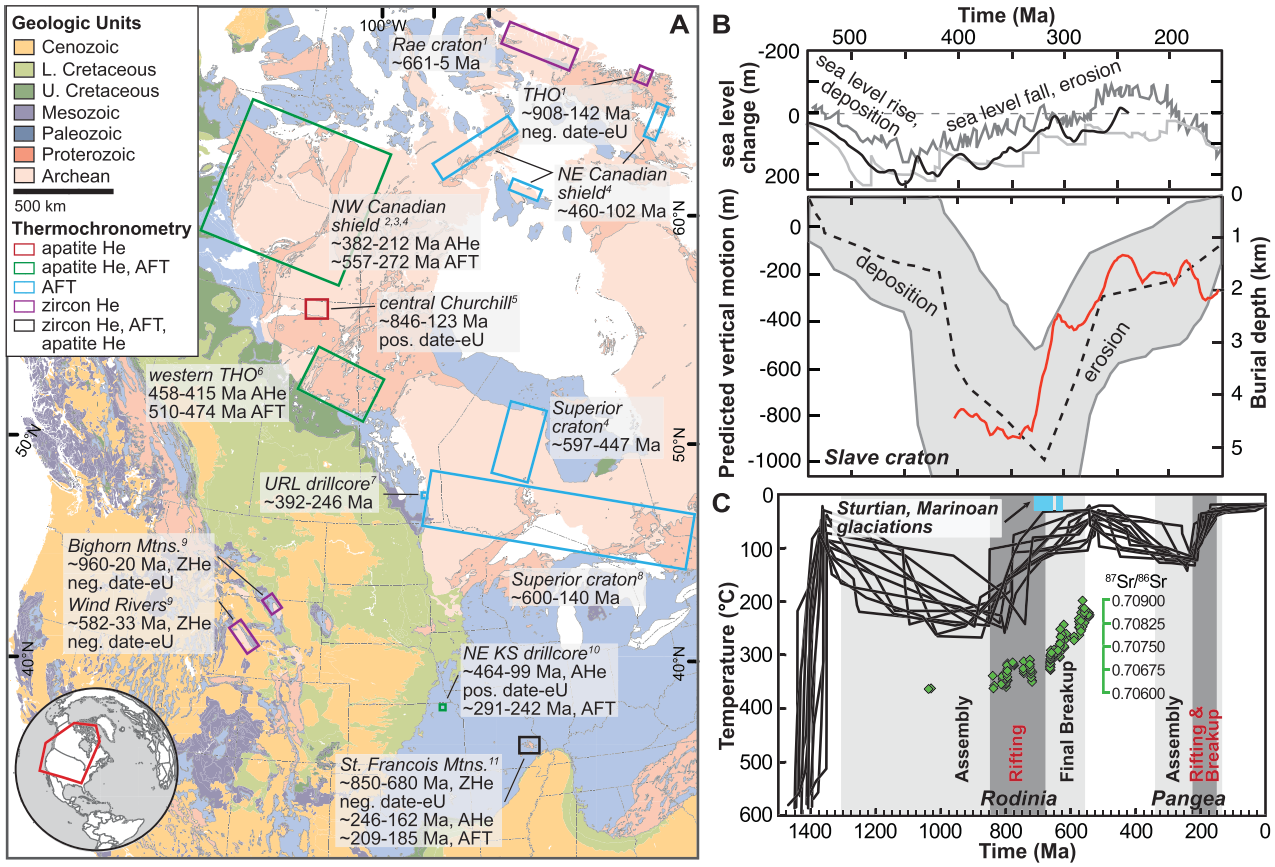

Figure 8. Application of deep time thermochronometry to cratonic North America. (a) Simplified geologic map showing results of apatite and zircon (U–Th)/He (He), fission track (AFT and ZFT) thermochronometry studies. 1: Ault et al. (2018); 2 and 3: Ault et al. (2009, 2013); 4: McDannell et al. (2019); 5: Flowers (2009); 6: Flowers et al. (2012); 7: Feinstein et al. (2009); 8: Kohn et al. (2005); 9: Orme et al. (2016); 10: Flowers and Kelley (2011); 11: DeLucia et al. (2018). (b) Example of thermochronometry-derived thermal history compared to a model of dynamic topography and sea level curves, modified from Flowers et al. (2012). Upper panel: Paleozoic-early Mesozoic sea level curve reconstructions relative to modern sea level from Haq and Al-Qahtani (2005; black line), Haq and Schutter (2008; dark gray line), and Vail et al. (1977; light gray line). Lower panel: Predicted Slave craton vertical motion history (red line, left *y* axis) relative to mean global dynamic topography from a mantle convection model (Zhang et al., 2012), compared with thermal history (gray-shaded region) derived from apatite He data (Ault et al., 2009) and damage-diffusivity model of Flowers et al. (2009). Thermal history converted to burial history (right *y* axis) assuming a 0 °C surface temperature and 25 °C/km geotherm. Slave craton surface history compares favorably with modeled pattern of subduction-related dynamic topography in the Paleozoic-Mesozoic and is out of phase with sea level change, suggesting the former drives subsidence in the continental interior. (c) Thermochronometry data reported in (a) constrain two supercontinent cycles. Time-temperature paths from zircon He, AFT, and apatite He data from the Ozark Plateau (DeLucia et al., 2018). Timing of Rodinia and Pangea supercontinent amalgamation and breakup (from Whitmeyer & Karlstrom, 2007), Sr isotope data (Cox et al., 2016), and global glaciations shown. Modified from DeLucia et al. (2018).

interior of continental North America. Apatite He and AFT data reveal phases of substantial burial (1–4 km), unroofing, and elevation change long after initial cratonic stabilization (Figures 8a and 8b; Ault et al., 2009, 2013; Feinstein et al., 2009; Flowers, 2009; Flowers et al., 2012; Flowers & Kelley, 2011; Kohn et al., 2005; McDannell et al., 2019). The long wavelength (>1,000 km) nature of this elevation change is out of phase with sea level change (Figure 8b). Elevation change distal from plate boundaries and the lack of significant associated crustal deformation suggest dynamic topography as a probable cause (Figure 8b; Ault et al., 2013; Flowers et al., 2012; Zhang et al., 2012).

Recent work extends the low-temperature thermal history of cratonic North American into deeper geologic time (Figures 8a and 8c; Ault et al., 2018; DeLucia et al., 2018; McDannell, Zeitler, & Schneider, 2018; Orme et al., 2016). For example, zircon He thermochronometry date-eU patterns from the North American mid-continent cratonic basement reveal ~850- to 680-Ma cooling and exhumation associated with the development of the Great Unconformity, an erosion surface representing ~100–1,000 Ma of missing geologic time between Precambrian and Phanerozoic rocks (DeLucia et al., 2018). In addition, ^{40}Ar–^{39}Ar multidiffusion

data suggest prolonged residence in the midcrust through the Proterozoic and exhumation initiating at ~1.0 Ga related to the development of the Midcontinent Rift System (McDannell, Zeitler, & Schneider, 2018). Collectively, low-temperature thermochronometry from across the North American craton reveals phases of burial and subsequent unroofing associated with processes operative during two supercontinent cycles, Rodinia and Pangea, raising possible links between cratonic exhumation and dramatic, possibly global, paleoenvironmental change (Figure 8c; Ault et al., 2013; DeLucia et al., 2018; Flowers et al., 2012).

FT and (U–Th)/He thermochronometry are also valuable tools for linking southern Africa's unique surface history with mantle processes. Southern Africa, a continental shield residing at a mean elevation of ~1 km (Nyblade & Robinson, 1994) is widely cited as an example of dynamically supported topography (Gurnis et al., 2000; Lithgow-Bertelloni & Silver, 1998). Combined AFT and apatite He data from Archean rocks of the Kaapvaal craton and off-craton Paleozoic mobile belts suggests Early Cretaceous cooling and unroofing focused on craton margins with comparatively limited erosion in the cratonic interior (Wildman et al., 2017). Apatite He thermochronometry from kimberlites document a Cretaceous eastward wave of erosion and imply disparate lithospheric responses to deep mantle processes on and off craton (Stanley et al., 2015). Off-craton kimberlite apatite He thermochronometry data reveals Cenozoic unroofing, concomitant with increasing temperature and metasomatism in the mantle, which may be connected with surface uplift (Stanley et al., 2013). Researchers are now extending the low-temperature thermal history of southern Africa into deep time, using zircon and titanite date-eU patterns to document Proterozoic burial across the Kaapvaal craton for which the geologic evidence has been erased (Baughman & Flowers, 2018) and Pan-African orogenesis in the Zimbabwe craton (Mackintosh et al., 2017). Collectively, these studies highlight the potential of FT and (U–Th)/He thermochronometry to decipher cryptic thermal histories in cratons and connect surface processes with geodynamics in deep geologic time.

5.3. Fault Zone Processes: Earthquakes, Creep, and Geofluid Flow

Documenting fault zone behavior in space and time is integral for understanding the mechanical, chemical, and thermal conditions of crustal deformation and illuminating dynamic interactions between tectonics and Earth surface processes (Huntington & Klepeis, 2018). Fault activity can be inferred from variations in bedrock FT and (U–Th)/He thermochronometry dates and/or extrapolated cooling rates (e.g., Abbey & Niemi, 2018; Bidgoli et al., 2015; Brady, 2002; Carter et al., 2006; Clark et al., 2005; Colgan et al., 2008; Collett et al., 2019; Curry et al., 2016; d'Alessio & Williams, 2007; Ehlers & Farley, 2003; Johnstone & Colgan, 2018; McDermott et al., 2013; Stockli et al., 2000; Tagami, 2012; Wells et al., 2000).

Exhumed fault zones provide a target for dating deformation and a bridge to geophysical and geochemical observations of deformation processes (e.g., Rowe & Griffith, 2015, and references therein). Radioisotopic methods used to place direct temporal constraints on fault slip include $^{40}Ar/^{39}Ar$ and K–Ar dating of neoformed, fault gouge clay (Duvall et al., 2011; Fitz-Diaz & van der Pluijm, 2013; Haines & van der Pluijm, 2008; van der Pluijm et al., 2001; van der Pluijm et al., 2006; Vrolijk & van der Pluijm, 1999; Zwingmann & Mancktelow, 2004), muscovite (Pachell & Evans, 2002), and pseudotachylytes (Cosca et al., 2005; Di Vincenzo et al., 2013; Magloughlin et al., 2001; Reimold et al., 1990; Sherlock et al., 2004; Sherlock et al., 2008; Sherlock et al., 2009); and U–Pb and U–Th dating of carbonate and opal (Nuriel et al., 2011, 2012, 2013, 2017, 2019; Pagel et al., 2018; Rittner & Muller, 2011; Roberts & Walker, 2016; Uysal et al., 2007; Verhaert et al., 2003; Watanabe et al., 2008).

Minerals on or adjacent to fault surfaces record strain, friction-generated heat, and fluid circulation associated with fault slip. Low-temperature thermochronometry of these phases offers the potential to document the timing, temperature, and nature of brittle fault zone processes, provided that fault-specific thermal signatures can be isolated from the ambient thermal history. For example, ZFT annealing kinetics respond to short duration, high-temperature thermal pulses (Murakami, Yamada, & Tagami, 2006) due to frictional (shear) heating (Ben-Zion & Sammis, 2013), asperity flash heating (Rice, 2006), or melting (Sibson, 1975). ZFT thermochronometry has been used to identify paleoearthquakes that generate pseudotachylytes or shear heating (Murakami, Košler, et al., 2006; Murakami & Tagami, 2004; Tagami, 2005, 2012, 2019; Tagami & Murakami, 2007). Friction-generated heat has also been detected using zircon He thermochronometry (Maino et al., 2015) and ferrimagnetic resonance signals via ESR (Fukuchi et al., 2007). Luminescence and ESR signals of quartz and feldspar can be reset within fault gouge (Ding & Lai, 1997; Fukuchi, 2001; Lee & Yang, 2007; Mukul et al., 2007; Singhvi et al., 1994; Spencer et al., 2012), although it is challenging to

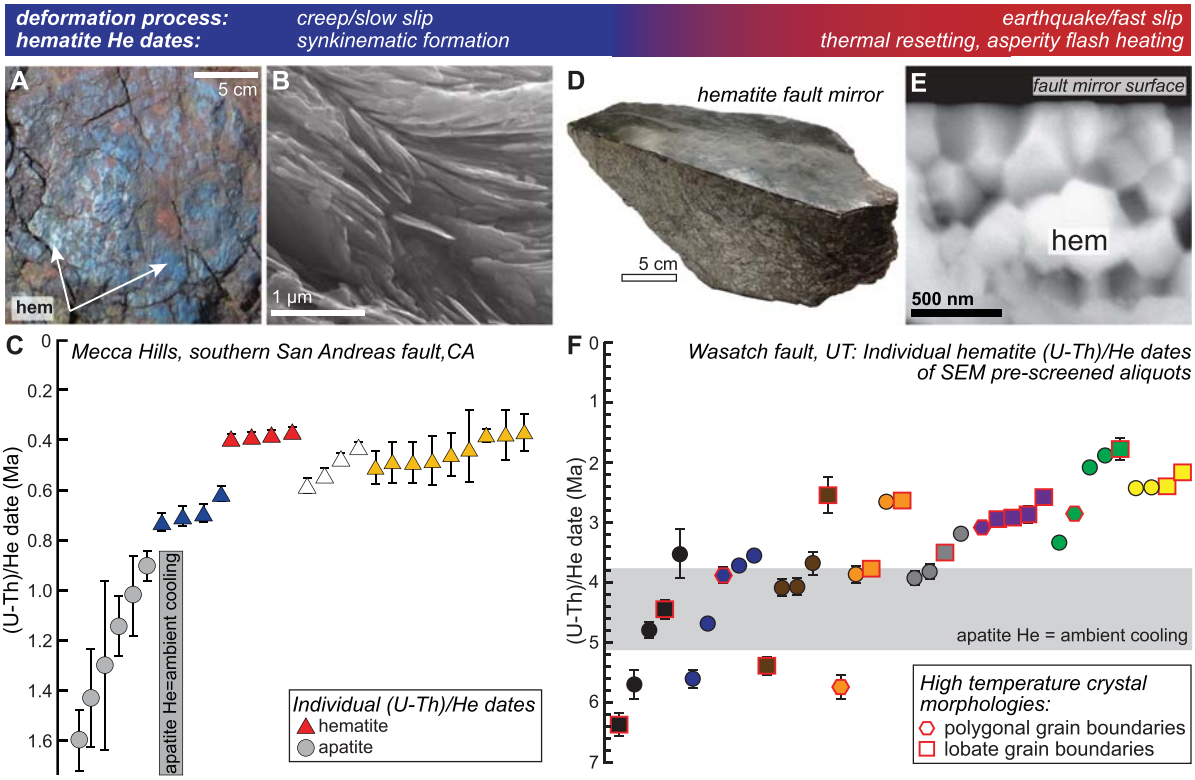

Figure 9. Examples of integrated hematite nanotextures and (U–Th)/He data patterns that inform fault zone processes from creep (a–c) to earthquakes (d–f). (a) Hematite-coated minor fault surfaces in fault damage zones that parallel the southern San Andreas fault in Mecca Hills, CA, comprise thin, high-aspect ratio, densely stacked hematite plates visible in high-resolution scanning electron microscope (SEM) images (b). (c) Comparison of hematite He and apatite He thermochronometry dates reveals the former record phases of Pleistocene synkinematic mineralization during slow slip events. Modified from Moser et al. (2017). (d) Hematite fault mirrors exposed in Wasatch fault damage zone comprise nanoparticles that locally exhibit polygonal morphology visible in SEM (e) from asperity flash heating. (f) Individual hematite He dates with 2σ analytical uncertainty from eight samples (different colors), which were prescreened with SEM to identify a variety of hematite crystal morphologies. Hematite aliquots with these distinctive high-temperature morphologies yield hematite He dates younger than apatite He-derived ambient cooling, reflecting thermal resetting during microearthquake to nanoearthquakes accommodated on these thin slip surfaces. Modified from McDermott et al. (2017).

empirically reproduce signal resetting under equivalent conditions in the laboratory (e.g., Fukuchi & Imai, 1998; Toyoda et al., 2000).

Hematite He thermochronometry informs fault slip timing and processes (Figure 9). Accurate interpretation of hematite He data requires hematite textural characterization, grain size (T_c) distribution data, and constraints on ambient thermal conditions during and after hematite formation from apatite He thermochronometry (e.g., Ault, Reiners, et al., 2015; McDermott et al., 2017; Moser et al., 2017). For example, hematite fault mirrors in the exhumed Wasatch fault damage zone, UT, preserve textural and thermochronometric evidence for asperity flash heating during earthquake aftershocks <4.5 Ma (Figures 9d–9f; Ault, Reiners, et al., 2015; Evans et al., 2014; McDermott et al., 2017). In the Mecca Hills, CA, adjacent to the San Andreas fault, hematite textures analogous to "scaly" fabrics observed in clays and thermochronometric data document Late Pleistocene episodes of synkinematic hematite mineralization in fault damage zones via creep processes (Figures 9a–9c; Moser et al., 2017). Similar scaly hematite fabrics are documented on small faults in the Kuh-e-Faghan strike-slip fault system, central Iran, from punctuated Miocene mineralization during fault-related exhumation (Calzolari et al., 2018).

Fluids circulating in fault systems advect heat, influencing local and regional temperature gradients and low-thermochronometry systematics in fault-bounded mountain ranges (e.g., Whipp & Ehlers, 2007). Minerals forming from fluids and entrained in fault zones also provide a record of these processes. (U–Th)/He and FT thermochronometry of minerals precipitated from fluids (e.g., hematite and Mn–K oxides) and entrained in faults (e.g., apatite and zircon) inform the timing and geologic significance of modern

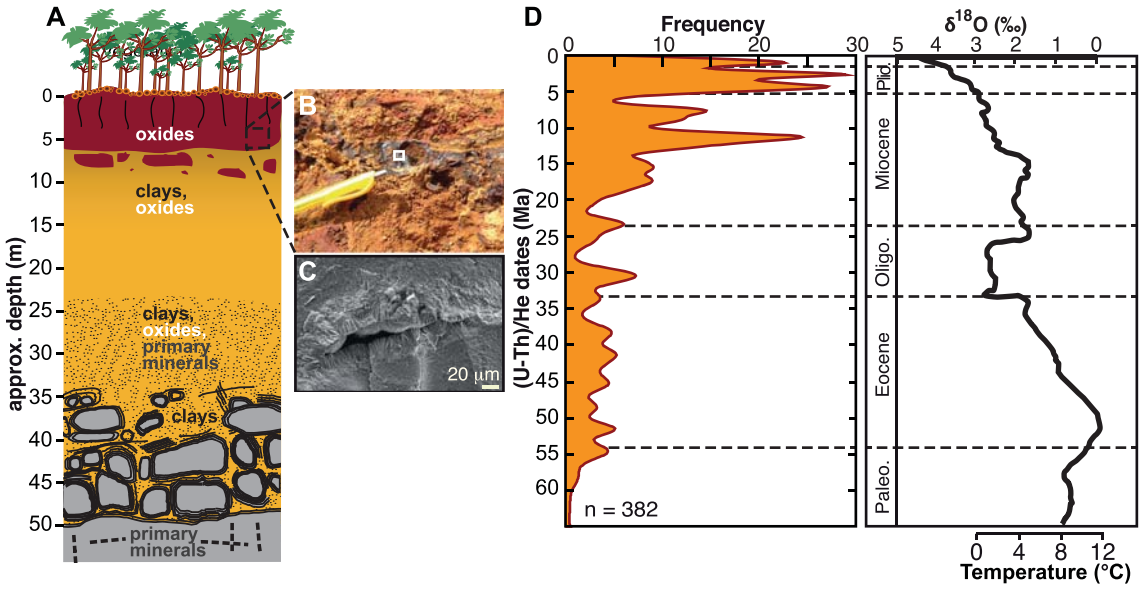

Figure 10. Schematic illustration of a typical lateritic profile that develops in intertropical regions with associated goethite He and hematite He thermochronometry. (a) Lateritic profile from surface to bedrock, with mineralogical constituents. Top of profile comprises a duricrust, formed during intense weathering. Depth scale is approximate, as weathering profile thickness is variable and can be >100 m. Insets (b, c) show metallic, Fe oxide enrichment and a scanning electron microscope image of a goethite concretion (Allard et al., 2018), respectively. (d) Frequency of supergene goethite He and hematite He dates from northern Brazil (Allard et al., 2018; Monteiro, Vasconcelos, & Farley, 2018; Monteiro, Vasconcelos, Farley, & Lopes, 2018; Shuster et al., 2005, 2012). (e) Temperature variations based on $\delta^{18}O$ isotopic composition over the Cenozoic (Zachos et al., 2001). Fe oxide He dates may reflect generations of hematite or goethite mineralization associated to multiple weathering episodes due to climatic change since ~65 Ma.

and paleofluid migration (Ault et al., 2016; Garcia et al., 2017; MacNamee & Stockli, 2015; Reiners et al., 2014; Tagami, 2019; Tagami & Murakami, 2007; Wolfler et al., 2010). For example, faults in the Gower Peninsula, Wales contain hematite that preserves a thermochronologic fingerprint of hydrothermal fluid circulation and hematite growth, contemporaneous with the opening of the North Atlantic Ocean ~140 million years ago (Ault et al., 2016). Some fault systems host paleo and juvenile geothermal systems. Bedrock and borehole apatite He thermochronometry can document transient and long-lived thermal anomalies in faults and, together with other low-temperature thermochronometers, are useful tools for geothermal research and exploration (Gorynski et al., 2014; MacNamee & Stockli, 2015; Valla, Rahn, et al., 2016; Whipp & Ehlers, 2007).

5.4. Weathering and Paleoclimate Changes

Earth's landscapes evolve by physical erosion and chemical weathering, processes that reflect tectonics and climatic change (West et al., 2005). The dynamics of the Earth's surface and especially of soils that cover most of it influence climate through the production and consumption of greenhouse gases such as CO_2 (Berner et al., 1983). Up to ~30% of continental surfaces comprise tectonically quiescent, low relief landscapes in intertropical regions with deep weathering profiles (i.e., laterites). As such, laterites and their components (e.g., primary and secondary minerals, water, and plants) are a tropical expression of the CZ (Anderson et al., 2007). The formation of laterites, like that of all soils, results from the transfer of chemical elements between different compartments of the CZ (Brantley & Lebedeva, 2011). The release of chemical elements from the parent rock will lead to the precipitation of secondary supergene phases such as clays (e.g., kaolinite), Fe oxides (e.g., hematite and goethite), and Mn–K oxides, which host less soluble elements such as Al, Fe, or Ti (Nahon, 1991).

Laterites factor significantly in the global geochemical budget of weathering and erosion processes. The deep weathering profiles can accumulate only through the combination of intense chemical weathering and slow physical erosion (Retallack, 2010). Figure 10 depicts a typical lateritic profile and its mineralogical compartments, capped by a strong Fe-enriched weathering horizon, referred to as a duricrust horizon. Mesozoic to Cenozoic laterite chronology has enhanced our understanding of soil formation and opens new research

avenues as laterites also record past climatic conditions (e.g., Vasconcelos et al., 2015) or landscape evolution (e.g., Bonnet et al., 2016). ^{40}Ar–^{39}Ar analysis of Mn oxides, and more recently, hematite and goethite He geochronology from laterites inform the timing, tempo, and geochemical processes of laterite formation via past climate change (Allard et al., 2018; Deng et al., 2017; Monteiro et al., 2014; Monteiro, Vasconcelos, Farley, & Lopes, 2018; Shuster, Vasconcelos, et al., 2005; Vasconcelos et al., 1994; Vasconcelos et al., 2013). For example, Figure 10d presents a compilation of published supergene goethite and hematite (U–Th)/He dates from northern Brazilian laterites. For comparison, temperature changes over the Cenozoic are shown inferred from stable isotope data. This compilation highlights the longevity of continental landscapes and protracted laterite formation during multiple weathering episodes. In addition, supergene hematite or goethite formation can also be used to date paleochannel evolution and water table drawdown during climate (e.g., Danišík et al., 2013; Heim et al., 2006) or landscape (Monteiro, Vasconcelos, & Farley, 2018; Riffel et al., 2015) changes.

6. Frontiers in Low-Temperature Thermochronometry

In this contribution we highlight advances and new directions in FT, (U–Th)/He, and trapped charge thermochronometry. The power and utility of these approaches to resolve Earth surface and upper crustal thermal histories has enabled researchers to quantify the timing and tempo of a cornucopia of fundamental Earth processes (Figure 6). In the coming decades, researchers will continue to push the boundaries of each of these methods and their applications to constrain increasingly complex—from seconds to billions of years—thermal histories. Innovation in theory and analytical methods, combined with numerical modeling, materials science, integrated thermochronometric approaches, and leveraging independent textural, geochemical, geophysical, and/or climatic observations, will usher in new Earth science discoveries and breakthroughs.

6.1. Theory and Systematics

Empirical, experimental, and theoretical observations fuel the low-temperature thermochronology community's desire to improve our understanding of diffusion, radiation damage accumulation, damage annealing, and trapped charge saturation ratios. Important advances in these topics will occur as thermochronologists engage with other scientific communities, such as theoretical chemists, nuclear or material physicists, and mineralogists. Investigations of atomic to crystal-cell-scale phenomena will allow us to address persistent questions centered on He diffusion and/or annealing behavior. For example, DFT calculations provide foundational insights into He diffusion in crystal structures (e.g., Djimbi et al., 2015), and ongoing analysis of apatite, zircon, goethite, magnetite, and quartz will allow us to better understand noble gas diffusion in those minerals. In addition, new material science characterization of radiation damage using Raman spectroscopy, transmission electron microscopy, atom microprobe, and/or ion beam techniques (e.g., elastic recoil detection analysis, nuclear reaction analysis, and Rutherford backscattering spectroscopy) can refine our understanding of damage annealing. Complementary laboratory and empirical characterization of crystal damage accumulation and annealing will help improve damage-He diffusivity and FT annealing models (Gerin et al., 2017; Ginster et al., 2019; McDannell et al., 2019; Recanati et al., 2017; Willett et al., 2017).

Trapped charge thermochronometry will also benefit from material science investigations into the physical nature of defects within quartz and feldspar, as well as new approaches to probing their trapped charge populations using spectroscopic methods (e.g., photoluminescence, radioluminescence, ESR, and time-resolved luminescence; cf. Krbetschek et al., 1997; Prasad et al., 2017; Riedesel et al., 2018). Understanding the nature of these defects will aid the development of robust physical models that accurately describe the processes of electron trapping and detrapping in these minerals, reducing the potential error caused by the extrapolation of thermal histories from poorly estimated kinetic parameters. Collectively, these advances directly translate to our ability to decipher more precise thermal histories over a variety of timescales and improve modeling packages that quantify the thermal evolution of rocks and minerals.

6.2. Emerging Tools and Analytical Approaches

Analytical improvements to low-temperature thermochronometry systems will similarly promote discovery and innovation. For example, ongoing application of a new continuous ramped heating approach can assess anomalous He diffusion behavior (Idleman et al., 2018; McDannell, Zeitler, Janes, et al., 2018). This

approach, currently used for apatite, offers the promise of identifying the source(s) of (U–Th)/He data dispersion during near routine He degassing analysis and, importantly, provides new insights into He mobility in target grains. Improved understanding of He diffusion in accessory and secondary phases from atomistic calculations and $^{4}He/^{3}He$ diffusion experiments will expand applications. For example, $^{4}He/^{3}He$ thermochronometry allows us to recover thermal history information from a single crystal or aliquot (e.g., Farley & McKeon, 2015; Flowers & Farley, 2012; Garcia et al., 2017; Schildgen et al., 2010; Tripathy-Lang et al., 2015; Valla et al., 2011). Advances in our understanding of He diffusion in hematite, magnetite, goethite, and Mn oxides (e.g., Balout et al., 2017; Farley, 2018; Garcia et al., 2017), new aliquot selection approaches (e.g., Jensen et al., 2018), and integration of nanotextural observations with oxide thermochronometry (e.g., Ault et al., 2016; Ault, Reiners, et al., 2015; McDermott et al., 2017; Moser et al., 2017) enable robust application of these thermochronometry tools to hydrothermal systems, faults, and surficial deposits in recent and deep time.

Recent development of (U–Th)/Ne thermochronometry opens up new and exciting research avenues. This system is based on ^{21}Ne production during alpha decay, capture on ^{18}O in O-rich minerals, and strong retention in O-bearing phases and requires measurement of U, Th, and ^{21}Ne in excess of atmospheric neon (Cox et al., 2015; Farley & Flowers, 2012; Farley & McKeon, 2015; Gautheron et al., 2006). For example, (U–Th)/Ne dating can provide Fe oxide formation ages and complementary thermal history information from oxides, apatite, and zircon to the (U–Th)/He and FT systems. This method offers the potential to date fluid circulation and concomitant mineralization in faults as well as deformation processes.

Analytical advances in detrital low-temperature thermochronometry will facilitate tracking sediment routing patterns in ancient basins due to tectonics and/or paleoclimate change as well as modern systems in response to anthropogenic climate change. Refinement of double- and triple-dating analytical procedures and expansion of these approaches to other detrital accessory phases is critical to this. For example, ongoing development of laser ablation (U–Th)/He thermochronometry and evaluation of method challenges will enable high sample throughput necessary for detrital studies in sedimentary rocks and modern drainage systems (e.g., Horne et al., 2016, 2019).

6.3. Emerging Applications

New applications will combine multiple low-temperature and trapped charge thermochronometry data sets (e.g., King, Herman, & Guralnik, 2016), as well as leverage other geochemical, geophysical, and geobiological data to tackle new science questions in the societally relevant fields of climate change, planetary geology, geomicrobiology, and sustainable resource development. For example, hematite He, goethite He, and magnetite He dating will be combined with stable isotope geochemistry to reconstruct paleoclimate (e.g., Miller et al., 2017; Yapp & Shuster, 2017). This also opens new avenues of soil science research, shedding light on paleoenvironmental and modern climate change. Comparison of magnetite, hematite, and goethite He dates can also reveal changes in oxidation-reduction conditions of Earth's surface in recent and deep time. These changes may be microbially mediated and future thermochronometry research will sit at the intersection of geochemistry and geomicrobiology. The aforementioned lines of inquiry are not restricted to Earth. Hematite and goethite He dating can be used to date weathering and thus the presence of water on Mars (Heim et al., 2006; Kula & Baldwin, 2012; Riffel et al., 2016). Investigation of oxide minerals on Mars may shed light rock-powered life on another planet. (U–Th)/He thermochronometry has been used to document terrestrial (van Soest et al., 2011; Young et al., 2013) and lunar (Kelly et al., 2018) impacts events and, in the future, may be applied to such events on Mars.

Applications of thermochronometry are also relevant for current and future geothermal, hydrocarbon, and mineral resource research and exploration. Apatite He and AFT thermochronometry have long been used to characterize basin and reservoir thermal histories, owing to the overlap between the T_c of these systems and oil production window temperatures (~120–60 °C, Hunt, 1996). High radiation-damaged zircon is sensitive to temperatures less than the apatite He T_c (e.g., Johnson et al., 2017), in line with hydrocarbon maturation temperatures. High damage and thus high eU zircon can be identified via visual metamictization (e.g., Ault et al., 2018). Together with greater preservation potential versus apatite in continental and submarine basin systems and ongoing refinement to zircon damage-diffusivity models (Ginster et al., 2019), the zircon He system is attractive and complementary tool for reconstructing basement and basin thermal histories for hydrocarbon research. FT, (U–Th)/He, and $^{4}He/^{3}He$ thermochronometry of minerals on and adjacent to fault

damage zone slip surfaces and in fault cores are well suited to detect signatures of fluid circulation in these systems and thus serves as a tool for geothermal exploration. Fe oxide and Mn oxide He thermochronometry will be applied to ore deposit research. For example, hematite and goethite coprecipitate with economically valuable ore minerals and thus hematite and goethite He chronology will be applied to Ni-rich laterites and Au–Ag–Cu–Zn deposits (Reich & Vasconcelos, 2015; Wernicke & Lippolt, 1997) to guide resource development.

Acknowledgments
We thank Pierre Valla, Matthew Fox, and Associate Editor Andrew Carter for constructive reviews; Laurent Tassan-Got, Peter Reiners, Gabriele Calzolari, and Robert McDermott for helpful discussions and perspectives during writing of the manuscript; and feedback from William Guenthner, Jessica Stanley, Leah Houser, Devon Orme, Kendra Murray, and Cailey Condit on earlier versions of the manuscript and figures. A. K. A. acknowledges the National Science Foundation for support via NSF CAREER EAR-1654628 and NSF EAR-1419828. C. G. acknowledges support from the HeDiff ANR-12-NS06-0005-01 and RECA ANR-17-CE01-0012-01 projects. G. E. K. acknowledges support from Swiss National Science Foundation (SNSF) Grant PZ00P2_167960. All presented data are available in contributions cited and provided in the reference list.

References

Abbey, A. L., & Niemi, N. A. (2018). Low-temperature thermochronometric constraints on fault initiation and growth in the northern Rio Grande rift, upper Arkansas River valley, Colorado, USA. *Geology*, *46*(7), 627–630. https://doi.org/10.1130/G40232.1

Aitken, M. J. (1985). Thermoluminescence dating: Past progress and future trends. *Nuclear Tracks and Radiation Measurements (1982)*, *10*(1-2), 3–6. https://doi.org/10.1016/0735-245X(85)90003-1

Aitken, M. J. (1998). *Introduction to optical dating: The dating of Quaternary sediments by the use of photon-stimulated luminescence*. Oxford, UK: Clarendon Press.

Allard, T., Gautheron, C., Riffel, S. B., Balan, E., Soares, B. F., Pinna-Jamme, R., et al. (2018). Combined dating of goethites and kaolinites from ferruginous duricrusts. Deciphering the Late Neogene erosion history of Central Amazonia. *Chemical Geology*, *479*, 136–150. https://doi.org/10.1016/j.chemgeo.2018.01.004

Anderson, A. J., Hodges, K. V., Van Soest, M. C., & Hanchar, J. M. (2019). Helium diffusion in natural xenotime. *Geochemistry, Geophysics, Geosystems*, *20*, 417–433. https://doi.org/10.1029/2018GC007849

Anderson, S. P., von Blanckenburg, F., & White, A. F. (2007). Physical and chemical controls on the Critical Zone. *Elements*, *3*(5), 315–319. https://doi.org/10.2113/gselements.3.5.315

Ault, A. K., & Flowers, R. M. (2012). Is apatite U-Th zonation information necessary for accurate interpretation of apatite (U-Th)/He thermochronometry data? *Geochimica et Cosmochimica Acta*, *79*, 60–78. https://doi.org/10.1016/j.gca.2011.11.037

Ault, A. K., Flowers, R. M., & Bowring, S. A. (2009). Phanerozoic burial and unroofing history of the western Slave craton and Wopmay orogen from apatite (U-Th)/He thermochronometry. *Earth and Planetary Science Letters*, *284*(1-2), 1–11. https://doi.org/10.1016/j.epsl.2009.02.035

Ault, A. K., Flowers, R. M., & Bowring, S. A. (2013). Phanerozoic surface history of the Slave craton. *Tectonics*, *32*, 1066–1083. https://doi.org/10.1002/tect.20069

Ault, A. K., Flowers, R. M., & Bowring, S. A. (2015). Synchroneity of cratonic burial phases and gaps in the kimberlite record: Episodic magmatism or preservational bias? *Earth and Planetary Science Letters*, *410*, 97–104. https://doi.org/10.1016/j.epsl.2014.11.017

Ault, A. K., Frenzel, M., Reiners, P. W., Woodcock, N. H., & Thomson, S. N. (2016). Record of paleofluid circulation in faults revealed by hematite (U-Th)/He and apatite fission-track dating: An example from Gower Peninsula fault fissures, Wales. *Lithosphere*, *8*(4), 379–385. https://doi.org/10.1130/L522.1

Ault, A. K., Guenthner, W. R., Moser, A. C., Miller, G. H., & Refsnider, K. A. (2018). Zircon selection reveals (de)coupled zircon metamictization, radiation damage, and He diffusivity. *Chemical Geology*, *490*, 1–12. https://doi.org/10.1016/j.chemgeo.2018.04.023

Ault, A. K., Reiners, P. W., Evans, J. P., & Thomson, S. N. (2015). Linking hematite (U-Th)/He dating with the microtextural record of seismicity in the Wasatch fault damage zone, Utah. *Geology*, *43*(9), 771–774. https://doi.org/10.1130/G36897.1

Avdeev, B., & Niemi, N. A. (2011). Rapid Pliocene exhumation of the Central Greater Caucasus constrained by low-temperature thermochronometry. *Tectonics*, *30*, TC2009. https://doi.org/10.1029/2010TC002808

Balout, H., Roques, J., Gautheron, C., Tassan-Got, L., & Mbongo-Djimbi, D. (2017). Helium diffusion in pure hematite (□-Fe2O3) for thermochronometric applications: A theoretical multi-scale study. *Computational and Theoretical Chemistry*, *1099*, 21–28. https://doi.org/10.1016/j.comptc.2016.11.001

Barbarand, J., Carter, A., Wood, I., & Hurford, A. J. (2003). Compositional and structural control of fission-track annealing in apatite. *Chemical Geology*, *198*(1-2), 107–137. https://doi.org/10.1016/S0009-2541(02)00424-2

Bartz, M., Rixhon, G., Duval, M., King, G. E., Posada, C. A., Parés, J. M., & Brückner, H. (2018). Successful combination of electron spin resonance, luminescence and palaeomagnetic dating methods allows reconstruction of the Pleistocene evolution of the lower Moulouya river (NE Morocco). *Quaternary Science Reviews*, *185*, 153–171. https://doi.org/10.1016/j.quascirev.2017.11.008

Batt, G. E., & Braun, J. (1997). On the thermomechanical evolution of compressional orogens. *Geophysical Journal International*, *128*(2), 364–382. https://doi.org/10.1111/j.1365-246X.1997.tb01561.x

Baughman, J. S., & Flowers, R. M. (2018). Deciphering a 2 Gyr-long thermal history from a multichronometer (U-Th)/He study of the Phalaborwa Carbonatite, Kaapvaal craton, South Africa. *Geochemistry, Geophysics, Geosystems*, *19*, 1581–1594. https://doi.org/10.1029/2017GC007198

Baughman, J. S., Flowers, R. M., Metcalf, J. R., & Dhansay, T. (2017). Influence of radiation damage on titanite diffusion kinetics. *Geochimica et Cosmochimica Acta*, *205*, 50–64. https://doi.org/10.1016/j.gca.2017.01.049

Beirau, T., Nix, W. D., Ewing, R. C., Pöllmann, H., & Salje, E. K. H. (2018). Radiation-damage-induced transitions in zircon: Percolation theory applied to hardness and elastic moduli as a function of density. *Applied Physics Letters*, *112*(20). https://doi.org/10.1063/1.5030626

Bengtson, A., Ewing, R. C., & Becker, U. (2012). He diffusion and closure temperatures in apatite and zircon: A density functional theory investigation. *Geochimica et Cosmochimica Acta*, *86*, 228–238. https://doi.org/10.1016/j.gca.2012.03.004

Ben-Zion, Y., & Sammis, C. G. (2013). Shear heating during distributed fracturing and pulverization of rocks. *Geology*, *41*(2), 139–142. https://doi.org/10.1130/G33665.1

Berner, R. A., Lasaga, A. C., & Garrels, R. M. (1983). The carbonate-silicate geochemical cycle and its effect on atmospheric carbon dioxide over the past 100 million years. *American Journal of Science*, *283*(7), 641–683. https://doi.org/10.2475/ajs.283.7.641

Bernet, M. (2009). A field-based estimate of the zircon fission-track closure temperature. *Chemical Geology*, *259*(3-4), 181–189. https://doi.org/10.1016/j.chemgeo.2008.10.043

Bernet, M., Brandon, M. T., Garver, J. I., Balestieri, M. L., Ventura, B., & Zattin, M. (2009). Exhuming the Alps through time: Clues fromdetrital zircon fission-track thermochronology. *Basin Research*, *21*(6), 781–798. https://doi.org/10.1111/j.1365-2117.2009.00400.x

Bernet, M., & Garver, J. I. (2005). Fission-track analyses of detrital zircon. *Reviews in Mineralogy and Geochemistry*, *58*(1), 205–237. https://doi.org/10.2138/rmg.2005.58.8

Bernet, M., van der Beek, P. A., Pik, R., Huyghe, P., Mugnier, J.-L., Labrin, E., & Szulc, A. (2006). Miocene to recent exhumation of the central Himalaya determined from combined detrital zircon fission-track and U/Pb analysis of Siwalik sediments, western Nepal. *Basin Research*, *18*(4), 393–412. https://doi.org/10.1111/j.1365-2117.2006.00303.x

Bidgoli, T. S., Stockli, D. F., & Walker, J. D. (2015). Low-temperature thermochronologic constraints on the kinematic histories of the Castle Cliffs, Tule Springs, and Mormon Peak detachments, southwestern Utah and southeastern Nevada. *Geosphere*, *11*(3), 850–867. https://doi.org/10.1130/GES01083.1

Biswas, R. H., Herman, F., King, G. E., & Braun, J. (2018). Thermoluminescence of feldspar as a multi-thermochronometer to constrain the temporal variation of rock exhumation in the recent past. *Earth and Planetary Science Letters*, *495*, 56–68. https://doi.org/10.1016/j.epsl.2018.04.030

Blackburn, T. J., Bowring, S. A., Schoene, B., Mahan, K. H., & Dudas, F. (2011). U-Pb thermochronology: Creating a temporal record of lithosphere thermal evolution. *Contributions to Mineralogy and Petrology*, *162*(3), 479–500. https://doi.org/10.1007/s00410-011-0607-6

Blackburn, T. J., Stockli, D. F., & Walker, J. D. (2007). Magnetite (U-Th)/He dating and its application to the geochronology of intermediate to mafic volcanic rocks. *Earth and Planetary Science Letters*, *259*(3-4), 360–371. https://doi.org/10.1016/j.epsl.2007.04.044

Blythe, A., Burbank, D., Carter, A., Schmidt, K., & Putkonen, J. (2007). Plio-Quaternary exhumation history of the central Nepalese Himalaya: 1. Apatite and zircon fission track and apatite (U-Th)/He analyses. *Tectonics*, *26*, TC3002. https://doi.org/10.1029/2006TC001990

Bonnet, N. J., Beauvais, A., Arnaud, N., Chardon, D., & Jayananda, M. (2016). Cenozoic lateritic weathering and erosion history of Peninsular India from 40Ar/39Ar dating of supergene K–Mn oxides. *Chemical Geology*, *446*, 33–53. https://doi.org/10.1016/j.chemgeo.2016.04.018

Bøtter-Jensen, L., Bulur, E., Duller, G. A. T., & Murray, A. S. (2000). Advances in luminescence instrument systems. *Radiation Measurements*, *32*(5-6), 523–528. https://doi.org/10.1016/S1350-4487(00)00039-1

Boyce, J. W., Hodges, K. V., Olszewski, W. J., & Jercinovic, M. J. (2005). He diffusion in monazite: Implications for (U-Th)/He thermochronometry. *Geochemistry, Geophysics, Geosystems*, *6*, Q12004. https://doi.org/10.1029/2005GC001058

Boyce, J. W., Hodges, K. V., Olszewski, W. J., Jercinovic, M. J., Carpenter, B. D., & Reiners, P. W. (2006). Laser microprobe (U-Th)/He geochronology. *Geochimica et Cosmochimica Acta*, *70*(12), 3031–3039. https://doi.org/10.1016/j.gca.2006.03.019

Brady, R. J. (2002). Very high slip rates on continental extensional faults: New evidence from (U-Th)/He thermochronometry of the Buckskin Mountains, Arizona. *Earth and Planetary Science Letters*, *197*(1-2), 95–104. https://doi.org/10.1016/S0012-821X(02)00460-0

Brantley, S. L., & Lebedeva, M. (2011). Learning to read the chemistry of regolith to understand the Critical Zone. *Annual Review of Earth and Planetary Sciences*, *39*(1), 387–416. https://doi.org/10.1146/annurev-earth-040809-152321

Braun, J. (2003). Pecube: A new finite-element code to solve the 3-D heat transport equation including the effects of a time-varying finite amplityde surface topography. *Computers and Geosciences*, *29*(6), 787–794. https://doi.org/10.1016/S0098-3004(03)00052-9

Braun, J., van der Beek, P. A., Valla, P. G., Robert, X., Herman, F., Glotzbach, C., et al. (2012). Quantifying rates of landscape evolution and tectonic processes by thermochronology and numerical modeling of crustal heat transport using PECUBE. *Tectonophysics*, *524*, 1–28.

Brown, N. D., Rhodes, E. J., & Harrison, T. M. (2017). Using thermoluminescence signals from feldspars for low-temperature thermochronology. *Quaternary Geochronology*, *42*, 31–41. https://doi.org/10.1016/j.quageo.2017.07.006

Brown, R. W., Beucher, R., Roper, S., Persano, C., Stuart, F. M., & Fitzgerald, P. G. (2013). Broken crystals, Part 1: Theoretical basis and implications for the apatite (U-Th)/He thermochronometer. *Geochimica et Cosmochimica Acta*, *122*, 478–497. https://doi.org/10.1016/j.gca.2013.05.041

Brown, R. W., Gallagher, K., Gleadow, A. J. W., & Summerfield, M. A. (2000). Morphotectonic evolution of the south Atlantic margins of Africa and South America. In M. A. Summerfield (Ed.), *Geomorphology and global tectonics* (pp. 255–281). New York: John Wiley and Sons, Inc.

Brown, R. W., Rust, D. J., Summerfield, M. A., Gleadow, A. J. W., & De Wit, M. C. J. (1990). An early Cretaceous phase of accelerated erosion on the south-western margin of Africa: Evidence from apatite fission track analysis and the offshore sedimentary recrod. *International Journal of Radiation and Applied Instrumentation, Part D*, *17*, 339–350.

Brown, R. W., Summerfield, M. A., & Gleadow, A. J. W. (2002). Denudational history along a transect across the Drakensberg Escarpment of southern Africa derived from apatite fission track thermochronology. *Journal of Geophysical Research*, *107*(B12), 2350. https://doi.org/10.1029/2001JB000745

Buylaert, J. P., Ujvari, G., Murray, A. S., Smedley, R. K., & Kook, M. (2018). On the relationship between K concentration, grain size, and dose in feldspar. *Radiation Measurements*, *120*, 181–187. https://doi.org/10.1016/j.radmeas.2018.06.003

Calzolari, G., Rossetti, F., Ault, A. K., Lucci, F., Olivetti, V., & Nozaem, R. (2018). Hematite (U-Th)/He thermochronometry constrains strike-slip faulting on the Kuh-e-Faghan fault, central Iran. *Tectonophysics*, *728-729*, 41–54. https://doi.org/10.1016/j.tecto.2018.01.023

Calzolari, G., Rossetti, F., Della Seta, M., Nozaem, R., Olivetti, V., Balestrieri, M. L., et al. (2016). Spatio-temporal evolution of intraplate strike-slip faulting: The Neogene–Quaternary Kuh-e-Faghan Fault, central Iran. *Bulletin*, *128*, 374–396.

Campbell, I. H., Reiners, P. W., Allen, C. M., Nicolescu, S., & Upadhyay, R. (2005). He–Pb double dating of detrital zircons from the Ganges and Indus Rivers: Implication for quantifying sediment recycling and provenance studies. *Earth and Planetary Science Letters*, *237*(3-4), 402–432. https://doi.org/10.1016/j.epsl.2005.06.043

Carlson, W. D., Donelick, R. A., & Ketcham, R. A. (1999). Variability of apatite fission-track annealing kinetics: I. Experimental results. *American Mineralogist*, *84*(9), 1213–1223. https://doi.org/10.2138/am-1999-0901

Carrapa, B., DeCelles, P. C., Reiners, P. W., Gehrels, G. E., & Sudo, M. (2009). Apatite triple dating and white mica $^{40}Ar/^{39}Ar$ thermochonology of syntectonci detritus in the Central Andes: A multiphase tectonothermal history. *Geology*, *37*(5), 407–410. https://doi.org/10.1130/G25698A.1

Carter, A. (2019). *Thermochronology on sand and sandstones for stratigraphic and provenance studies, fission-track thermochronology and its application to geology*, (pp. 259–268). Cham: Springer.

Carter, A., & Moss, S. J. (1999). Combined detrital-zircon fission-track and U-Pb dating: A new approach to understanding hinterland evolution. *Geology*, *27*(3), 235–238. https://doi.org/10.1130/0091-7613(1999)027<0235:CDZFTA>2.3.CO;2

Carter, T. J., Kohn, B. P., Foster, D. A., Gleadow, A. J. W., & Woodhead, J. D. (2006). Late-stage evolution of the Chemehuevi and Sacramento detachment faults from apatite (U-Th)/He thermochronometry - Evidence for mid-Miocene accelerated slip. *GSA Bulletin*, *118*(5-6), 689–709. https://doi.org/10.1130/B25736.1

Chapot, M. S., Roberts, H. M., Duller, G. A. T., & Lai, Z. P. (2012). A comparison of natural-and laboratory-generated dose response curves for quartz optically stimulated luminescence signals from Chinese Loess. *Radiation Measurements*, *47*(11-12), 1045–1052. https://doi.org/10.1016/j.radmeas.2012.09.001

Chew, D. M., & Donelick, R. A. (2012). Combined apatite fission track and U-Pb dating by LA-ICP-MS and its application in apatite provenance analysis. *Mineralogical Association of Canada Short Course*, *42*, 219–247.

Christeleit, E. C., Brandon, M. T., & Shuster, D. L. (2017). Miocene development of alpine glacial relief in the Patagonian Andes, as revealed by low-temperature thermochronometry. *Earth and Planetary Science Letters*, *460*, 152–163. https://doi.org/10.1016/j.epsl.2016.12.019

Clark, M. K., House, M. A., Royden, L. H., Whipple, K. X., Burchfiel, B. C., Zhang, X., & Tang, W. (2005). Late Cenozoic uplift of southeastern Tibet. *Geology*, *33*(6), 525–528. https://doi.org/10.1130/G21265.1

Cochrane, R., Spikings, R. A., Chew, D., Wotzlaw, J.-F., Chiaradia, M., Tyrrell, S., et al. (2014). High temperature (> 350 °C) thermochronology and mechanisms of Pb loss in apatite. *Geochimica et Cosmochimica Acta*, *127*, 39–56. https://doi.org/10.1016/j.gca.2013.11.028

Cockburn, H. A. P., Brown, R. W., Summerfield, M. A., & Seidl, M. A. (2000). Quantifying passive margin denudation and landscape development using a combined fission-track thermochronology and cosmogenic isotope analysis approach. *Earth and Planetary Science Letters*, *179*(3-4), 429–435. https://doi.org/10.1016/S0012-821X(00)00144-8

Colgan, J. P., Shuster, D. L., & Reiners, P. W. (2008). Two-phase Neogene extension in the northwestern Basin and Range recorded in a single thermochronology sample. *Geology*, *36*(8), 631–634. https://doi.org/10.1130/G24897A.1

Collett, C. M., Duvall, A. R., Flowers, R. M., Tucker, G. E., & Upton, P. (2019). The timing and style of oblique deformation within New Zealand's Kaikōura Ranges and Marlborough Fault System based on low-temperature thermochronology. *Tectonics*, *38*, 1250–1272. https://doi.org/10.1029/2018TC005268

Cooperdock, E. H., & Stockli, D. F. (2016). Unraveling alterations histories in serpentinites and associated ultramafic rocks with magnetite (U-Th)/He geochronology. *Geology*, *44*(11), 967–970. https://doi.org/10.1130/G38587.1

Cooperdock, E. H., & Stockli, D. F. (2018). Dating exhumed peridotite with spinel (U-Th)/He chronometry. *Earth and Planetary Science Letters*, *489*, 219–227. https://doi.org/10.1016/j.epsl.2018.02.041

Copeland, P., Cox, K., & Watson, E. B. (2015). The potential of crinoids as (U+Th+Sm)/He thermochronometers. *Earth and Planetary Science Letters*, *422*, 1–10. https://doi.org/10.1016/j.epsl.2015.04.007

Copeland, P., Watson, E. B., Urizar, S. C., Patterson, D., & Lapen, T. L. (2007). Alpha thermochronology of carbonates. *Geochimica et Cosmochimica Acta*, *71*, 4448–4487.

Cosca, M. A., Caby, P., & Bussya, F. (2005). Geochemistry and $^{40}Ar/^{39}Ar$ geochronology of pseudotachylite associated with UHP whiteschists from the Dora Maira massif, Italy. *Tectonophysics*, *402*(1-4), 93–110. https://doi.org/10.1016/j.tecto.2004.12.033

Cox, G. M., Halverson, G. P., Stevenson, R. K., Vokaty, M., Poirier, A., Kunzmann, M., et al. (2016). Continental flood basalt weathering as a trigger for Neoproterozoic Snowball Earth. *Earth and Planetary Science Letters*, *446*, 89–99. https://doi.org/10.1016/j.epsl.2016.04.016

Cox, S. E., Farley, K. A., & Cherniak, D. J. (2015). Direct measurement of neon production rates by (α,n) reaction in minerals. *Geochimica et Cosmochimica Acta*, *148*, 130–144. https://doi.org/10.1016/j.gca.2014.08.036

Cros, A., Gautheron, C., Pagel, M., Berthet, P., Tassan-Got, L., Douville, E., et al. (2014). ^{4}He behavior in calcite filling viewed by (U-Th)/He dating, ^{4}He diffusion and crystallographic studies. *Geochimica et Cosmochimica Acta*, *125*, 414–432. https://doi.org/10.1016/j.gca.2013.09.038

Curry, M. A. E., Barnes, J. B., & Colgan, J. P. (2016). Testing fault growth models with low-temperature thermochronology in the northwest Basin and Range, USA. *Tectonics*, *35*, 2467–2492. https://doi.org/10.1002/2016TC004211

d'Alessio, M. A., & Williams, C. F. (2007). Putting it all together: Exhumation histories from a formal combination of heat flow and a suite of thermochronometers. *Journal of Geophysical Research*, *112*, B08412. https://doi.org/10.1029/2006JB004725

Danišík, M. (2019). *Integration of fission-track thermochronology with other geochronologic methods on single crystals, fission-track thermochronology and its application to geology*, (pp. 93–108). Cham: Springer.

Danišík, M., Evans, N. J., Ramanaidou, E. R., McDonald, B. J., Mayers, C., & McInnes, B. I. A. (2013). (U–Th)/He chronology of the Robe River channel iron deposits, Hamersley Province, Western Australia. *Chemical Geology*, *354*, 150–162. https://doi.org/10.1016/j.chemgeo.2013.06.012

Danišík, M., Pfaff, K., Evans, N. J., Manoloukos, C., Staude, S., McDonald, B. J., & Markl, G. (2010). Tectonothermal history of the Schwarzwald Ore District (Germany): An apatite triple dating approach. *Chemical Geology*, *278*(1-2), 58–69. https://doi.org/10.1016/j.chemgeo.2010.08.022

De Sarkar, S., Mathew, G., Pande, K., Chauhan, N., & Singhvi, A. (2013). Rapid denudation of Higher Himalaya during late Pliestocence, evidence from OSL thermochronology. *Geochronometria*, *40*(4), 304–310. https://doi.org/10.2478/s13386-013-0124-7

DeLucia, M. S., Guenthner, W. R., Marshak, S., Thomson, S. N., & Ault, A. K. (2018). Thermochronology links denudation of the Great Unconformity surface to the supercontinent cycle and snowball Earth. *Geology*, *46*(2), 167–170. https://doi.org/10.1130/G39525.1

Deng, X.-D., Li, J.-W., & Shuster, D. L. (2017). Late Mio-Pliocene chemical weathering of the Yulong porphyry Cu deposit in the eastern Tibetan Plateau constrained by goethite (U–Th)/He dating: Implication for Asian summer monsoon. *Earth and Planetary Science Letters*, *472*, 289–298. https://doi.org/10.1016/j.epsl.2017.04.043

Di Vincenzo, G., Rossetti, F., Viti, C., & Balsamo, F. (2013). Constraining the timing of fault reactivation: Eocene coseismic slip along a Late Ordovician ductile shear zone (northern Victoria Land, Antarctica). *Geological Society of America Bulletin*, *125*(3-4), 609–624. https://doi.org/10.1130/B30670.1

Ding, Y. Z., & Lai, K. W. (1997). Neotectonic fault activity in Hong Kong: Evidence from seismic events and thermoluminescence dating of fault gouge. *Journal of the Geological Society*, *154*(6), 1001–1007. https://doi.org/10.1144/gsjgs.154.6.1001

Djimbi, D. M., Gautheron, C., Roques, J., Tassan-Got, L., Gerin, C., & Simoni, E. (2015). Impact of apatite chemical composition on (U-Th)/He thermochronometry: An atomistic point of view. *Geochimica et Cosmochimica Acta*, *167*, 162–176. https://doi.org/10.1016/j.gca.2015.06.017

Dodson, M. H. (1973). Closure temperatures in cooling geological and petrological systems. *Contributions to Mineralogy and Petrology*, *40*(3), 259–274. https://doi.org/10.1007/BF00373790

Donelick, R. A., Ketcham, R. A., & Carlson, W. D. (1999). Variability of apatite fission-track annealing kinetics II. Crystallographic orientation effects. *American Mineralogist*, *84*(9), 1224–1234. https://doi.org/10.2138/am-1999-0902

Donelick, R. A., O'Sullivan, P. B., & Ketcham, R. A. (2005). Apatite fission-track analysis. *Reviews in Mineralogy and Geochemistry*, *58*(1), 49–94. https://doi.org/10.2138/rmg.2005.58.3

Durcan, J. A., King, G. E., & Duller, G. A. T. (2015). DRAC: Dose rate and age calculator for trapped charge dating. *Quaternary Geochronology*, *28*, 54–61. https://doi.org/10.1016/j.quageo.2015.03.012

Duvall, A. R., Clark, M. K., van der Pluijm, B. A., & Li, C. (2011). Direct dating of Eocene reverse faulting in northeastern Tibet using Ar-dating of fault clays and low-temperature thermochronometry. *Earth and Planetary Science Letters*, *304*(3-4), 520–526. https://doi.org/10.1016/j.epsl.2011.02.028

Ehlers, T. A., & Farley, K. A. (2003). Apatite (U-Th)/He thermochronometry: Methods and applications to problems in tectonics and surface processes. *Earth and Planetary Science Letters*, *206*(1-2), 1–14. https://doi.org/10.1016/S0012-821X(02)01069-5

Ehlers, T. A., Szameitat, A., Enkelmann, E., Yanites, B. J., & Woodsworth, G. J. (2015). Identifying spatial variations in glacial catchment erosion with detrital thermochronology. *Journal of Geophysical Research: Earth Surface*, *120*, 1023–1039. https://doi.org/10.1002/2014JF003432

Enkelmann, E., & Ehlers, T. A. (2015). Evaluation of detrital thermochronology for quantification of glacial catchment denudation and sediment mixing. *Chemical Geology*, *411*, 299–309. https://doi.org/10.1016/j.chemgeo.2015.07.018

Espurt, N., Baby, P., Brusset, S., Roddaz, M., Hermoza, W., & Barbarand, J. (2010). The Nazca Ridge and uplift of the Fitzcarrald Arch: Implications for regional geology in northern South America. In *Amazoni a: Landscape and Species Evolution: A Look into the Past* (pp. 89–100). West Sussex, UK: Wiley-Blackwell.

Evans, J. P., Prante, M. R., Janecke, S. U., Ault, A. K., & Newell, D. N. (2014). Hot faults: Iridescent slip surfaces with metallic luster document high-temperature ancient seismicity in the Wasatch fault zone. *Geology*, *42*, 636–626.

Evans, N. J., Byrne, J. P., Keegan, J. T., & Dotter, L. E. (2005). Determination of uranium and thorium in zircons, apatite, and fluorite: Application to laser (U-Th)/He thermochronology. *Journal of Analytical Chemistry*, *60*, 1300–1307.

Evans, N. J., Wilson, N. S. F., Cline, J. S., McInnes, B. I. A., & Byrne, J. (2005). Fluorite (U–Th)/He thermochronology: Constraints on the low temperature history of Yucca Mountain, Nevada. *Applied Geochemistry*, *20*(6), 1099–1105. https://doi.org/10.1016/j.apgeochem.2005.02.008

Evenson, N. S., Reiners, P. W., Spencer, J., & Shuster, D. L. (2014). Hematite and Mn oxide (U-Th)/He dates from the Buckskin-Rawhide detachment system, western Arizona: Constraining the timing of mineralization and hematite (U-Th)/He systematics. *American Journal of Science*, *314*(10), 1373–1435. https://doi.org/10.2475/10.2014.01

Ewing, R. C., Meldrum, A., Wang, L., & Wang, S. (2000). Radiation-induced amorphization. *Reviews in Mineralogy and Geochemistry*, *391*, 319–361.

Fang, F., Martin, L., Williams, I. S., Brink, F., Mercier, N., & Grün, R. (2018). 2D modelling: A Monte Carlo approach for assessing heterogeneous beta dose rates in luminescence and ESR dating: Paper II, application to igneous rocks. *Quaternary Geochronology*, *48*, 195–206. https://doi.org/10.1016/j.quageo.2018.07.005

Farley, K. A. (2000). Helium diffusion from apatite: General behavior as illustrated by Durango fluorapatite. *Journal of Geophysical Research*, *105*(B2), 2903–2914. https://doi.org/10.1029/1999JB900348

Farley, K. A. (2002). (U-Th)/He dating: Techniques, calibrations, and applications. In D. Porcelli, C. J. Ballentine, & R. Wieler (Eds.), *Noble Gasses in Geochemistry and Cosmochemistry*, *Reviews in Mineralogy and Geochemistry* (Vol. 47, pp. 819–844). Washington, D.C.: Mineralogical Society of America. https://doi.org/10.1515/9781501509056-020

Farley, K. A. (2007). He diffusion systematics in minerals: Evidence from synthetic monazite and zircon structure phosphates. *Geochimica et Cosmochimica Acta*, *71*(16), 4015–4024. https://doi.org/10.1016/j.gca.2007.05.022

Farley, K. A. (2018). Helium diffusion parameters of hematite from a single-diffusion-domain crystal. *Geochimica et Cosmochimica Acta*, *231*, 117–129. https://doi.org/10.1016/j.gca.2018.04.005

Farley, K. A., & Flowers, R. M. (2012). (U-Th)/Ne and multidomain (U-Th)/He systematics of a hydrothermal hematite from eastern Grand Canyon. *Earth and Planetary Science Letters*, *359-360*, 131–140. https://doi.org/10.1016/j.epsl.2012.10.010

Farley, K. A., & McKeon, R. E. (2015). Radiometric dating and temperature history of banded iron formation-associated hematite, Gogebic iron range, Michigan, USA. *Geology*, *43*, 1083–1086.

Farley, K. A., Reiners, P. W., & Nemow, V. (1999). An apparatus for high-precision helium diffusion measurements from minerals. *Analytical Chemistry*, *71*(10), 2059–2061. https://doi.org/10.1021/ac9813078

Farley, K. A., Shuster, D. L., & Ketcham, R. A. (2011). U and Th zonation in apatite observed by laser ablation ICPMS an implications for the (U-Th)/He system. *Geochimica et Cosmochimica Acta*, *75*, 4194–4215.

Farley, K. A., Shuster, D. L., Watson, E. B., Wanser, K., & Balco, G. (2010). Numerical investigations of apatite $^{4}He/^{3}He$ thermochronometry. *Geochemistry, Geophysics, Geosystems*, *11*, Q10001. https://doi.org/10.1029/2010GC003243

Farley, K. A., & Stockli, D. F. (2002). (U-Th)/He dating of phosphates: Apatite, monazite, and xenotime. *Phosphates: Geochemical, Geobiological, and Materials Importance*. *Reviews in Mineralogy and Geochemistry*, *48*(1), 559–577. https://doi.org/10.2138/rmg.2002.48.15

Farley, K. A., Wolf, L. T., & Silver, L. T. (1996). The effects of long alpha-stopping distances on (U-Th)/He ages. *Geochimica et Cosmochimica Acta*, *60*(21), 4223–4229. https://doi.org/10.1016/S0016-7037(96)00193-7

Feinstein, S., Kohn, B. P., Osadetz, K. G., & O'Sullivan, P. B. (2009). Variable Phanerozoic thermal history in the Southern Canadian Shield: Evidence from an apatite fission track profile at the Underground Research Laboratory (URL), Manitoba. *Tectonophysics*, *475*(1), 190–199. https://doi.org/10.1016/j.tecto.2009.01.016

Filleaudeau, P.-Y., Mouthereau, F., & Pik, R. (2012). Thermo-tectonic evolution of the south-central Pyrenees from rifting to orogeny: Insights from detrital zircon U/Pb and (U-Th)/He thermochronometry. *Basin Research*, *24*(4), 401–417. https://doi.org/10.1111/j.1365-2117.2011.00535.x

Fitz-Diaz, E., & van der Pluijm, B. A. (2013). Fold dating: A new Ar/Ar illite dating application to constrain the age of deformation in shallow crustal rocks. *Journal of Structural Geology*, *54*, 174–179. https://doi.org/10.1016/j.jsg.2013.05.011

Fleischer, R. L., Price, P. B., & Walker, R. M. (1975). *Nuclear tracks in solids: Principles and applications* (p. 605). Berkeley: University of California Press.

Flowers, R. M. (2009). Exploiting radiation damage control on apatite (U-Th)/He dates in cratonic regions. *Earth and Planetary Science Letters*, *277*(1-2), 148–155. https://doi.org/10.1016/j.epsl.2008.10.005

Flowers, R. M., Ault, A. K., Kelley, S. A., Zhang, N., & Zhong, S. (2012). Eperiogeny or eustasy? Paleozoic-Mesozoic vertical motion of the North American continental interior from thermochronometry and implications for mantle dynamics. *Earth and Planetary Science Letters*, *317-318*, 436–445. https://doi.org/10.1016/j.epsl.2011.11.015

Flowers, R. M., Bowring, S. A., & Reiners, P. W. (2006). Low long-term erosion rates and extreme continental stability documented by ancient (U-Th)/He dates. *Geology*, *34*(11), 925–928. https://doi.org/10.1130/G22670A.1

Flowers, R. M., & Farley, K. A. (2012). Apatite $^{4}He/^{3}He$ and (U-Th)/He evidence for an ancient Grand Canyon. *Science*, *338*(6114), 1616–1619. https://doi.org/10.1126/science.1229390

Flowers, R. M., Farley, K. A., & Ketcham, R. A. (2015). A reporting protocol for thermochronologic modeling illustrated with data from the Grand Canyon. *Earth and Planetary Science Letters*, *432*, 425–435. https://doi.org/10.1016/j.epsl.2015.09.053

Flowers, R. M., & Kelley, S. A. (2011). Interpreting data dispersion and "inverted" dates in apatite (U-Th)/He and fission track datasets: An example from the U.S. midcontinent. *Geochimica et Cosmochimica Acta*, *75*(18), 5169–5186. https://doi.org/10.1016/j.gca.2011.06.016

Flowers, R. M., Ketcham, R. A., Shuster, D. L., & Farley, K. A. (2009). Apatite (U-Th)/He thermochronometry using a radiation damage accumulation and annealing model. *Geochimica et Cosmochimica Acta*, *73*(8), 2347–2365. https://doi.org/10.1016/j.gca.2009.01.015

Flowers, R. M., & Schoene, B. (2010). (U-Th)/He thermochronometry constraints on unroofing of the eastern Kaapvall craton and significance for uplift of the southern African Plateau. *Geology*, *38*(9), 827–830. https://doi.org/10.1130/G30980.1

Flowers, R. M., Shuster, D. L., Wernicke, B. P., & Farley, K. A. (2007). Radiation damage control on apatite (U-Th)/He dates from the Grand Canyon region, Colorado Plateau. *Geology*, *35*(5), 447–450. https://doi.org/10.1130/G23471A.1

Fosdick, J. C., Grove, M., Graham, S. A., Hourigan, J. K., Lovera, O. M., & Romans, B. W. (2015). Detrital thermochronologic record of burial heating and sediment recycling in the Magallanes foreland basin, Patagonian Andes. *Basin Research*, *27*(4), 546–572. https://doi.org/10.1111/bre.12088

Fox, M., Dai, J. G., & Carter, A. (2019). Badly behaved detrital (U-Th)/He ages: Problems with He diffusion models or geological models? *Geochemistry, Geophysics, Geosystems*, *20*, 2418–2432. https://doi.org/10.1029/2018GC008102

Fox, M., Herman, F., Willett, S. D., & May, D. A. (2014). A linear inversion method to infer exhumation rates in space and time from thermochronometric data. *Earth Surface Dynamics*, *2*(1), 47–65. https://doi.org/10.5194/esurf-2-47-2014

Fox, M., McKeon, R. E., & Shuster, D. L. (2014). Incorporating 3-D parent nuclide zonation for apatite 4He/3He thermochronometry: An example from the Appalachian Mountains. *Geochemistry, Geophysics, Geosystems*, *15*, 4217–4229. https://doi.org/10.1002/2014GC005464

Fox, M., & Shuster, D. L. (2014). The influence of burial heating on the (U-Th)/He system in apatite: Grand Canyon case study. *Earth and Planetary Science Letters*, *397*, 174–183. https://doi.org/10.1016/j.epsl.2014.04.041

Fox, M., Tripathy-Lang, A., Shuster, D. L., Winn, C., Karlstrom, K. E., & Kelley, S. A. (2017). Westernmost Grand Canyon incision: Testing thermochronometric resolution. *Earth and Planetary Science Letters*, *474*, 248–256. https://doi.org/10.1016/j.epsl.2017.06.049

Fukuchi, T. (2001). Assessment of fault activity by ESR dating of fault gouge; an example of the 500 m core samples drilled into the Nojima earthquake fault in Japan. *Quaternary Science Reviews*, *20*(5-9), 1005–1008. https://doi.org/10.1016/S0277-3791(00)00064-0

Fukuchi, T., & Imai, N. (1998). Resetting experiment of E′ centres by natural faulting—The case of the Nojima earthquake fault in Japan. *Quaternary Science Reviews*, *17*(11), 1063–1068. https://doi.org/10.1016/S0277-3791(97)00102-9

Fukuchi, T., Yurugi, J.-I., & Imai, N. (2007). ESR detection of seismic frictional heating events in the Nojima fault drill core samples, Japan. *Tectonophysics*, *443*(3-4), 127–138. https://doi.org/10.1016/j.tecto.2007.01.020

Galbraith, R. F., & Laslett, G. M. (1993). Statistical models for mixed fission track ages. *Nuclear Tracks and Radiation Measurements*, *21*(4), 459–470. https://doi.org/10.1016/1359-0189(93)90185-C

Gallagher, K. (2012). Transdimensional inverse thermal history modeling for quantitative thermochronology. *Journal of Geophysical Research*, *117*, B02408. https://doi.org/10.1029/2011JB008825

Gallagher, K., & Brown, R. W. (1999). Denudation and uplift at passive margins: The record on the Atlantic Margin of southern Africa. *Philosophical Transactions of the Royal Society of London*, *357*(1753), 835–859. https://doi.org/10.1098/rsta.1999.0354

Gallagher, K., Hawkesworth, C., & Montovani, M. (1994). The denudation history of the onshore continental margin of S.E. Brazil inferred from fission track data. *Journal of Geophysical Research*, *99*(B9), 18,117–18,145. https://doi.org/10.1029/94JB00661

Garcia, V. H., Reiners, P. W., Shuster, D. L., Idleman, B. D., & Zeitler, P. K. (2017). Thermochronology of sandstone-hosted secondary Fe- and Mn-oxides near Moab, Utah: Record of paleo-fluid flow along a fault. *Geological Society of America Bulletin*, *130*(1-2), 93–113.

Garver, J. I., & Kamp, P. J. J. (2002). Integration of zircon color and zircon fission-track zonation patterns in orogenic belts: Application to the Southern Alps, New Zealand. *Tectonophysics*, *349*(1-4), 203–219. https://doi.org/10.1016/S0040-1951(02)00054-9

Gastil, R. G., DeLisle, M., & Morgan, J. (1967). Some effects of progressive metamorphism on zircons. *Geological Society of America Bulletin*, *78*(7), 879–906. https://doi.org/10.1130/0016-7606(1967)78[879:SEOPMO]2.0.CO;2

Gautheron, C., Barbarand, J., Ketcham, R. A., Tassan-Got, L., van der Beek, P. A., Pagel, M., et al. (2013). Chemical influence on α-recoil damage annealing in apatite: Implications for (U-Th)/He dating. *Chemical Geology*, *351*, 257–267. https://doi.org/10.1016/j.chemgeo.2013.05.027

Gautheron, C., Espurt, N., Barbarand, J., Roddaz, M., Baby, P., Brusset, S., et al. (2013). Direct dating of thick-and thin-skin thrusts in the Peruvian Subandean zone through apatite (U–Th)/He and fission track thermochronometry. *Basin Research*, *25*(4), 419–435. https://doi.org/10.1111/bre.12012

Gautheron, C., & Tassan-Got, L. (2010). A Monte Carlo approach of diffusion applied to noble gas/helium thermochronology. *Chemical Geology*, *273*(3-4), 212–224. https://doi.org/10.1016/j.chemgeo.2010.02.023

Gautheron, C., Tassan-Got, L., Barbarand, J., & Pagel, M. (2009). Effect of alpha-damage annealing on apatite (U-Th)/He thermochronology. *Chemical Geology*, *266*(3-4), 157–170. https://doi.org/10.1016/j.chemgeo.2009.06.001

Gautheron, C., Tassan-Got, L., & Farley, K. A. (2006). (U-Th)/Ne chronometry. *Earth and Planetary Science Letters*, *243*(3-4), 520–535. https://doi.org/10.1016/j.epsl.2006.01.025

Gautheron, C., Tassan-Got, L., Ketcham, R. A., & Dobson, K. J. (2012). Accounting for long alpha-particle stopping distances in (U-Th-Sm)/He geochronology: 3D modeling of diffusion, zoning, implantation, and abrasion. *Geochimica et Cosmochimica Acta*, *96*, 44–56. https://doi.org/10.1016/j.gca.2012.08.016

Gerin, C., Gautheron, C., Oliviero, E., Bachelet, C., Djimbi, D. M., Seydoux-Guillaume, A.-M., et al. (2017). Influence of vacancy damage on He diffusion in apatite, investigated at atomic to mineralogical scales. *Geochimica et Cosmochimica Acta*, *197*, 87–103. https://doi.org/10.1016/j.gca.2016.10.018

Ginster, U., Reiners, P. W., Nasdala, L., & Chanmuang, N. C. (2019). Annealing kinetics of radiation damage in zircon. *Geochimica et Cosmochimica Acta*, *249*, 225–246. https://doi.org/10.1016/j.gca.2019.01.033

Gleadow, A. J. W. (1981). Fission-track dating methods: What are the real alternatives? *Nuclear Tracks*, *5*(1-2), 3–14. https://doi.org/10.1016/0191-278X(81)90021-4

Gleadow, A. J. W., Duddy, I. R., Green, P. F., & Lovering, J. F. (1986). Confined fission track lengths in apatite: A diagnostic tool for thermal history analysis. *Contributions to Mineralogy and Petrology*, *94*(4), 405–415. https://doi.org/10.1007/BF00376334

Gleadow, A. J. W., Kohn, B. P., Brown, R. W., O'Sullivan, P. B., & Raza, A. (2002). Fission track thermotectonic imaging of the Australian continent. *Tectonophysics*, *349*(1-4), 5–21. https://doi.org/10.1016/S0040-1951(02)00043-4

Glotzbach, C., Bernet, M., & van der Beek, P. A. (2011). Detrital thermochronology records changing source areas and steady exhumation in the Western European Alps. *Geology*, *39*(3), 239–242. https://doi.org/10.1130/G31757.1

Glotzbach, C., Lang, K. A., Avdievitch, N. N., & Ehlers, T. A. (2019). Increasing the accuracy of (U-Th(-Sm))/He dating with 3D grain modelling. *Chemical Geology*, *506*, 113–125. https://doi.org/10.1016/j.chemgeo.2018.12.032

Gorynski, K. E., Walker, J. D., Stockli, D. F., & Sabin, A. (2014). Apatite (U–Th)/He thermochronometry as an innovative geothermal exploration tool: A case study from the southern Wassuk Range, Nevada. *Journal of Volcanology and Geothermal Research*, *270*, 99–114. https://doi.org/10.1016/j.jvolgeores.2013.11.018

Gottardi, R., Schaper, M. C., Barnes, J. D., & Heizler, M. T. (2018). Fluid–Rock Interaction and Strain Localization in the Picacho Mountains Detachment Shear Zone, Arizona, USA. *Tectonics*, *37*, 3244–3260. https://doi.org/10.1029/2017TC004835

Green, P. F., Duddy, I. R., Gleadow, A. J. W., Tingate, P. R., & Laslett, G. M. (1985). Fission-track annealing in apatite: Track length measurements and the form of the Arrhenius plot. *Nuclear Tracks and Radiation Measurements (1982)*, *10*(3), 323–328. https://doi.org/10.1016/0735-245X(85)90121-8

Green, P. F., Duddy, I. R., Gleadow, A. J. W., Tingate, P. R., & Laslett, G. M. (1986). Thermal annealing of fission tracks in apatite 1. A Qualitative description. *Chemical Geology*, *59*, 237–253. https://doi.org/10.1016/0168-9622(86)90074-6

Grün, R., Tani, A., Gurbanov, A., Koshchug, D., Williams, I., & Braun, J. (1999). A new method for the estimation of cooling and denudation rates using paramagnetic centers in quartz: A case study on the Eldzhurtinskiy Granite, Caucasus. *Journal of Geophysical Research*, *104*(B8), 17,531–17,549. https://doi.org/10.1029/1999JB900173

Guenthner, W. R., Reiners, P. W., & Chowdhury, U. (2016). Isotope dilution analysis of Ca and Ze in apatite and zircon (U-Th)/He chronometry. *Geochemistry, Geophysics, Geosystems*, *17*, 1623–1640. https://doi.org/10.1002/2016GC006311

Guenthner, W. R., Reiners, P. W., DeCelles, P. G., & Kendall, J. (2015). Sevier belt exhumation in central Utah constrained from complex zircon (U-Th)/He data sets: Radiation damage and He inheritance effects on partially reset detrital zircons. *Geological Society of America Bulletin*, *127*(3-4), 323–348. https://doi.org/10.1130/B31032.1

Guenthner, W. R., Reiners, P. W., Drake, H., & Tillberg, M. (2017). Zircon, titanite, and apatite (U-Th)/He ages and age-eU correlations from the Fennoscandian Shield, southern Sweden. *Tectonics*, *36*, 1254–1274. https://doi.org/10.1002/2017TC004525

Guenthner, W. R., Reiners, P. W., Ketcham, R. A., Nasdala, L., & Giester, G. (2013). Helium diffusion in natural zircon: Radiation damage, anisotropy, and the interpretation of zircon (U-Th)/He thermochronology. *American Journal of Science*, *313*(3), 145–198. https://doi.org/10.2475/03.2013.01

Guenthner, W. R., Reiners, P. W., & Tian, Y. (2014). Interpreting date-eU correlations in zircon (U-Th)/He datasets: A case study from the Longmen Shan, China. *Earth and Planetary Science Letters*, *403*, 328–339. https://doi.org/10.1016/j.epsl.2014.06.050

Guralnik, B., Ankjærgaard, C., Jain, M., Murray, A. S., Müller, A., Wälle, M., et al. (2015). OSL-thermochronometry using bedrock quartz: A note of caution. *Quaternary Geochronology*, *25*, 37–48. https://doi.org/10.1016/j.quageo.2014.09.001

Guralnik, B., Jain, M., Herman, F., Ankjærgaard, C., Murray, A. S., Valla, P. G., et al. (2015). OSL-thermochronometry of feldspar from the KTB borehole, Germany. *Earth and Planetary Science Letters*, *423*, 232–243. https://doi.org/10.1016/j.epsl.2015.04.032

Guralnik, B., Jain, M., Herman, F., Paris, R. B., Harrison, T. M., Murray, A. S., et al. (2013). Effective closure temperature in leaky and/or saturating thermochronometers. *Earth and Planetary Science Letters*, *384*, 209–218. https://doi.org/10.1016/j.epsl.2013.10.003

Guralnik, B., and R. Sohbati, 2019, Fundamentals of luminescence photo- and thermochronometry, 399 p, DOI: https://doi.org/10.1142/9781786345790_0011.

Gurnis, M., Mitrovica, J. X., Ritsema, J., & van Heijst, H.-J. (2000). Constraining mantle density structure using geological evidence of surface uplift rates: The case of the African superplume. *Geochemistry, Geophysics, Geosystems*, *1*(7). https://doi.org/10.1029/1999GC000035

Hackspacher, P. C., Ribeiro, L. F. B., Ribeiro, M. C. S., Fetter, A. H., Neto, J. C. H., Tello, C. E. S., & Dantas, E. L. (2004). Consolidation and break-up of the South American Platform in southeastern Brazil: Tectonothermal and denudation histories. *Gondwana Research*, *7*(1), 91–101. https://doi.org/10.1016/S1342-937X(05)70308-7

Haines, S. H., & van der Pluijm, B. A. (2008). Clay quantification and Ar-Ar dating of synthetic and natural gouge: Application to the Miocene Sierra Mazatan detachment fault, Sonora, Mexico. *Journal of Structural Geology*, *30*(4), 525–538. https://doi.org/10.1016/j.jsg.2007.11.012

Haq, B. U., & Al-Qahtani, A. M. (2005). Phanerozoic cycles of sea-level change on the Arabian Platform. *GeoArabia*, *10*, 127–160.

Haq, B. U., & Schutter, S. R. (2008). A chronology of Paleozoic sea-level changes. *Science*, *322*(5898), 64–68. https://doi.org/10.1126/science.1161648

Hasebe, N., Barbarand, J., Jarvis, K., Carter, A., & Hurford, A. J. (2004). Apatite fission-track chronometry using laser ablation ICP-MS. *Chemical Geology*, *207*(3-4), 135–145. https://doi.org/10.1016/j.chemgeo.2004.01.007

Hawthorne, F. C., Groat, L. A., Raudsepp, M., Ball, N. A., Kimata, M., Spike, F. D., et al. (1991). Alpha-decay damage in titanite. *American Mineralogist*, *76*, 370–396.

Heim, J. A., Vasconcelos, P. M., Shuster, D. L., Farley, K. A., & Broadbent, G. (2006). Dating paleochannel iron ore by (U-Th)/He analysis of supergene goethite, Hamersley province, Australia. *Geology*, *34*(3), 173–176. https://doi.org/10.1130/G22003.1

Hendriks, B. W. H., & Redfield, T. F. (2005). Apatite fission track and (U-Th)/He data from Fennoscandia: An example of underestimation of fission track annealing in apatite. *Earth and Planetary Science Letters*, *236*(1-2), 443–458. https://doi.org/10.1016/j.epsl.2005.05.027

Herman, F., Braun, J., Senden, T. J., & Dunlap, W. J. (2007). (U–Th)/He thermochronometry: Mapping 3D geometry using micro-X-ray tomography and solving the associated production–diffusion equation. *Chemical Geology*, *242*(1-2), 126–136. https://doi.org/10.1016/j.chemgeo.2007.03.009

Herman, F., & King, G. E. (2018). Luminescence thermochronometry: Investigating the link between mountain erosion, tectonics and climate. *Elements: An International Magazine of Mineralogy, Geochemistry, and Petrology*, *14*(1), 33–38. https://doi.org/10.2138/gselements.14.1.33

Herman, F., Rhodes, E. J., Braun, J., & Heiniger, L. (2010). Uniform erosion rates and relief amplitude during glacial cycles in the Southern Alps of New Zealand, as revealed from OSL-thermochronology. *Earth and Planetary Science Letters*, *297*(1-2), 183–189. https://doi.org/10.1016/j.epsl.2010.06.019

Hodges, K. V., Ruhl, K. W., Wobus, C. W., & Pringle, M. S. (2005). $^{40}Ar/^{39}Ar$ thermochronology of detrital minerals. *Reviews in Mineralogy and Geochemistry*, *58*(1), 239–257. https://doi.org/10.2138/rmg.2005.58.9

Holland, H. D., & Gottfried, D. (1955). The effect of nuclear radiation on the structure of zircon. *Acta Crystallographica*, *8*(6), 291–300. https://doi.org/10.1107/S0365110X55000947

Horne, A. M., van Soest, M. C., & Hodges, K. V. (2019). U/Pb and (U-Th-Sm)/He "double" dating of detrital apatite by laser ablation: A critical evaluation. *Chemical Geology*, *506*, 40–50. https://doi.org/10.1016/j.chemgeo.2018.12.004

Horne, A. M., van Soest, M. C., Hodges, K. V., Tripathy-Lang, A., & Hourigan, J. K. (2016). Integrated single crystal laser ablation U/Pb and (U-Th)/He dating of detrital accessory minerals—Proof-of-concept studies of titanites and zircons from the Fish Canyon Tuff. *Geochimica et Cosmochimica Acta*, *178*, 106–123. https://doi.org/10.1016/j.gca.2015.11.044

Horton, B. K., Saylor, J. E., Nie, J., Mora, A., Parra, M., Reyes-Harker, A., & Stockli, D. F. (2010). Linking sedimentation in the northern Andes to basement configuration, Mesozoic extension, and Cenozoic shortening: Evidence from detrital zircon U-Pb ages, Eastern Cordillera, Colombia. *Bulletin*, *122*, 1423–1442.

Hourigan, J. K., Reiners, P. W., & Brandon, M. T. (2005). U-Th zonation-dependent alpha-ejection in (U-Th)/He chronometry. *Geochimica et Cosmochimica Acta*, *69*(13), 3349–3365. https://doi.org/10.1016/j.gca.2005.01.024

Houtermans, F. G., Jager, E., Schon, M., & Stauffer, H. (1957). Messungen der Thermolumineszenz als Mittel zur Untersuchung der thermischen und der Strahlungsgeschichte von naturlucken Mineralien und Gesteinen. *Annual Reviews in Physics*, *20*, 283–292.

Hunt, J. M. (1996). *Petroleum Geochemistry and Geology* (Second ed.p. 743). Cambridge, UK: Cambridge University Press.

Huntington, K.W., Klepeis, K. A., & w.c. contributors. (2018). Challenges and opportunities for research in tectonics: Understanding deformation and the processes that link Earth systems from geologic time to human time. A community vision document submitted to the U.S. National Science Foundation. University of Washington, 84 pp. https://doi.org/10.6069/H52R3PQ5

Huntley, D. J. (1985). On the zeroing of the thermoluminescence of sediments. *Physics and Chemistry of Minerals*, *12*(2), 122–127. https://doi.org/10.1007/BF01046837

Huntley, D. J. (2006). An explanation of the power-law decay of luminescence. *Journal of Physics: Condensed Matter*, *18*, 1359.

Hurley, P. M. (1952). Alpha ionization damage as a cause of low helium ratios. *Transactions of the American Geophysical Union*, *33*(2), 174–183. https://doi.org/10.1029/TR033i002p00174

Idleman, B. D., Zeitler, P. K., & McDannell, K. T. (2018). Characterization of helium release from apatite by continuous ramped heating. *Chemical Geology*, *476*, 223–232. https://doi.org/10.1016/j.chemgeo.2017.11.019

Issler, D. R., Grist, A. M., & Stasiuk, L. D. (2005). Post-Early Devonian thermal constraints on hydrocarbon source rock maturation in the Keele Tectonic Zone, Tulita area, NWT, Canada, from multi-kinetic apatite fission track thermochronology, vitrinite reflectance and shale compaction. *Bulletin of Canadian Petroleum Geology*, *53*(4), 405–431. https://doi.org/10.2113/53.4.405

van der Beek, P. A., Summerfield, M. A., Braun, J., Brown, R. W., & Fleming, A. (2002). Modeling postbreakup landscape development and denudational history across the southeast African (Drakensberg Escarpment) margin. *Journal of Geophysical Research*, *107*(12), 2350. https://doi.org/10.1029/2001JB000745

Japsen, P., Bonow, J. M., Green, P. F., Chalmers, J. A., & Lidmar-Bergstrom, K. (2009). Formation, uplift and dissection of planation surfaces at passive continental margins—A new approach. *Earth Surface Processes and Landforms*, *34*(5), 683–699. https://doi.org/10.1002/esp.1766

Jensen, J. L., Reiners, P. W., Siddoway, C. S., Ault, A. K., Thomson, S. N., & Steele-MacInnis, M. (2018). Single-crystal hematite (U-Th)/He dates and fluid inclusions document Cryogenian seismic clastic injection in granite. *Earth and Planetary Science Letters*, *500*, 145–155. https://doi.org/10.1016/j.epsl.2018.08.021

Jess, S., Stephenson, R., & Brown, R. J. (2018). Evolution of the central West Greenland margin and the Nuussuaq Basin: Localised basin uplift along a stable continental margin proposed from thermochronological data. *Basin Research*, *30*(6), 1230–1246. https://doi.org/10.1111/bre.12301

Jess, S., Stephenson, R. A., Roberts, D. H., & Brown, R. J. (2019). Differential erosion of a Mesozoic rift flank: Establishing the source of topography across Karrat, central West Greenland. *Geomorphology*, *334*, 138–150. https://doi.org/10.1016/j.geomorph.2019.02.026

Johnson, J. E., Flowers, R. M., Baird, G. B., & Mahan, K. H. (2017). "Inverted" zircon and apatite (U-Th)/He dates from the Front Range, Colorado: High-damage zircon as a low-temperature (< 50 °C) thermochronometer. *Earth and Planetary Science Letters*, *466*, 80–90. https://doi.org/10.1016/j.epsl.2017.03.002

Johnstone, S. A., & Colgan, J. P. (2018). Interpretation of low-temperature thermochronometer ages from tilted normal fault blocks. *Tectonics*, *37*, 3647–3667. https://doi.org/10.1029/2018TC005207

Jónsson, H., G. Mills, and K.W. Jacobsen, 1998, Nudged elastic band method for finding minimum energy paths of transitions, 385 p.

Kars, R. H., Wallinga, J., & Cohen, K. M. (2008). A new approach towards anomalous fading correction for feldspar IRSL dating—Tests on samples in field saturation. *Radiation Measurements*, *43*(2-6), 786–790. https://doi.org/10.1016/j.radmeas.2008.01.021

Kelly, N. M., Flowers, R. M., Metcalf, J. R., & Mojzsis, S. J. (2018). Late accretion to the Moon recorded in zircon (U–Th)/He thermochronometry. *Earth and Planetary Science Letters*, *482*, 222–235. https://doi.org/10.1016/j.epsl.2017.11.009

Ketcham, R. A. (2005). Forward and inverse modeling of low-temperature thermochronometry data. *Reviews in Mineralogy and Geochemistry*, *58*(1), 275–314. https://doi.org/10.2138/rmg.2005.58.11

Ketcham, R. A., Carter, A., Donelick, R. A., Barbarand, J., & Hurford, A. J. (2007). Improved modeling of fission-track annealing in apatite. *American Mineralogist*, *92*(5-6), 799–810. https://doi.org/10.2138/am.2007.2281

Ketcham, R. A., Carter, A., & Hurford, A. J. (2015). Inter-laboratory comparison of fission track confined length and etch figure measurements in apatite. *American Mineralogist*, *100*(7), 1452–1468. https://doi.org/10.2138/am-2015-5167

Ketcham, R. A., Donelick, R. A., & Carlson, W. D. (1999). Variability of apatite fission-track annealing kinetics: III. Extrapolation to geological time scales. *American Mineralogist*, *84*(9), 1235–1255. https://doi.org/10.2138/am-1999-0903

Ketcham, R. A., Gautheron, C., & Tassan-Got, L. (2011). Accounting for long alpha-particle stopping distances in (U-Th-Sm)/He geochronology: Refinement of the baseline case. *Geochimica et Cosmochimica Acta*, *75*(24), 7779–7791. https://doi.org/10.1016/j.gca.2011.10.011

Ketcham, R. A., Guenthner, W. R., & Reiners, P. W. (2013). Geometric analysis of radiation damage connectivity in zircon and its implications for He diffusion. *American Mineralogist*, *98*(2-3), 350–360. https://doi.org/10.2138/am.2013.4249

Ketcham, R. A., Mora, A., & Parra, M. (2018). Deciphering exhumation and burial history with multi-sample down-well thermochronometric inverse modeling. *Basin Research*, *30*, 48–64. https://doi.org/10.1111/bre.12207

Ketcham, R. A., van der Beek, P. A., Barbarand, J., Bernet, M., & Gautheron, C. (2018). Reproducibility of thermal history reconstruction from apatite fission-track and (U-Th)/He data. *Geochemistry, Geophysics, Geosystems*, *19*, 2411–2436. https://doi.org/10.1029/2018GC007555

King, G. E., Burow, C., Roberts, H. M., & Pearce, N. J. G. (2018). Age determination using feldspar: Evaluating fading-correction model performance. *Radiation Measurements*, *119*, 58–73. https://doi.org/10.1016/j.radmeas.2018.07.013

King, G. E., Guralnik, B., Valla, P. G., & Herman, F. (2016). Trapped-charge thermochronometry and thermometry: A status review. *Chemical Geology*, *446*, 3–17. https://doi.org/10.1016/j.chemgeo.2016.08.023

King, G. E., Herman, F., & Guralnik, B. (2016). Northward migration of the eastern Himalayan syntaxis revealed by OSL thermochronometry. *Science*, *353*(6301), 800–804. https://doi.org/10.1126/science.aaf2637

King, G. E., Herman, F., Lambert, R., Valla, P. G., & Guralnik, B. (2016). Multi-OSL-thermochronometry of feldspar. *Quaternary Geochronology*, *33*, 76–87. https://doi.org/10.1016/j.quageo.2016.01.004

Kohn, B. P., Gleadow, A. J. W., Brown, R. W., Gallagher, K., Lorencak, M., & Noble, W. R. (2005). Visualizing thermotectonic and denudation histories using apatite fission track thermochronology. *Reviews in Mineralogy and Geochemistry*, *58*(1), 527–565. https://doi.org/10.2138/rmg.2005.58.20

Kohn, B. P., Gleadow, A. J. W., Brown, R. W., Gallagher, K., O'Sullivan, P. B., & Foster, D. A. (2002). Shaping the Australian crust over the last 300 million years: Insights from fission track thermotectonic imaging and denudation studies of key terranes. *Australian Journal of Earth Sciences*, *49*(4), 697–717. https://doi.org/10.1046/j.1440-0952.2002.00942.x

Kounov, A., Viola, G., De Wit, M., & Andreoli, M. A. G. (2009). Deundation along the Atlantic passive margin: New insights from apatite fission-track analysis on the western coast of South Africa. *Geological Society of America Special Papers*, *324*(1), 287–306. https://doi.org/10.1144/SP324.19

Krbetschek, M. R., Gotze, J., Dietrich, A., & Trautmann, T. (1997). Spectral information from minerals relevant for luminescence dating. *Radiation Measurements*, *27*(5-6), 695–748. https://doi.org/10.1016/S1350-4487(97)00223-0

Kresse, G., & Furthmüller, J. (1996a). Efficiency of ab-initio total energy calculations for metals and semiconductors using a plane-wave basis set. *Computational Materials Science*, *6*(1), 15–50. https://doi.org/10.1016/0927-0256(96)00008-0

Kresse, G., & Furthmüller, J. (1996b). Efficient iterative schemes for ab initio total-energy calculations using a plane-wave basis set. *Physical Review B*, *54*(16), 11,169–11,186. https://doi.org/10.1103/PhysRevB.54.11169

Kresse, G., & Hafner, J. (1993). Ab initio molecular dynamics for liquid metals. *Physical Review B*, *47*(1), 558–561. https://doi.org/10.1103/PhysRevB.47.558

Kula, J., & Baldwin, S. L. (2012). On hematite as a target for dating aqueous conditions on Mars. *Planetary and Space Science*, *67*(1), 101–108 . https://doi.org/10.1016/j.pss.2012.03.005

Landman, R. L., Flowers, R. M., Rosenau, N. A., & Powell, J. (2016). Conodont (U-Th)/He thermochronology: A case study from the Illinois Basin. *Earth and Planetary Science Letters*, *456*, 55–65. https://doi.org/10.1016/j.epsl.2016.10.003

Lang, K. A., Ehlers, T. A., Kamp, P. J. J., & Ring, U. (2018). Sediment storage in the Southern Alps of New Zealand: New observations from tracer thermochronology. *Earth and Planetary Science Letters*, *493*, 140–149. https://doi.org/10.1016/j.epsl.2018.04.016

Laslett, G., Green, P. F., Duddy, I., & Gleadow, A. (1987). Thermal annealing of fission tracks in apatite 2. A quantitative analysis. *Chemical Geology: Isotope Geoscience Section*, *65*(1), 1–13. https://doi.org/10.1016/0168-9622(87)90057-1

Lease, R. O., Ehlers, T. A., & Enkelmann, E. (2016). Large along-strike variations in the onset of Subandean exhumation: Implications for Central Andean orogenic growth. *Earth and Planetary Science Letters*, *451*, 62–76. https://doi.org/10.1016/j.epsl.2016.07.004

Lease, R. O., Haeussler, P. J., & O'Sullivan, P. B. (2016). Changing exhumation patterns during Cenozoic growth and glaciation of the Alaska Range: Insights from detrital thermochronology and geochronology. *Tectonics*, *35*, 934–955. https://doi.org/10.1002/2015TC004067

Lee, H.-K., & Yang, J.-S. (2007). ESR dating of the Eupchon fault, South Korea. *Quaternary Geochronology*, *2*(1-4), 392–397. https://doi.org/10.1016/j.quageo.2006.04.009

Li, B., & Li, S.-H. (2012). Determining the cooling age using luminescence-thermochronology. *Tectonophysics*, *580*, 242–248. https://doi.org/10.1016/j.tecto.2012.09.023

Li, W., Kluth, P., Schauries, D., Rodriguez, M. D., Lang, M., Zhang, F., et al. (2014). Effect of orientation on ion track formation in apatite and zircon. *American Mineralogist*, *99*(5-6), 1127–1132. https://doi.org/10.2138/am.2014.4669

Li, W., Shen, Y., Zhou, Y., Nan, S., Chen, C.-H., & Ewing, R. C. (2017). In situ TEM observation of alpha-particle induced annealing of radiation damage in Durango apatite. *Scientific Reports*, *7*(1), 14,108. https://doi.org/10.1038/s41598-017-14379-9

Li, W., Wang, L., Lang, M., Trautmann, C., & Ewing, R. C. (2011). Thermal annealing mechanisms of latent fission tracks: Apatite vs. zircon. *Earth and Planetary Science Letters*, *302*(1-2), 227–235. https://doi.org/10.1016/j.epsl.2010.12.016

Lippolt, H. J., Leitz, M., Wernicke, R. S., & Hagedorn, B. (1994). (U+Th)/He dating of apatite experience with samples from different geochemical environments. *Chemical Geology*, *112*(1-2), 179–191. https://doi.org/10.1016/0009-2541(94)90113-9

Lithgow-Bertelloni, C., & Silver, P. (1998). Dynamic topography, plate driving forces, and the African superswell. *Nature*, *395*(6699), 269–272. https://doi.org/10.1038/26212

Lock, J., & Willett, S. D. (2008). Low-temperature thermochronometric ages in fold-and-thrust belts. *Tectonophysics*, *456*(3-4), 147–162. https://doi.org/10.1016/j.tecto.2008.03.007

Lovera, O. M., Richter, F., & Harrison, T. M. (1991). Diffusion domains determined by ^{39}Ar released during step heating. *Journal of Geophysical Research*, *96*(B2), 2057–2069. https://doi.org/10.1029/90JB02217

Lumpkin, G. R., Eby, R. K., & Ewing, R. C. (1991). Alpha-recoil damage in titanite ($CaTiSiO_5$): Direct observation and annealing study using high resolution transmission electron microscopy. *Journal of Materials Research*, *6*(3), 560–564. https://doi.org/10.1557/JMR.1991.0560

Mackintosh, V., Kohn, B. P., Gleadow, A. J. W., & Tian, Y. (2017). Phanerozoic morphotectonic evolution of the Zimbabwe Craton: Unexpected outcomes from a multiple low-temperature thermochronology study. *Tectonics*, *36*, 2044–2067. https://doi.org/10.1002/2017TC004703

MacNamee, A., and D.F. Stockli, 2015, Constraining age and locations of active and paleofluid flow systems in Dixie Valley, Nevada, with apatite (U-Th)/He thermochronometry, AGU Fall Meeting Abstracts.

Magloughlin, J. F., Hall, C. M., & van der Pluijm, B. A. (2001). ^{40}Ar-^{39}Ar geochronometry of pseydotachylytes by vacuum encapsulation: North Cascade Mountains, Washington, USA. *Geology*, *29*(1), 51–54. https://doi.org/10.1130/0091-7613(2001)029<0051:AAGOPB>2.0.CO;2

Maino, M., Casini, L., Ceriani, A., Decarlis, A., Di Giulio, A., Seno, S., et al. (2015). Dating shallow thrusts with zircon (U-Th)/He thermochronometry—The shear heating connection. *Geology*, *43*(6), 495–498. https://doi.org/10.1130/G36492.1

Marfunin, A. S. (2012). *Spectroscopy, luminescence and radiation centers in minerals*. Berlin, Germany and New York, New York, USA: Springer Science & Business Media.

McDannell, K. T., Issler, D. R., & O'Sullivan, P. B. (2019). Radiation-enhanced fission-track annealing revisited and consequences for apatite thermochronometry. *Geochimica et Cosmochimica Acta*, *252*, 213–239. https://doi.org/10.1016/j.gca.2019.03.006

McDannell, K. T., Zeitler, P. K., Janes, D. G., Idleman, B. D., & Fayon, A. K. (2018). Screening apatites for (U-Th)/He thermochronometry via continuous ramped heating: He age components and implications for age dispersion. *Geochimica et Cosmochimica Acta*, *223*, 90–106. https://doi.org/10.1016/j.gca.2017.11.031

McDannell, K. T., Zeitler, P. K., & Schneider, D. A. (2018). Instability of the southern Canadian Shield during the late Proterozoic. *Earth and Planetary Science Letters*, *490*, 100–109. https://doi.org/10.1016/j.epsl.2018.03.012

McDermott, J. A., Whipple, K. X., Hodges, K. V., & van Soest, M. C. (2013). Evidence for Plio-Pleistocene north-south extension at the southern margin of the Tibetal Plateau, Nyalam region. *Tectonics*, *32*, 317–333. https://doi.org/10.1002/tect.20018

McDermott, R.G., A.K. Ault, J.S. Caine, and S.N. Thomson, 2019, Thermotectonic history of the Kluane Ranges and evolution of the eastern Denali fault zone in southwestern Yukon, Canada, *Tectonics, 38*. *DOI:* https://doi.org/10.1029/2019TC005545.

McDermott, R. G., Ault, A. K., Evans, J. P., & Reiners, P. W. (2017). Thermochronometric and textural evidence for seismicity via asperity flash heating on exhumed hematite fault mirrors, Wasatch fault zone, UT, USA. *Earth and Planetary Science Letters*, *471*, 85–93. https://doi.org/10.1016/j.epsl.2017.04.020

McQuarrie, N., & Ehlers, T. A. (2015). Influence of thrust belt geometry and shortening rate on thermochronometer cooling ages: Insights from thermokinematic and erosion modeling of the Bhutan Himalaya. *Tectonics*, *34*, 1055–1079. https://doi.org/10.1002/2014TC003783

Meesters, A. G. C. A., & Dunai, T. J. (2002). Solving the production-diffusion equation for finite diffusion domain of various shapes Part II. Application to cases with α-ejection and nonhomogeneous distribution of the source. *Chemical Geology*, *186*, 57–73.

Metcalf, J. R., & Flowers, R. M. (2013). Initial development of baddeleyite (U-Th)/He thermochronology. *Geological Society of America Abstracts with Programs*, *45*, 223.

Miller, H. B. D., Vasconcelos, P. M., Eiler, J. M., & Farley, K. A. (2017). A Cenozoic terrestrial paleoclimate record from He dating and stable isotope geochemistry of goethite from Western Australia. *Geology*, *45*(10), 895–898. https://doi.org/10.1130/G38989.1

Mills, G., Jónsson, H., & Schenter, G. K. (1995). Reversible work transition state theory: Application to dissociative adsorption of hydrogen. *Surface Science*, *324*(2-3), 305–337. https://doi.org/10.1016/0039-6028(94)00731-4

Monteiro, H., Vasconcelos, P. M., Farley, K. A., Spier, C. A., & Mello, C. L. (2014). (U-Th)/He geochronology of goethite and the origin and evolution of cangas. *Geochimica et Cosmochimica Acta*, *131*, 267–289. https://doi.org/10.1016/j.gca.2014.01.036

Monteiro, H. S., Vasconcelos, P. M. P., & Farley, K. A. (2018). A combined (U-Th)/He and cosmogenic ^{3}He record of landscape armoring by biogeochemical iron cycling. *Journal of Geophysical Research: Earth Surface*, *123*, 298–323. https://doi.org/10.1002/2017JF004282

Monteiro, H. S., Vasconcelos, P. M. P., Farley, K. A., & Lopes, C. A. M. (2018). Age and evolution of diachronous erosion surfaces in the Amazon: Combining (U-Th)/He and cosmogenic ^{3}He records. *Geochimica et Cosmochimica Acta*, *229*, 162–183. https://doi.org/10.1016/j.gca.2018.02.045

Moser, A. C., Evans, J. P., Ault, A. K., Janecke, S. U., & Bradbury, K. K. (2017). (U-Th)/He thermochronometry reveals Pleistocene punctuated deformation and synkinematic hematite mineralization in the Mecca Hills, southernmost San Andreas Fault zone. *Earth and Planetary Science Letters*, *476*, 87–99. https://doi.org/10.1016/j.epsl.2017.07.039

Mukul, M., Jaiswal, M., & Singhvi, A. K. (2007). Timing of recent out-of-sequence active deformation in the frontal Himalayan wedge: Insights from the Darjiling sub-Himalaya, India. *Geology*, *35*(11), 999–1002. https://doi.org/10.1130/G23869A.1

Murakami, M., Košler, J., Takagi, H., & Tagami, T. (2006). Dating pseudotachylyte of the Asuke Shear Zone using zircon fission-track and U–Pb methods. *Tectonophysics*, *424*(1-2), 99–107. https://doi.org/10.1016/j.tecto.2006.06.006

Murakami, M., & Tagami, T. (2004). Dating pseudotachylyte of the Nojima fault using the zircon fission-track method. *Geophysical Research Letters*, *31*, L12604. https://doi.org/10.1029/2004GL020211

Murakami, M., Yamada, R., & Tagami, T. (2006). Short-term annealing characteristics of spontaneous fission tracks in zircon: A qualitative description. *Chemical Geology*, *227*(3-4), 214–222. https://doi.org/10.1016/j.chemgeo.2005.10.002

Murray, A. S., & Olley, J. M. (2002). Precision and accuracy in the optically stimulated luminescence dating of sedimentary quartz: A status review. *Geochronometria*, *21*, 1–16.

Murray, A. S., & Wintle, A. G. (2000). Luminescence dating of quartz using an improved single-aliquot regenerative-dose protocol. *Radiation Measurements*, *32*(1), 57–73. https://doi.org/10.1016/S1350-4487(99)00253-X

Murray, A. S., & Wintle, A. G. (2003). The single aliquot regenerative dose protocol: Potential for improvements in reliability. *Radiation Measurements*, *37*(4-5), 377–381. https://doi.org/10.1016/S1350-4487(03)00053-2

Murray, K. E., Orme, D. A., & Reiners, P. W. (2014). Effects of U-Th-rich grain boundary phases on apatite helium ages. *Chemical Geology*, *390*, 135–151. https://doi.org/10.1016/j.chemgeo.2014.09.023

Murray, K. E., Reiners, P. W., & Thomson, S. N. (2016). Rapid Pliocene-Pleistocene erosion of the central Colorado Plateau documented by apatite thermochronology from the Henry Mountains. *Geology*, *44*(6), 483–486. https://doi.org/10.1130/G37733.1

Murrell, G. R., Sobel, E. R., Carrapa, B., & Andriessen, P. A. M. (2009). Calibration and comparison of etching techniques for apatite fission-track thermochronology. *Geological Society, London, Special Publications*, *324*(1), 73–85. https://doi.org/10.1144/SP324.6

Naeser, C. W. (1967). The use of apatite and sphene for fission track age determinations. *Geological Society of America Bulletin*, *78*(12), 1523–1526. https://doi.org/10.1130/0016-7606(1967)78[1523:TUOAAS]2.0.CO;2

Nahon, D., 1991, Introduction to the petrology of soils and chemical weathering. .

Nasdala, L., Irmer, G., & Wolf, D. (1995). The degree of metamictization in zircon: A Raman spectroscopic study. *European Journal of Mineralogy*, *7*, 471–478.

Nasdala, L., Reiners, P. W., Garver, J. I., Kennedy, A. K., Stern, R. A., Balan, E., & Wirth, R. (2004). Incomplete retention of radiation damage in zircon from Sri Lanka. *American Mineralogist*, *89*(1), 219–231. https://doi.org/10.2138/am-2004-0126

Nuriel, P., K. Maher, and D.M. Miller, 2013, Time constraints on fault activity in the Eastern California Shear Zone from U-Pb (SHRIMP-RG) dating of syntectonic opal. Eos Trans., AGU v. 94 Fall Meeting Suppl., T34B-02.

Nuriel, P., Miller, D. M., Schmidt, K. M., Coble, M. A., & Maher, K. (2019). Ten-million years of activity within the Eastern California Shear Zone from U–Pb dating of fault-zone opal. *Earth and Planetary Science Letters*, *521*, 37–45. https://doi.org/10.1016/j.epsl.2019.05.047

Nuriel, P., Rosenbaum, G., Uysal, T. I., Zhao, J., Golding, S. D., Weinberger, R., et al. (2011). Formation of fault-related calcite precipitates and their implications for dating fault activity in the East Anatolian and Dead Sea fault zones. *Geological Society of London, Special Publication*, *359*(1), 229–248. https://doi.org/10.1144/SP359.13

Nuriel, P., Rosenbaum, G., Zhao, J.-X., Feng, Y., Golding, S. D., Villement, B., & Weinberger, R. (2012). U-Th dating of striated fault planes. *Geology*, *40*(7), 647–650. https://doi.org/10.1130/G32970.1

Nuriel, P., Weinberger, R., Kylander-Clark, A. R. C., Hacker, B. R., & Craddock, J. P. (2017). The onset of the Dead Sea transform based on calcite age-strain analyses. *Geology*, *45*(7), 587–590. https://doi.org/10.1130/G38903.1

Nyblade, A. A., & Robinson, S. W. (1994). The African superwell. *Geophysical Research Letters*, *21*(9), 765–768. https://doi.org/10.1029/94GL00631

Odlum, M. L., & Stockli, D. F. (2019). Thermotectonic evolution of the North Pyrenean Agly Massif during Early Cretaceous hyperextension using multi-mineral U-Pb thermochronometry. *Tectonics*, *38*, 1509–1531. https://doi.org/10.1029/2018TC005298

Orme, D. A., Guenthner, W. R., Laskowski, A. K., & Reiners, P. W. (2016). Long-term tectonothermal history of Laramide basement from zircon-He age-eU correlations. *Earth and Planetary Science Letters*, *453*, 119–130. https://doi.org/10.1016/j.epsl.2016.07.046

Orme, D. A., Reiners, P. W., Hourigan, J. K., & Carrapa, B. (2015). Effects of inherited cores and magmatic overgrowths on zircon (U-Th)/He ages and age-eU trends from Greater Himalayan sequence rocks, Mount Everest region, Tibet. *Geochemistry, Geophysics, Geosystems*, *16*, 2499–2507. https://doi.org/10.1002/2015GC005818

Pachell, M. A., & Evans, J. P. (2002). Structural analysis of the Gemini strike-slip fault zone, Central Sierra Nevada, California. *Journal of Structural Geology*, *24*(12), 1903–1924. https://doi.org/10.1016/S0191-8141(02)00027-5

Pagel, M., Bonifacie, M., Schneider, D. A., Gautheron, C., Brigaud, B., Calmels, D., et al. (2018). Improving paleohydrological and diagenetic reconstructions in calcite veins and breccia of a sedimentary basin by combining Δ47 temperature, δ18Owater and U-Pb age. *Chemical Geology*, *481*, 1–17. https://doi.org/10.1016/j.chemgeo.2017.12.026

Peppe, D. J., & Reiners, P. W. (2007). Conodont (U-Th)/He thermochronology: Initial results, potential, and problems. *Earth and Planetary Science Letters*, *258*(3-4), 569–580. https://doi.org/10.1016/j.epsl.2007.04.022

van der Pluijm, B. A., Hall, C. M., Vrolijk, P. J., Pevear, D. R., & Covey, M. C. (2001). The dating of shallow faults in the Earth's crust. *Nature*, *412*(6843), 172–175. https://doi.org/10.1038/35084053

van der Pluijm, B. A., Vrolijk, P. J., Pevear, D. R., Hall, C. M., & Solum, J. G. (2006). Fault dating in the Canadian Rocky Mountains: Evidence for late Cretaceous and early Eocene orogenic pulses. *Geology*, *34*(10), 837–840. https://doi.org/10.1130/G22610.1

Powell, J., Schneider, D., Stockli, D. F., & Fallas, K. (2016). Zircon (U-Th)/He thermochronology of Neoproterozoic strata from the Mackenzie Mountains, Canada: Implications for the Phanerozoic exhumation and deformation history of the northern Canadian Cordillera. *Tectonics*, *35*, 663–689. https://doi.org/10.1002/2015TC003989

Prasad, A. K., Poolton, N. R. J., Kook, M., & Jain, M. (2017). Optical dating in a new light: A direct, non-destructive probe of trapped electrons. *Scientific Reports*, *7*(1), 12,097. https://doi.org/10.1038/s41598-017-10174-8

Price, P. B., & Walker, R. M. (1962a). Chemical etching of charged particle tracks in solids. *Journal of Applied Physics*, *33*(12), 3407–3412. https://doi.org/10.1063/1.1702421

Price, P. B., & Walker, R. M. (1962b). Electron microscope observation of etched tracks from spallation recoils in mica. *Physical Review Letters*, *8*(5), 217–219. https://doi.org/10.1103/PhysRevLett.8.217

Price, P. B., & Walker, R. M. (1962c). Observation of fossil particle tracks in natural micas. *Nature*, *196*(4856), 732–734. https://doi.org/10.1038/196732a0

Rahl, J. M., Reiners, P. W., Campbell, I. H., Nicolescu, S., & Allen, C. M. (2003). Combined single-grain (U-Th)/He and U/Pb dating of detrital zircons from the Navajo Sandstone, Utah. *Geology*, *31*(9), 761–764. https://doi.org/10.1130/G19653.1

Ravenhurst, C. E., Roden-Tice, M. K., & Miller, D. S. (2003). Thermal annealing of fission tracks in fluorapatite, chlorapatite, manganoapatite, and Durango apatite: Experimental results. *Canadian Journal of Earth Sciences*, *40*(7), 995–1007. https://doi.org/10.1139/e03-032

Recanati, A., Gautheron, C., Barbarand, J., Missenard, Y., Rinna-Jamme, R., Tassan-Got, L., et al. (2017). Helium trapping in apatite damage: Insights from (U-Th-Sm)/He dating of different granitoid lithologies. *Chemical Geology*, *470*, 116–131. https://doi.org/10.1016/j.chemgeo.2017.09.002

Reich, M., Ewing, R. C., Ehlers, T., & Becker, U. (2007). Low-temperature anisotropic diffusion of helium in zircon: Implications for zircon (U-Th)/He thermochronometry. *Geochemica et Cosmochimica Acta*, *71*(12), 3119–3130. https://doi.org/10.1016/j.gca.2007.03.033

Reich, M., & Vasconcelos, P. M. (2015). Geologic and economic significance of supergene metal deposits. *Elements*, *11*(5), 305–310. https://doi.org/10.2113/gselements.11.5.305

Reimold, W. U., Jessberger, E. K., & Stephan, T. (1990). ^{40}Ar-^{39}Ar dating of pseudotachylite from the Vredefort dome, South Africa: A progress report. *Tectonophysics*, *171*(1-4), 139–152. https://doi.org/10.1016/0040-1951(90)90095-P

Reiners, P. W. (2005). Zircon (U-Th)/He thermochronometry. *Reviews in Mineralogy and Geochemistry*, *58*(1), 151–179. https://doi.org/10.2138/rmg.2005.58.6

Reiners, P. W., Campbell, I. H., Nicolescu, S., Allen, C. M., Hourigan, J. K., Garver, J. I., et al. (2005). (U-Th)/(He-Pb) double dating of detrital zircons. *American Journal of Science*, *305*(4), 259–311. https://doi.org/10.2475/ajs.305.4.259

Reiners, P. W., Chan, M. A., & Evenson, N. S. (2014). Radiogenic helium dating and chemistry of diagenetic Fe- and Mn-oxides in Mesozoic sandstones of the Colorado Plateau. *Geological Society of America Bulletin*, *126*(9-10), 1363–1383. https://doi.org/10.1130/B30983.1

Reiners, P. W., & Farley, K. A. (1999). Helium diffusion and (U-Th)/He thermochronometry of titanite. *Geochimica et Cosmochimica Acta*, *63*(22), 3845–3859. https://doi.org/10.1016/S0016-7037(99)00170-2

Reiners, P. W., & Farley, K. A. (2001). Influence of crystal size on apatite (U-Th)/He thermochronology: An example from the Bighorn Mountains, Wyoming. *Earth and Planetary Science Letters*, *188*(3-4), 413–420. https://doi.org/10.1016/S0012-821X(01)00341-7

Reiners, P. W., Farley, K. A., & Hiskes, H. J. (2002). He diffusion and (U-Th)/He thermochronology of zircon: Initial results from Fish Canyon Tuff and Gold Butte. *Tectonophysics*, *349*(1-4), 297–308. https://doi.org/10.1016/S0040-1951(02)00058-6

Reiners, P. W., Spell, T. L., Nicolescu, S., & Zanetti, K. A. (2004a). Zircon (U-Th)/He thermochronology: He diffusion and comparisons with ^{40}Ar/^{39}Ar dating. *Geochimica et Cosmochimica Acta*, *68*(8), 1857–1887. https://doi.org/10.1016/j.gca.2003.10.021

Reiners, P. W., Spell, T. L., Nicolescu, S., & Zanetti, K. A. (2004b). Zircon (U–Th)/He thermochronometry: He diffusion and comparison with ^{40}Ar/^{39}Ar dating. *Geochemica et Cosmochimica Acta*, *68*(8), 1857–1887. https://doi.org/10.1016/j.gca.2003.10.021

Resor, P. G., Chamberlain, K. R., Frost, C. D., Frost, B. R., & Snoke, A. W. (1996). Directly dating of deformation: U-Pb age of syndeformational sphene growth in the Proterozoic Laramie Peak shear zone. *Geology*, *24*(7), 623–626. https://doi.org/10.1130/0091-7613(1996)024<0623:DDODUP>2.3.CO;2

Retallack, G. J. (2010). Lateritization and bauxitization *Events*. *Economic Geology*, *105*(3), 655–667. https://doi.org/10.2113/gsecongeo.105.3.655

Rice, J. R. (2006). Heating and weakening of faults during earthquake slip. *Journal of Geophysical Research*, *111*, B05311. https://doi.org/10.1029/2005JB004006

Riedesel, S., King, G. E., Prasad, A. K., Kumar, R., Finch, A. A., & Jain, M. (2018). Optical determination of the width of the band-tail states, and the excited state and ground state energies of the principal dosimetric trap in feldspar. *Radiation Measurements*, *125*, 40–51.

Riffel, S. B., Vasconcelos, P. M., Carmo, I. O., & Farley, K. A. (2015). Combined ^{40}Ar/^{39}Ar and (U-Th)/He geochronological constraints on long-term landscape evolution of the Second Parana Plateau and its ruiniform surface features, Parana, Brazil. *Geomorphology*, *233*, 52–63. https://doi.org/10.1016/j.geomorph.2014.10.041

Riffel, S. B., Vasconcelos, P. M., Carmo, I. O., & Farley, K. A. (2016). Goethite (U-Th)/He geochronology and precipitation mechanisms during weathering of basalts. *Chemical Geology*, *446*, 18–32. https://doi.org/10.1016/j.chemgeo.2016.03.033

Rink, W. J. (1997). Electron spin resonance (ESR) dating and ESR applications in Quaternary science and archaeometry. *Radiation Measurements*, *27*(5-6), 975–1025. https://doi.org/10.1016/S1350-4487(97)00219-9

Rittner, M., and W. Muller, 2011, Dating brittle deformation with the U-Pb method. Geophysical Research Abstracts *13*, EGU2011-13443.
Roberts, N. M. W., & Walker, R. J. (2016). U-Pb geochronology of calcite-mineralized faults: Absolute timing of rift-related fault events on the northeast Atlantic margin. *Geology*, *44*(7), 531–534. https://doi.org/10.1130/G37868.1
Roberts, R. G., & Lian, O. B. (2015). Dating techniques: Illuminating the past. *Nature*, *520*(7548), 438–439. https://doi.org/10.1038/520438a
Roselieb, K., Dersch, O., Büttner, H., & Rauch, F. (2006). Diffusivity and solubility of He in garnet: An exploratory study using nuclear reaction analysis. *Nuclear Instruments and Methods in Physics Research Section B: Beam Interactions with Materials and Atoms*, *244*(2), 412–418. https://doi.org/10.1016/j.nimb.2005.10.016
Rowe, C. D., & Griffith, W. A. (2015). Do faults preserve a record of seismic slip: A second opinion. *Journal of Structural Geology*, *78*, 1–26. https://doi.org/10.1016/j.jsg.2015.06.006
Saadoune, I., & De Leeuw, N. H. (2009). A computer simulation study of the accommodation and diffusion of He in uranium-and plutonium-doped zircon ($ZrSiO_4$). *Geochimica et Cosmochimica Acta*, *73*(13), 3880–3893. https://doi.org/10.1016/j.gca.2009.03.019
Saadoune, I., Purton, J. A., & De Leeuw, N. H. (2009). He incorporation and diffusion pathways in pure and defective zircon $ZrSiO_4$: A density functional theory study. *Chemical Geology*, *258*(3-4), 182–196. https://doi.org/10.1016/j.chemgeo.2008.10.015
Schildgen, T. F., Balco, G., & Shuster, D. L. (2010). Canyon incision and knickpoint propagation recorded by apatite $^4He/^3He$ thermochronometry. *Earth and Planetary Science Letters*, *293*(3-4), 377–387. https://doi.org/10.1016/j.epsl.2010.03.009
Schneider, S., Hammerschmidt, K., & Rosenberg, C. L. (2013). Dating the longevity of ductile shear zones: Insight from $^{40}Ar/^{39}Ar$ in situ analyses. *Earth and Planetary Science Letters*, *369-370*, 43–58. https://doi.org/10.1016/j.epsl.2013.03.002
Schoene, B., & Bowring, S. A. (2007). Determining accurate temperature-time paths from U-Pb thermochronology: An example from the Kaapvaal craton, southern Africa. *Geochimica et Cosmochimica Acta*, *71*(1), 165–185. https://doi.org/10.1016/j.gca.2006.08.029
Schwartz, S., Gautheron, C., Audin, L., Dumont, T., Nomade, J., Barbarand, J., et al. (2017). Foreland exhumation controlled by crustal thickening in the Western Alps. *Geology*, *45*(2), 139–142. https://doi.org/10.1130/G38561.1
Seman, S., D.F. Stockli, A.J. Smye, and E.J. Hernandez Goldstein, 2014, Garnet (U-Th)/He thermochronometry and its application to exhumed high-pressure low-temperature metamorphic rocks. *Thermo 2014,* 14th International Conference on Thermochronology*,* Chamonix*,* France.
Sherlock, S. C., Jones, K. A., & Park, R. G. (2008). Grenville-age pseudotachylite in the Lewisian: Laserprobe $^{40}Ar/^{39}Ar$ ages from the Gairloch region of Scotland (UK). *Journal of the Geological Society of London*, *165*(1), 73–83. https://doi.org/10.1144/0016-76492006-134
Sherlock, S. C., Strachan, R. A., & Jones, K. A. (2009). High spatial resolution $^{40}Ar/^{39}Ar$ dating of pseudotachylites: Geochronological evidence for multiple phases of faulting within basement gneisses of the Outer Hebrides (UK). *Journal of the Geological Society of London*, *166*(6), 1049–1059. https://doi.org/10.1144/0016-76492008-125
Sherlock, S. C., Watts, L. M., Holdsworth, R., & Roberts, D. (2004). Dating fault reactivation by Ar/Ar laserprobe: An alternative view of apparently cogenetic mylonite-pseudotachylite assemblages. *Journal of the Geological Society of London*, *161*(3), 335–338. https://doi.org/10.1144/0016-764903-160
Shuster, D. L., Cuffey, K. M., Sanders, J. W., & Balco, G. (2011). Thermochronology reveals headward propagation of erosion in an alpine landscape. *Science*, *332*(6025), 84–88. https://doi.org/10.1126/science.1198401
Shuster, D. L., Ehlers, T. A., Rusmore, M. E., & Farley, K. A. (2005). Rapid glacial erosion at 1.8 Ma revealed by $^4He/^3He$ thermochronometry. *Science*, *310*(5754), 1668–1670. https://doi.org/10.1126/science.1118519
Shuster, D. L., & Farley, K. A. (2004). $^4He/^3He$ thermochronometry. *Earth and Planetary Science Letters*, *217*(1-2), 1–17. https://doi.org/10.1016/S0012-821X(03)00595-8
Shuster, D. L., & Farley, K. A. (2005). $^4He/^3He$ thermochronometry: Theory, practice, and potential complications. In P. Reiners, & T. Ehlers (Eds.), *Reviews in Mineralogy and Geochemistry: Low-Temperature Thermochronology: Techniques, Interpretations, and Applications*, (Vol. 58, pp. 181–203). Washington, D.C.: Mineralogical Society of America.
Shuster, D. L., & Farley, K. A. (2009). The influence of artificial radiation damage and thermal annealing on helium diffusion kinetics in apatite. *Geochimica et Cosmochimica Acta*, *73*(1), 183–196. https://doi.org/10.1016/j.gca.2008.10.013
Shuster, D. L., Farley, K. A., Sisterson, J. M., & Burnett, D. S. (2004). Quantifying the diffusion kinetics and spatial distributions of radiogenic ^4He in minerals containing proton-induced ^3He. *Earth and Planetary Science Letters*, *217*(1-2), 19–32. https://doi.org/10.1016/S0012-821X(03)00594-6
Shuster, D. L., Farley, K. A., Vasconcelos, P. M., Balco, G., Monteiro, H. S., Waltenberg, K., & Stone, J. O. (2012). Cosmogenic ^3He in hematite and goethite from Brazilian "canga" duricrust demonstrates the extreme stability of these surfaces. *Earth and Planetary Science Letters*, *329-330*, 41–50. https://doi.org/10.1016/j.epsl.2012.02.017
Shuster, D. L., Flowers, R. M., & Farley, K. A. (2006). The influence of natural radiation damage on helium diffusion kinetics in apatite. *Earth and Planetary Science Letters*, *249*(3-4), 148–161. https://doi.org/10.1016/j.epsl.2006.07.028
Shuster, D. L., Vasconcelos, P. M., Heim, J. A., & Farley, K. A. (2005). Weathering geochronology by (U-Th)/He dating of goethite. *Geochimica et Cosmochimica Acta*, *69*(3), 659–673. https://doi.org/10.1016/j.gca.2004.07.028
Sibson, R. H. (1975). Generation of pseudotachylyte by ancient seismic faulting. *Geophysical Journal of the Royal Astronomical Society*, *43*(3), 775–794. https://doi.org/10.1111/j.1365-246X.1975.tb06195.x
Silk, E. C. H., & Barner, R. S. (1959). Examination of fission fragment tracks with an electron microscope. *Philosophical Magazine*, *4*(44), 970–972. https://doi.org/10.1080/14786435908238273
Singhvi, A. K., Banerjee, D., Pande, K., Gogte, V., & Valdiya, K. S. (1994). Luminescence studies on neotectonic events in south-central Kumaun Himalaya—A feasibility study. *Quaternary Science Reviews*, *13*(5-7), 595–600. https://doi.org/10.1016/0277-3791(94)90083-3
Sobel, E. R., & Seward, D. (2010). Influence of etching conditions on apatite fission-track etch pit diameter. *Chemical Geology*, *271*(1-2), 59–69. https://doi.org/10.1016/j.chemgeo.2009.12.012
van Soest, M. C., Hodges, K. V., Wartho, J. A., Biren, M. B., Monteleone, B. D., Ramezani, J., et al. (2011). (U-Th)/He dating of terrestrial impact structures: The Manicouagan example. *Geochemistry, Geophysics, Geosystems*, *12*, Q0AA16. https://doi.org/10.1029/2010GC003465
Spencer, C. J., Danišík, M., Ito, H., Hoiland, C., Tapster, S., Jeon, H., et al. (2019). Rapid exhumation of Earth's youngest exposed granites driven by subduction of an oceanic arc. *Geophysical Research Letters*, *46*, 1259–1267. https://doi.org/10.1029/2018GL080579
Spencer, J. Q. G., Hadizadeh, J., Gratier, J.-P., & Doan, M.-L. (2012). Dating deep? Luminescence studies of fault gouge from the San Andreas Fault zone 2.6 km beneath Earth's surface. *Quaternary Geochronology*, *10*, 280–284. https://doi.org/10.1016/j.quageo.2012.04.023
Spiegel, C., Kohn, B. P., Belton, D., Brener, Z., & Gleadow, A. J. W. (2009). Apatite (U-Th-Sm)/He thermochronology of rapidly cooled samples: The effect of He implantation. *Earth and Planetary Science Letters*, *385*, 105–119.

Stanley, J. R., & Flowers, R. M. (2016). Dating kimberlite emplacement with zircon and perovskite (U-Th)/He geochronology. *Geochemistry, Geophysics, Geosystems*, *17*, 4517–4533. https://doi.org/10.1002/2016GC006519

Stanley, J. R., Flowers, R. M., & Bell, D. R. (2013). Kimberlite (U-Th)/He dating links surface erosion with lithospheric heating, thinning, and metasomatism in the southern African Plateau. *Geology*, *41*(12), 1243–1246. https://doi.org/10.1130/G34797.1

Stanley, J. R., Flowers, R. M., & Bell, D. R. (2015). Erosion patterns and mantle sources of topographic change across the southern African Plateau derived from the shallow and deep records of kimberlites. *Geochemistry, Geophysics, Geosystems*, *16*, 3235–3256. https://doi.org/10.1002/2015GC005969

Stevens, A. L., Balgord, E. A., & Carrapa, B. (2016). Revised exhumation history of the Wind River Range, WY, and implications for Laramide tectonics. *Tectonics*, *35*, 1121–1136. https://doi.org/10.1002/2016TC004126

Stock, G. M., Ehlers, T. A., & Farley, K. A. (2006). Where does sediment come from? Quantifying catchment erosion with detrital apatite (U-Th)/He thermochronometry. *Geology*, *34*(9), 725–728. https://doi.org/10.1130/G22592.1

Stockli, D. F., & Farley, K. A. (2004). Empirical constraints on the titanite (U-Th)/He partial retention zone from the KTB drill hole. *Chemical Geology*, *207*(3-4), 223–236. https://doi.org/10.1016/j.chemgeo.2004.03.002

Stockli, D. F., Farley, K. A., & Dumitru, T. A. (2000). Calibration of the (U-Th)/He thermochronometer on an exhumed fault block, White Mountains, California. *Geology*, *28*(11), 983–986. https://doi.org/10.1130/0091-7613(2000)28<983:COTAHT>2.0.CO;2

Stockli, D.F., M.R. Wolfe, T.J. Blackburn, T. Zack, J.D. Walker, and G.L. Luvizotto, 2007, He diffusion and (U-Th)/He thermochronometry of rutile, American Geophysical Union Fall Meeting, Volume V23C-1548: San Francisco.

Strutt, R. J. (1909). The accumulation of helium in geological time, II. *Proceedings of the Royal Society of London A*, *83*(560), 96–99. https://doi.org/10.1098/rspa.1909.0081

Stüwe, K., & Hintermüller, M. (2000). Topography and isotherms revisited: The influence of laterally migrating drainage divides. *Earth and Planetary Science Letters*, *184*(1), 287–303. https://doi.org/10.1016/S0012-821X(00)00315-0

Tagami, T. (2005). Zircon fission-track thermochronology and applications to fault studies. *Reviews in Mineralogy and Geochemistry*, *58*(1), 95–122. https://doi.org/10.2138/rmg.2005.58.4

Tagami, T. (2012). Thermochronological investigations of fault zones. *Tectonophysics*, *538-540*, 67–85. https://doi.org/10.1016/j.tecto.2012.01.032

Tagami, T. (2019). Application of fission-track thermochronology to understand fault zones. In: Malusà M., Fitzgerald P. (eds) *Fission-Track Thermochronology and its Application to Geology*. *Springer Textbooks in Earth Sciences, Geography and Environment* (pp. 221–233). Cham: Springer.

Tagami, T., Galbraith, R., Yamada, R., & Laslett, G. (1998). Revised annealing kinetics of fission tracks in zircon and geological implications. In: van den Haute P., de Corte F. (eds) *Advances in Fission-Track Geochronology*. *Solid Earth Sciences Library*, vol 10. p. 99–112, Dordrecht: Springer.

Tagami, T., & Murakami, T. (2007). Probing fault zone heterogeneity on the Nojima fault: Constraints from zircon fission-track analysis of borefole samples. *Tectonophysics*, *443*(3-4), 139–152. https://doi.org/10.1016/j.tecto.2007.01.013

Ternois, S., Odlum, M. L., Ford, M., Pik, R., Stockli, D. F., Tibari, D., et al. (2019). Thermochronological evidence of early orogenesis eastern Pyrenees, France. *Tectonics*, *38*, 1308–1336. https://doi.org/10.1029/2018TC005254

Thomson, K. D., Stockli, D. F., Clark, J. D., Puigdefàbregas, C., & Fildani, A. (2017). Detrital zircon (U-Th)/(He-Pb) double-dating constraints on provenance and foreland basin evolution of the Ainsa Basin, south-central Pyrenees, Spain. *Tectonics*, *36*, 1352–1375. https://doi.org/10.1002/2017TC004504

Tinker, J., de Wit, M., & Brown, R. W. (2008). Linking source and sink: Evaluating the balance between onshore erosion and offshore sediment accumulation since Gondwana break-up, South Africa. *Tectonophysics*, *455*(1-4), 94–103. https://doi.org/10.1016/j.tecto.2007.11.040

Toyoda, S., Rink, W., Schwarcz, H. P., & Rees-Jones, J. (2000). Crushing effects on TL and OSL on quartz: Relevance to fault dating. *Radiation Measurements*, *32*(5-6), 667–672. https://doi.org/10.1016/S1350-4487(00)00088-3

Tranel, L. M., Spotila, J. A., Kowalewski, M. J., & Waller, C. M. (2011). Spatial variation of erosion in a small, glaciated basin in the Teton Range, Wyoming, based on detrital apatite (U-Th)/He thermochronology. *Basin Research*, *23*(5), 571–590. https://doi.org/10.1111/j.1365-2117.2011.00502.x

Tremblay, M. M., Fox, M., Schmidt, J. L., Tripathy-Lang, A., Wielicki, M. M., Harrison, T. M., et al. (2015). Erosion in southern Tibet shut down at ~10 Ma due to enhanced rock uplift within the Himalaya. *Proceedings of the National Academy of Sciences*, *112*(39), 12,030–12,035. https://doi.org/10.1073/pnas.1515652112

Tremblay, M. M., Shuster, D. L., & Balco, G. (2014). Cosmogenic noble gas paleothermometry. *Earth and Planetary Science Letters*, *400*, 195–205. https://doi.org/10.1016/j.epsl.2014.05.040

Tremblay, M. M., Shuster, D. L., Balco, G., & Cassata, W. S. (2017). Neon diffusion kinetics and implications for cosmogenic neon paleothermometry in feldspars. *Geochimica et Cosmochimica Acta*, *205*, 14–30. https://doi.org/10.1016/j.gca.2017.02.013

Tremblay, M. M., Shuster, D. L., Spagnolo, M., Renssen, H., & Ribolini, A. (2019). Temperatures recorded by cosmogenic noble gases since the last glacial maximum in the Maritime Alps. *Quaternary Research*, *91*(2), 829–847. https://doi.org/10.1017/qua.2018.109

Tripathy-Lang, A., Fox, M., & Shuster, D. L. (2015). Zircon ^{4}He/^{3}He thermochronometry. *Geochimica et Cosmochimica Acta*, *166*, 1–14. https://doi.org/10.1016/j.gca.2015.05.027

Tsukamoto, S., Long, H., Richter, M., Li, Y., King, G. E., He, Z., et al. (2018). Quartz natural and laboratory ESR dose response curves: A first attempt from Chinese loess. *Radiation Measurements*, *120*, 137–142. https://doi.org/10.1016/j.radmeas.2018.09.008

Uysal, T. I., Feng, Y., Zhao, J.-X., Altunel, E., Weatherley, D., Karabacak, V., et al. (2007). U-series dating and geochemical tracing of late Quaternary travertine in co-seismic fissures. *Earth and Planetary Science Letters*, *257*(3-4), 450–462. https://doi.org/10.1016/j.epsl.2007.03.004

Vail, P.R., R.M. Mitchum Jr, and S. Thompson III, 1977, Seismic stratigraphy and global changes of sea level: Part 4. Global cycles of relative changes of sea level.: Section 2. Application of seismic reflection configuration to stratigraphic interpretation.

Valla, P. G., Lowick, S. E., Herman, F., Champagnac, J.-D., Steer, P., & Guralnik, B. (2016). Exploring IRSL50 fading variability in bedrock feldspars and implications for OSL thermochronometry. *Quaternary Geochronology*, *36*, 55–66. https://doi.org/10.1016/j.quageo.2016.08.004

Valla, P. G., Rahn, M. K. W., Shuster, D. L., & van der Beek, P. A. (2016). Multi-phase late-Neogene exhumation history of the Aar massif, Swiss central Alps. *Terra Nova*, *28*(6), 383–393. https://doi.org/10.1111/ter.12231

Valla, P. G., Shuster, D. L., & van der Beek, P. A. (2011). Significant increase in relief of the European Alps during mid-Pleistocene glaciations. *Nature Geoscience*, *4*, 688–692.

Valla, P. G., van der Beek, P. A., Shuster, D. L., Braun, J., Herman, F., Tassan-Got, L., & Gautheron, C. (2012). Late Neogene exhumation and relief development of the Ar and Aiguilles Rouges massifs (Swiss Alps) from low-temperature thermochronology and $^{4}He/^{3}He$ thermochronometry. *Journal of Geophysical Research*, *117*, F01004. https://doi.org/10.1029/2011JF002043

Vasconcelos, P., Renne, P. R., Brimhall, G. H., & Becker, T. A. (1994). Direct dating of weathering phenomena by 40Ar/36Ar and K-Ar analysis of supergene K-Mn oxides. *Geochimica et Cosmochimica Acta*, *58*(6), 1635–1665. https://doi.org/10.1016/0016-7037(94)90565-7

Vasconcelos, P. M., Heim, J. A., Farley, K. A., Monteiro, H., & Waltenberg, K. (2013). $^{40}Ar/^{39}Ar$ and (U-Th)/He–$^{4}He/^{3}He$ geochronology of landscape evolution and channel iron deposits genesis at Lynn Peak, Western Australia. *Geochimica et Cosmochimica Acta*, *117*, 283–312 . https://doi.org/10.1016/j.gca.2013.03.037

Vasconcelos, P. M., Reich, M., & Shuster, D. (2015). The paleoclimatic signatures of supergene metal deposits. *Elements*, *11*(5), 317–322. https://doi.org/10.2113/gselements.11.5.317

Verhaert, G., Muchez, P., Sintubin, M., Similox-Tohon, D., Vandycke, S., & Waelkens, M. (2003). Reconstruction of neotectonic activity using carbonate precipitates: A case study from northwestern extremity of the Isparta Angle (SW Turkey). *Journal of Geochemical Exploration*, *78-79*, 197–201. https://doi.org/10.1016/S0375-6742(03)00070-0

Vermeesh, P. (2009). RadialPlotter: A java application for fission track, luminescence, and other radial plots. *Nuclear Tracks and Radiation Measurements*, *44*(4), 409–410. https://doi.org/10.1016/j.radmeas.2009.05.003

Visocekas, R., Spponer, N. A., Zink, A., & Blanc, P. (1994). Tunnel afterglow, fading, and infrared emission in thermoluminescence of feldspars. *Radiation Measurements*, *23*(2-3), 377–385. https://doi.org/10.1016/1350-4487(94)90067-1

Vrolijk, P. J., & van der Pluijm, B. A. (1999). Clay gouge. *Journal of Structural Geology*, *21*(8-9), 1039–1048. https://doi.org/10.1016/S0191-8141(99)00103-0

Watanabe, Y., Nakai, S. I., & Lin, A. (2008). Attempt to determine U-Th ages of calcite veins in the Nojima fault zone, Japan. *Geochemical Journal*, *42*(6), 507–513. https://doi.org/10.2343/geochemj.42.507

Weber, W. J., & Matzke, H. J. (1986). Radiation effects in actinide host phases. *Radiation Effects*, *98*(1-4), 93–99. https://doi.org/10.1080/00337578608206101

Weisberg, W. R., Metcalf, J. R., & Flowers, R. M. (2018). Distinguishing slow cooling versus multiphase cooling and heating in zircon and apatite (U-Th)/He datasets: The case of the McClure Mountain syenite standard. *Chemical Geology*, *485*, 90–99.

Wells, M. L., Snee, L. W., & Blythe, A. E. (2000). Dating of major normal fault systems using thermochronology: An example from the Raft River detachment, Basin and Range, western United States. *Journal of Geophysical Research*, *105*(B7), 16,303–16,327. https://doi.org/10.1029/2000JB900094

Wernicke, R. S., & Lippolt, H. J. (1993). Botryoidal hematite from the Schwarzwald (Germany): Heterogeneous uranium distributions and their bearing on the helium dating method. *Earth and Planetary Science Letters*, *114*(2-3), 287–300. https://doi.org/10.1016/0012-821X(93)90031-4

Wernicke, R. S., & Lippolt, H. J. (1994). Dating of vein specularite using internal (U+Th)/^{4}He isochrons. *Geophysical Research Letters*, *21*(5), 345–347. https://doi.org/10.1029/94GL00014

Wernicke, R. S., & Lippolt, H. J. (1997). (U+Th)-He evidence of Jurassic continuous hydrothermal activity in the Schwarzwald basement, Germany. *Chemical Geology*, *138*(3-4), 273–285. https://doi.org/10.1016/S0009-2541(97)00020-X

West, A. J., Galy, A., & Bickle, M. (2005). Tectonic and climatic controls on silicate weathering. *Earth and Planetary Science Letters*, *235*(1-2), 211–228. https://doi.org/10.1016/j.epsl.2005.03.020

Whipp, D. M., & Ehlers, T. A. (2007). Influence of groundwater flow on thermochronometer-derived exhumation rates in the central Nepalese Himalaya. *Geology*, *35*(9), 851–854. https://doi.org/10.1130/G23788A.1

Whipp, D. M., Ehlers, T. A., Braun, J., & Spath, C. D. (2009). Effects of exhumation kinematics and topographic evolution on detrital thermochronometer data. *Journal of Geophysical Research*, *114*, F04021. https://doi.org/10.1029/2008JF001195

Whitmeyer, S. J., & Karlstrom, K. E. (2007). Tectonic model for the Proterozoic growth of North America. *Geosphere*, *3*(4), 220–259. https://doi.org/10.1130/GES00055.1

Wildman, M., Brown, R. J., Beucher, R., Persano, C., Stuart, F. M., Gallagher, K., et al. (2016). The chronology and tectonic style of landscape evolution along the elevated Atlantic continental margin of South Africa resolved by joint apatite fission track and (U-Th-Sm)/He thermochronology. *Tectonics*, *35*, 511–545. https://doi.org/10.1002/2015TC004042

Wildman, M., Brown, R. J., Persano, C., Beucher, R., Stuart, F. M., MacKintosh, V., et al. (2017). Contrasting Mesozoic evolution across the boundary between on and off craton regions of the South African plateau inferred from apatite fission track and (U-Th-Sm)/He thermochronology. *Journal of Geophysical Research: Solid Earth*, *122*, 1517–1547. https://doi.org/10.1002/2016JB013478

Willett, C. D., Fox, M., & Shuster, D. L. (2017). A helium-based model for the effects of radiation damage annealing on helium diffusion kinetics in apatite. *Earth and Planetary Science Letters*, *477*, 195–204. https://doi.org/10.1016/j.epsl.2017.07.047

Willett, S. D., & Brandon, M. T. (2013). Some analytical methods for converting thermochronometric age to erosion rate. *Geochemistry, Geophysics, Geosystems*, *14*, 209–222. https://doi.org/10.1029/2012GC004279

Winn, C., Karlstrom, K. E., Shuster, D. L., Kelley, S. A., & Fox, M. (2017). 6 Ma age of carving Westernmost Grand Canyon: Reconciling geologic data with combined AFT, (U-Th)/He, and $^{4}He/^{3}He$ thermochronologic data. *Earth and Planetary Science Letters*, *474*, 257–271. https://doi.org/10.1016/j.epsl.2017.06.051

Wintle, A. G. (1973). Anomalous fading of thermo-luminescence in mineral samples. *Nature*, *245*(5421), 143–144. https://doi.org/10.1038/245143a0

Wintle, A. G., & Murray, A. S. (2006). A review of quartz optically stimulated luminescence characteristics and their relevance in single-aliquot regeneration dating protocols. *Radiation Measurements*, *41*(4), 369–391. https://doi.org/10.1016/j.radmeas.2005.11.001

Wolf, R. A., Farley, K. A., & Silver, L. T. (1996). Helium diffusion and low temperature thermochronometry of apatite. *Geochimica et Cosmochimica Acta*, *60*(21), 4231–4240. https://doi.org/10.1016/S0016-7037(96)00192-5

Wolfe, M.R., 2009, Calibration of rutile (U-Th)/He Thermochronology: Assessing the thermal evolution of the KTB drill hole, Germany and adjacent Bohemian Massif, University of Kansas.

Wolff, R., Dunkl, I., Kempe, U., Stockli, D. F., Wiedenbeck, M., & von Eynatten, H. (2016). Variable helium diffusion characteristics in fluorite. *Geochimica et Cosmochimica Acta*, *188*, 21–34. https://doi.org/10.1016/j.gca.2016.05.029

Wolff, R., Dunkl, I., Kempe, U., & von Eynatten, H. (2015). The age of the latest thermal overprint of tin and polymetallic deposits in the Erzebirge, Germany: Constraints from fluorite (U-Th-Sm)/He thermochronology. *Economic Geology*, *110*(8), 2025–2040. https://doi.org/10.2113/econgeo.110.8.2025

Wolfler, A., Kurz, W., Danisik, M., & Rabitsch, R. (2010). Dating of fault zone activity by apatite fission track and apatite (U-Th)/He thermochronometry: A case study from the Lavanttal fault system (Eastern Alps). *Terra Nova*, *22*, 274–282.

Woodhead, J. A., Rossman, G. R., & Silver, L. T. (1991). The metamictization of zircon: Radiation dose-dependent structural characteristics. *American Mineralogist*, *76*, 74–82.

Yamada, R., Tagami, T., Nishimura, S., & Ito, H. (1995). Annealing kinetics of fission tracks in zircon: An experimental study. *Chemical Geology*, *122*(1-4), 249–258. https://doi.org/10.1016/0009-2541(95)00006-8

Yang, R., Herman, F., Fellin, M. G., & Maden, C. (2018). Exhumation and topographic evolution of the Namche Barwa Syntaxis, eastern Himalaya. *Tectonophysics*, *722*, 43–52. https://doi.org/10.1016/j.tecto.2017.10.026

Yapp, C. J., & Shuster, D. L. (2017). D/H of late Miocene meteoric waters in Western Australia: Paleoenvironmental conditions inferred from the δD of (U-Th)/He-dated CID goethite. *Geochimica et Cosmochimica Acta*, *213*, 110–136. https://doi.org/10.1016/j.gca.2017.06.036

Young, D. A. (1958). Etching of radiation damage in lithium fluoride. *Nature*, *182*(4632), 375–377. https://doi.org/10.1038/182375a0

Young, K. E., van Soest, M. C., Hodges, K. V., Watson, E. B., Adams, B. A., & Lee, P. (2013). Impact thermochronology and the age of Haughton impact structure, Canada. *Geophysical Research Letters*, *40*, 3836–3840. https://doi.org/10.1002/grl.50745

Zachos, J., Pagani, M., Sloan, L., Thomas, E., & Billups, K. (2001). Trends, rhythms, and aberrations in global climate 65 Ma to present. *Science*, *292*(5517), 686–693. https://doi.org/10.1126/science.1059412

Zattin, M., Pace, D., Andreucci, B., Rossetti, F., & Talarico, F. M. (2014). Cenozoic erosion of the Transantarctic Mountains: A source-to-sink thermochronological study. *Tectonophysics*, *630*, 158–165. https://doi.org/10.1016/j.tecto.2014.05.022

Zeitler, P. K., Enkelmann, E., Thomas, J. B., Watson, E. B., Ancuta, L. D., & Idleman, B. D. (2017). Solubility and trapping of helium in apatite. *Geochimica et Cosmochimica Acta*, *209*, 1–8. https://doi.org/10.1016/j.gca.2017.03.041

Zeitler, P. K., Herczig, A. L., McDougall, I., & Honda, M. (1987). U-Th-He dating of apatite: A potential thermochronometer. *Geochimica et Cosmochimica Acta*, *51*(10), 2865–2868. https://doi.org/10.1016/0016-7037(87)90164-5

Zhang, N., Zhong, S., & Flowers, R. M. (2012). Predicting and testing continental vertical motion histories since the Paleozoic. *Earth and Planetary Science Letters*, *317-318*, 426–435. https://doi.org/10.1016/j.epsl.2011.10.041

Zwingmann, H., & Mancktelow, N. (2004). Timing of Alpine fault gouges. *Earth and Planetary Science Letters*, *223*(3-4), 415–425. https://doi.org/10.1016/j.epsl.2004.04.041